Processing-Property Relationships of Hemp Fibre

by

Sandra Korte

A thesis submitted in partial fulfilment of the
requirements for the

Degree of Master of Engineering

University of Canterbury
September 2006

Contents

List of Figures

List of Tables

Abbreviations

3PB	Three-Point-Bending
a	Absorbtivity
A	Absorbance A = abc
AFM	Atomic Force Microscopy
b	Thickness of sample cell
c	Concentration of absorbing component
DMA	Dynamic Mechanical Analysis
E	Young's modulus
E	Enzyme concentration
FT-IR	Fourier transform infrared
I	Intensity transmitted by the sample
I_0	Intensity of monochromatic radiation entering a sample
IR	Infrared
PGU	Polygalacturonase units
SEM	Scanning Electron Microscopy
T	Transmittance = $I / I_0 = 10^{-abc}$
T_t	Transformation temperature

Abstract

There is great interest in the plant Cannabis sativa (hemp) as a source of technical fibres for the reinforcement of polymers in composite materials due to its high mechanical properties. As a natural fibre hemp also offers biodegradabilty and is therefore an inexpensive and renewable alternative to glass fibres However, the environmental benefits of natural fibres cannot be fully exploited if the manufacturing of their composites involves polluting processing steps. Unfortunately, there is still a lack of environmetally sustainable processing methods yielding technical fibres of sufficient quality. Enzyme application as a biotechnological processing method is a good candidate for this aim and is therefore actively investigated at present.

In this work the effects of a range of enzymes on the morphological, compositional and mechanical properties of hemp was investigated. The enzymes were firstly characterised and then applied to hemp fibre for differing periods of time. After visual inspection, a set of fibre samples were selected and subjected to further analysis by Fourier-Transform Infrared Spectroscopy (FTIR), tensile testing and scanning electron microscopy (SEM). The commercial formulation Pectinex® Ultra-SL emerged as the most efficient in terms of treatment time and fibre quality.

The effectiveness of treatments was further investigated by developing a novel experimental method that correlates the adhesion forces measured by atomic force microscopy (AFM) on the fibre surface to the properties of the fibres or composites. In order to identify correlations between the adhesion forces and fibre or composite properties, hemp fibre was subjected to four distinctly different treatments to obtain significant differences between fibre properties. The fibres and composites were then analyzed using a combination of FTIR, tensile testing, 3-point bend testing, dynamic mechanical analysis (DMA) and SEM. Based on this comprehensive dataset the AFM data was correlated using the software SPSS. The information derived from AFM (adhesion forces and surface topology) was useful in the clarification of fibre modifications evoked by the treatments.

1 Introduction

Increasingly, the selection and application of engineering materials is being governed by environmental impact and sustainability issues, especially in mass production sectors such as the transportation industry. Synthetically-made fibre-reinforced plastics (*e.g.* fibre-glass) fulfil the need for more lightweight materials but without being recyclable or degradable. Natural fibres (*e.g.* flax, hemp, sisal, etc.) are an alternative to synthetic fibres, offering CO_2-neutrality, biodegradability and specific mechanical properties comparable to those of glass fibres. After appropriate fibre pre-treatments, natural fibres have been successfully used to reinforce various polymers, leading to the class of composite materials known as *eco-composites* or *biocomposites*. Although natural fibres are used in various applications, extensive research is still required in order to fully understand the applied treatments and eventually optimise them to explore the full potential of natural fibres.

This thesis is split into two main parts. In the first part, different enzyme solutions and their effect on hemp fibre is examined. By the determination of the resulting mechanical, chemical and morphological properties of the fibres, the most suitable treatment for future projects will be identified.

The second part of the thesis also aims to improve the basis for future projects in the field of natural fibre composites. Several methods of analysis such as FTIR, tensile and bend testing, DMA and SEM were employed to characterize fibre properties. In order to facilitate a faster development of new treatments it is vital to be able to predict composite properties from direct analysis of the fibre so that the time and cost of fabricating and testing composites can be minimised.

In this work, AFM has been used to characterize the surface topology, surface energy and polarity of natural fibres. These properties can have an important influence on the interfacial bonding properties of the final composite and examination of the treated fibres by AFM is therefore a promising candidate in the search for an analytical method that improves prediction of composite properties *via* fibre analysis. In this thesis, four distinctly different fibre treatments (buffer solution, enzymatic, alkalization and acetylation) were applied to hemp fibres in

order to elucidate possible correlations between AFM measurements and fibre or composite characteristics. The necessary systematic characterization of the samples will involve FTIR, single fibre tensile tests, composite bending tests, SEM, DMA and AFM.

Thus, the main objectives of this thesis are to:

- compare a range of commercial and pure enzyme solutions for treatment of hemp fibre;
- develop a basis for the appropriate selection of an enzyme solution;
- creation of a comprehensive dataset on the effect of four different fibre treatments on the properties of hemp fibre and their composites; and
- correlate the data obtained from AFM to fibre and composite properties

2 Literature Review

2.1 Natural fibre composites

The rise of industrial composite materials began during the sixties, when glass fibres in combination with tough rigid resins could be produced on a large scale. However, although natural fibres had been used in ancient times, for example straw in clay bricks, the interest in natural fibres was low until recently. During the last decade reasons including required weight saving, a lower raw material price, 'caloric recycling' or ecological motivations such as the need for renewable resources constituted a renewed interest in natural fibres as a substitute for fibreglass.

The main advantages of a natural fibre composite are:

- Low specific weight, resulting in a higher specific strength and stiffness than glass fibre;
- It is a renewable resource, the production requires little energy, CO_2 is used while oxygen is given back to the environment;
- Producible with low investment at low cost, which makes the material an interesting product for low-wage countries;
- Reduced wear of tooling;
- Healthier working conditions, no skin irritation;
- Thermal recycling is possible while glass causes problems in combustion furnaces; and
- Good thermal and acoustic insulating properties.

Natural fibre composites also have their short-comings which are overcome to an extent by appropriate treatments and production technologies:

- Low strength properties, particularly impact strength; in comparison to fibre strength
- Variable quality that depends on unpredictable influences such as weather;
- Moisture absorption which causes swelling of the fibres;

- Limited maximum processing temperature;
- Lower durability although fibre treatments can improve this considerably;
- Poor fire resistance;
- Price can fluctuate due to harvesting results or agricultural politics; and
- Irregular fibre lengths such that spinning is required to obtain continuous yarns (for weaving or winding).

At present new applications of natural fibre composites are mainly found in the automotive industry. Figure 2.1 shows natural fibre composite parts typically to be found in cars. This image also illustrates the dominance of upholstery applications where acoustic and thermal insulation, low cost and an environmentally friendly image are advantageous. Intensive research in the areas of composite properties and production aims to support the future implementation of natural fibre composites for parts with structural functionalities.

Figure 2.1: 20 kg of recyclable biomass used in the Mercedes C-Class [1].

This work focuses on the fibre material to be treated for biocomposite production, in particular hemp fibres, and therefore an overview of typical characteristic values of natural fibres in comparison with glass fibres is given in Table 2.1.

Table 2.1: Comparison of characteristic values for E-glass and natural fibres [2].

Properties	E-glass	flax	hemp	jute	ramie	coir	sisal	abaca	cotton
density ρ [g/cm^{3}]	2.55	1.4	1.48	1.46	1.5	1.25	1.33	1.5	1.51
tensile strength [10E^{6} N/m^{2}]	2400	800-1500	550-900	400-800	500	220	600-700	980	400
E-modulus [GPa] specific [E/ρ]	73 29	60- 80 26- 46	70 47	10- 30 7- 21	44 29	6 5	38 29		12 8
elongation at failure (%)	3	1.2-1.6	1.6	1.8	2	15- 25	2- 3		3- 10
moisture absorption [%]	-	7	8	12	12- 17	10	11		8- 25
price / kg [$], raw (mat / fabric)	1.3 (1.7/ 3.8)	0.5–1.5 (2/4)	0.6–1.8 (2/4)	0.35 1.5/ 0.9-2	1.5– 2.5	0.25–0.5	0.6–0.7	1.5–2.5	1.5–2.2

* tensile strength strongly depends on type of fibre, being a bundle or a single filament

2.2 Hemp

Natural fibres are subdivided based on their origins, deriving from plant, animals or minerals. Hemp (*Cannabis sativa L*) as a plant fibre is additionally classified as bast fibre such as flax, kenaf, ramie and jute, whereas sisal, henequen and coir are hard-fibres.

Hemp can be cultured in temperate climates, while most of the other types of bast fibres can only be grown in subtropical or tropical climate zones [3]. Since visual differentiation is not possible between hemp that is cultivated for technical applications (“industrial hemp”) and hemp intended for drug use, the cultivation of hemp is restricted in most countries.

2.3 Composition and structure of hemp fibre

Bast fibres consist of a wooden core surrounded by a stem (Figure 2.2 (a) and (b)). Within the stem there are a number of fibre bundles, each containing individual fibre cells that are arranged and constructed as shown in Figure 2.2 (c).

The cell walls of the elementary fibres are composed of several layers. The outward layer is called middle lamella. It connects the macrofibrils and acts as “glue”, consisting mainly of pectin. The primary cell wall, made of a cellulose network, follows after the middle lamella. Being the first wall that is grown in a young cell, it stays very thin. After completion of the primary wall, the secondary wall is built and finally makes up to 98% of the wall thickness of the fibre. The secondary wall is formed out of three layers of crystalline microfibrils based on cellulose, which are connected by amorphous lignin and hemicellulose. The structure of the secondary wall is shown in Figure 2.2 (d). Enclosed by the thin tertiary wall lies the innermost part of the fibre, the lumen, which is filled with proteins and pectin.

Table 2.2: Mean composition (in%) and microfibril angles of natural cellulose fibres at 10% moisture content [4], [5].

	Cotton	Hemp	Jute	Flax	Ramie
Cellulose	92.7	67.0	64.4	62.1	68.8
Hemicellulose	5.7	16.1	12.0	16.7	13.1
Pectin	0.0	0.8	0.2	1.8	1.9
Lignin	0.0	3.3	11.8	2.0	0.6
Water solubles	1.0	2.1	1.1	3.9	5.5
Wax	0.6	0.7	0.5	1.5	0.3
Microfibril Angle		6.2	8.0	10.0	7.5

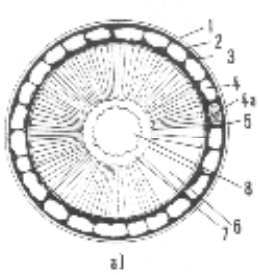

1 cuticula, 2 epidermis, 3 parenchyma, 4 sclerenchyma, 4a (fibre bundles and single fibres), 5 cambium, 6 xylem (wood cells), 7 pith, 8 lumen

(a) schematic layout of bast fibres [9]

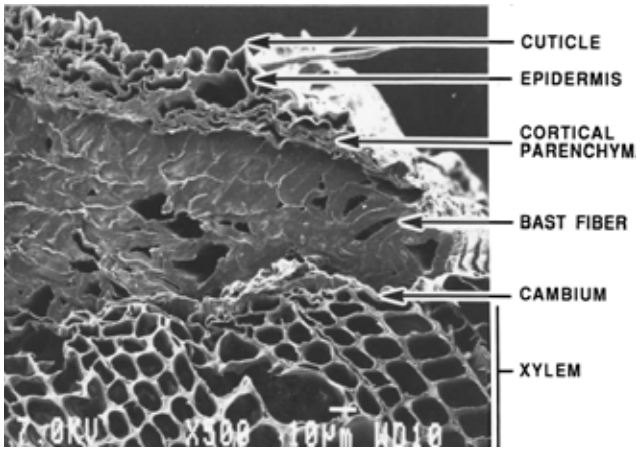

(b) Micrograph of a hemp stem cross-section, [6]

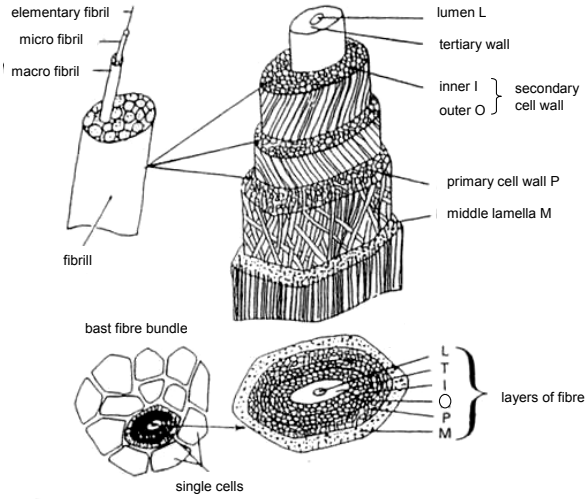

(c) Flax fibre model according to H.W. Haudek; E. Viti, [7].

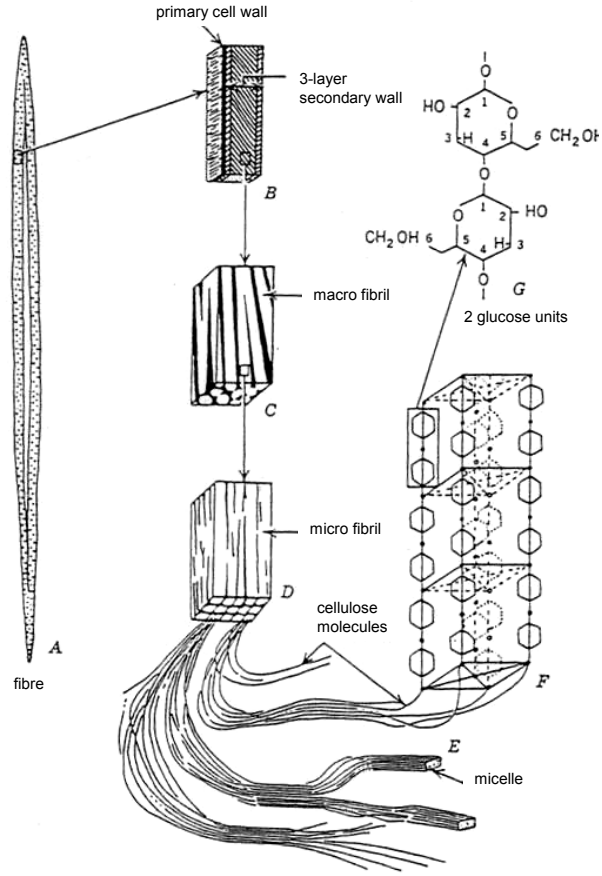

(d) Design of the secondary cell wall according to K. Esau, [8].

Figure 2.2: Layout of bast fibres

The mechanical properties of a natural fibre are generally determined by the cellulose content and the microfibril angle of the cellulose fibrils within the secondary cell wall [9]. Typical values for both the microfibril angles and the composition of natural fibres are given in Table 2.2. A small microfibril angle indicates predominantly parallel alignment of the cellulose fibrils in fibre direction. The fibre's stiffness therefore reaches a maximum at 0° and decreases as shown in Figure 2.3 towards larger angles. An FEM-model for the calculation of fibre stiffness was developed by Gassan *et al*. [10]. In contrast to earlier models of the fibre featuring a symmetric laminate, *e.g.* [11], the fibre structure is represented by a thick-walled tube. The fibre stiffness is described as a combination of parallel and serial connection, representing low and high microfibril angles respectively, of the cellulose fibrils in a hemicellulose/lignin matrix.

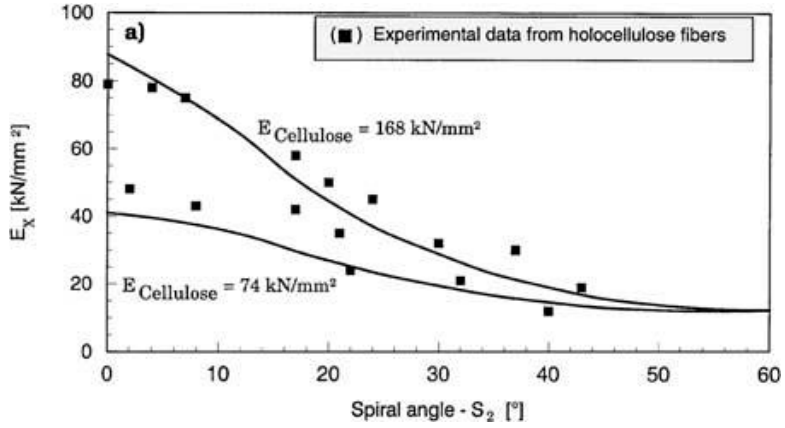

Figure 2.3: Influence of the second cell wall's microfibril angle on fibre stiffness. Experimental data from Page *et al*. [12], curves calculated by Gassan *et al*. [10].

Cellulose, hemicellulose and lignin as the basic components of natural fibres with regard to physical properties and fibre composite properties will be introduced in more detail.

Cellulose

Cellulose is the most abundant biopolymer. Cellulose is a linear condensation polymer consisting of D-anhydroglucopyranose units joined by β-1,4-glycosidic bonds (common abbreviations are anhydroglucose or simply glucose). The basic formula of cellulose is:

$$C_{6P}H_{10P+2}O_{5P+1} \approx (C_6H_{10}O_5)_P \text{ or } (C_6H_{10}O_5)_n$$

where *P* = the degree of polymerization and *n* = the number of units in the chain. Typical degrees of polymerization are listed in Table 2.3.

Table 2.3: Degrees of polymerization (P_n) of different natural fibres [13].

Fibre	P_n
Cotton, raw	7000
Flax	8000
Ramie	6500

As shown in the Hawthorne projection of cellulose in Figure 2.4, the pyranose rings are in the $^4C_1$ conformation, which means that the -CH_2OH and -OH groups, as well as the glycosidic bonds are equatorial with respect to the mean planes of the rings [5]. The actual base unit therefore is the cellubiose (4-O-β-d-glucopyranosyl-d-glucose) [4].

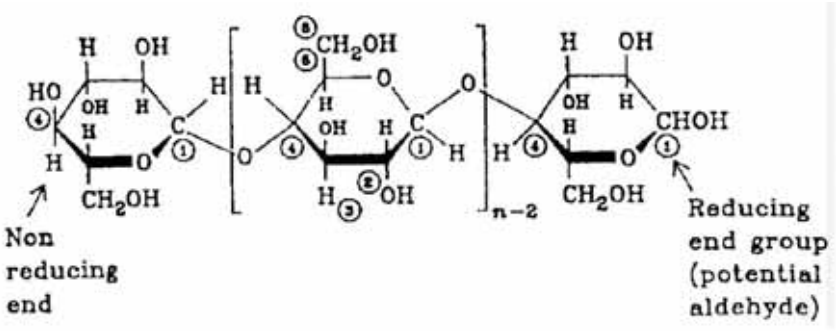

Figure 2.4: Hawthorne projection formula of cellulose [5].

As a naturally occurring polymer, cellulose always contains small amounts of other constituents in addition to glucose (over 99%). Most of these changes result from secondary reactions, *i.e.* hydrolysis or oxidation, during isolation of cellulose from natural resources. However, they also may already be partially built into or onto the cellulose molecules during biosynthesis, such as lignin-cellulose complexes [4].

The secondary structure of solid cellulose is characterized by high-order microcrystalline structures (crystalline regions) alternated with those of a distinctly lower order (amorphous regions). Cellulose is polymorphic; *i.e.*, depending on the origin or the conditions during isolation or conversion, cellulose can adopt various crystal lattice structures.

Native celluloses all show the so-called cellulose I lattice structure. Each unit cell houses two countercurrently arranged cellulose molecules. The lattice of cellulose I is of the monoclinic sphenolitic type. The cellulose chains are in line with the b axis of the unit cell. Figure 2.5 shows a schematic drawing of the cellulose I unit cell modification.

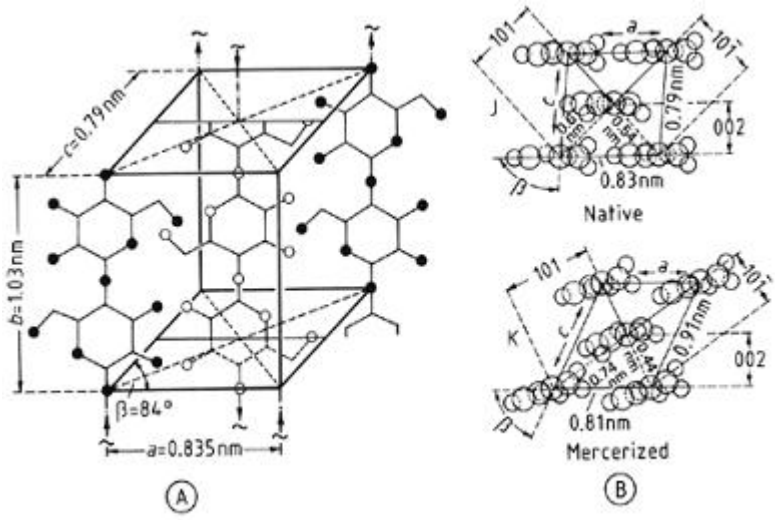

Figure 2.5: Crystal structure of cellulose.

A) Unit cell of the crystal lattice of cellulose I [4]

B) Comparison of the unit cell cross-sections of the native cellulose I and mercerized cellulose II [4]

The internal cohesion of the cellulose molecules in the unit cells and crystalline domains is due to intermolecular secondary valences - partly hydrogen bonds and partly van der Waals forces. These bonds can act either between molecules situated in the same crystal lattice plane (intraplanar bonds) or between molecules located in neighbouring lattice planes (interplanar bonds).

The unit cells of the other polymorphic structures of cellulose - the most important one being the so-called cellulose II - differ basically in the lengths of their *a* and *c* axis and the angle of inclination b. The cellulose II modification is formed as the thermodynamically most stable polymorph when cellulose fibres are treated with concentrated sodium hydroxide solution (> 14%) or precipitated (regenerated) from solution.

The ability of hydroxyl groups to form secondary valence hydrogen bonds is – together with the stiff and straight chain nature of the cellulose molecule – the cause for the high tendency to organize into crystallites in parallel arrangement and crystallite strands (elementary fibrils), the basic elements of the supermolecular structure of cellulose fibres.

The dimensions of the elementary crystallites differ only slightly for native or regenerated cellulose fibres. Their length ranges between 12 and 20 nm (= 24 – 40 glucose units) and their width between 2.5 and 4.0 nm.

The basic structural element of cellulose fibres is the so-called elementary fibril. The cross-dimensions of the elementary fibrils correspond with those of the elementary crystallites. The elementary fibril is a strand of elementary crystals linked together by segments of long cellulose molecules. The lateral order in the interlinking regions is distinctly less pronounced (amorphous). This structure is schematically shown in Figure 2.6 [4].

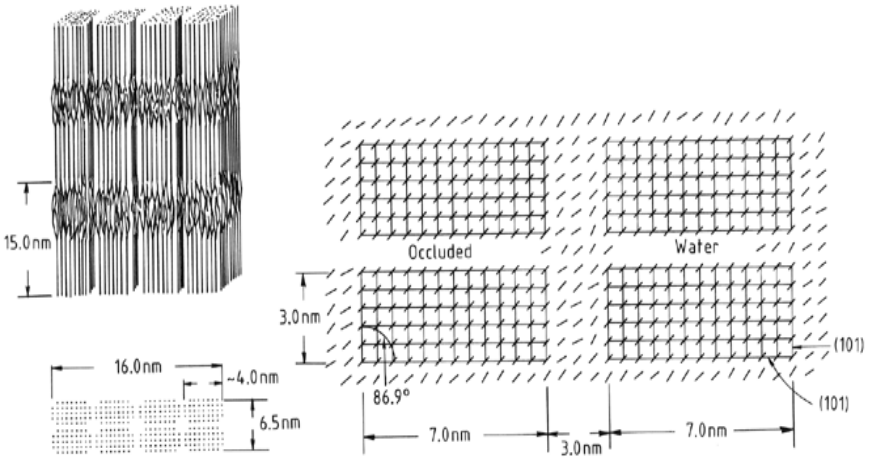

Figure 2.6: The architecture of elementary fibrils and microfibrils of native celluloses, [4]

Several elementary fibrils associate to form larger aggregations of so-called microfibrils and macrofibrils (Figure 2.2 (c)).

Cellulose is relatively hygroscopic and solution can only be achieved under severe degradation in concentrated acids. It is moreover non-melting with thermal decomposition starting at 180 °C [4].

The chemical reactivity is determined to a large extent by its solid-state supermolecular structure, resulting in heterogeneous reactions. With the two-phase system of well-ordered crystalline and amorphous regions the action of the reaction medium initially focuses on the latter. The interlinked crystallites offer only a very small surface area to be penetrated. In order to enhance the reactivity of cellulose, several activation treatments are in use. As such, swelling, solvent exchange, structure-loosening additives, degradation, and mechanical grinding enlarge the accessible surfaces by *opening* the crystalline aggregations. Especially the use of certain inorganic and organic bases (*e.g.* sodium hydroxide solution during mercerization) leads to an even more effective additional opening of the amorphous regions interlinking the crystallites.

Hemicellulose

Hemicelluloses comprise a group of polysaccharides (excluding pectin) that remain associated with cellulose after the removal of lignin. There are three main differences observed in comparison with cellulose. In the first place the composition of hemicellulose is heterogeneous containing several different sugars

(cellulose is composed of glucose units only). Secondly, hemicelluloses are in contrast to the strictly linear structure of cellulose as they are mainly branched molecules. Thirdly, the degree of polymerization of hemicellulose is 10-100 times lower than cellulose.

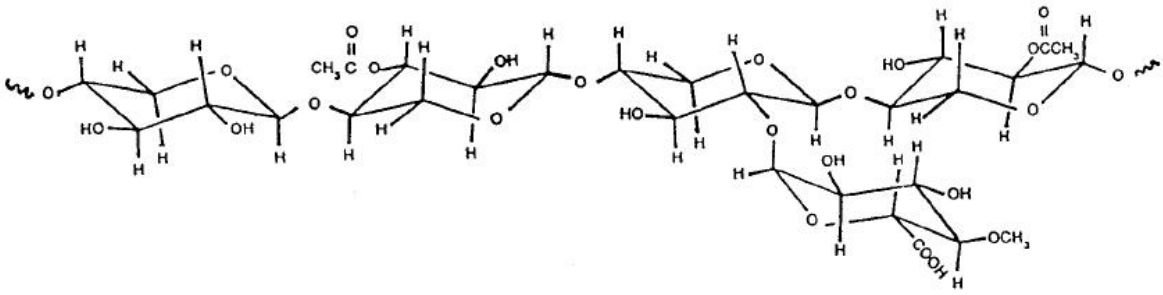

Figure 2.7: Schematic diagram of a representative section of the molecular structure of hemicellulose [5].

Lignin

Together with hemicellulose, lignin serves as a matrix for the embedded cellulose fibres. Lignins in fibres are complex hydrocarbon polymers with both aliphatic and aromatic constituents, forming an insoluble three dimensional network. Apart from forming the matrix in the secondary cell wall of plant fibres, lignin also acts as a water barrier, decreasing the permeation of water through the cell wall. Both the inferior mechanical properties of lignin (E = 4 GPa [5]) compared to cellulose (E = 70-135 GPa [5]) and the need to remove water through the cell walls of technical fibres during drying, make the removal of lignin from technical fibres desirable.

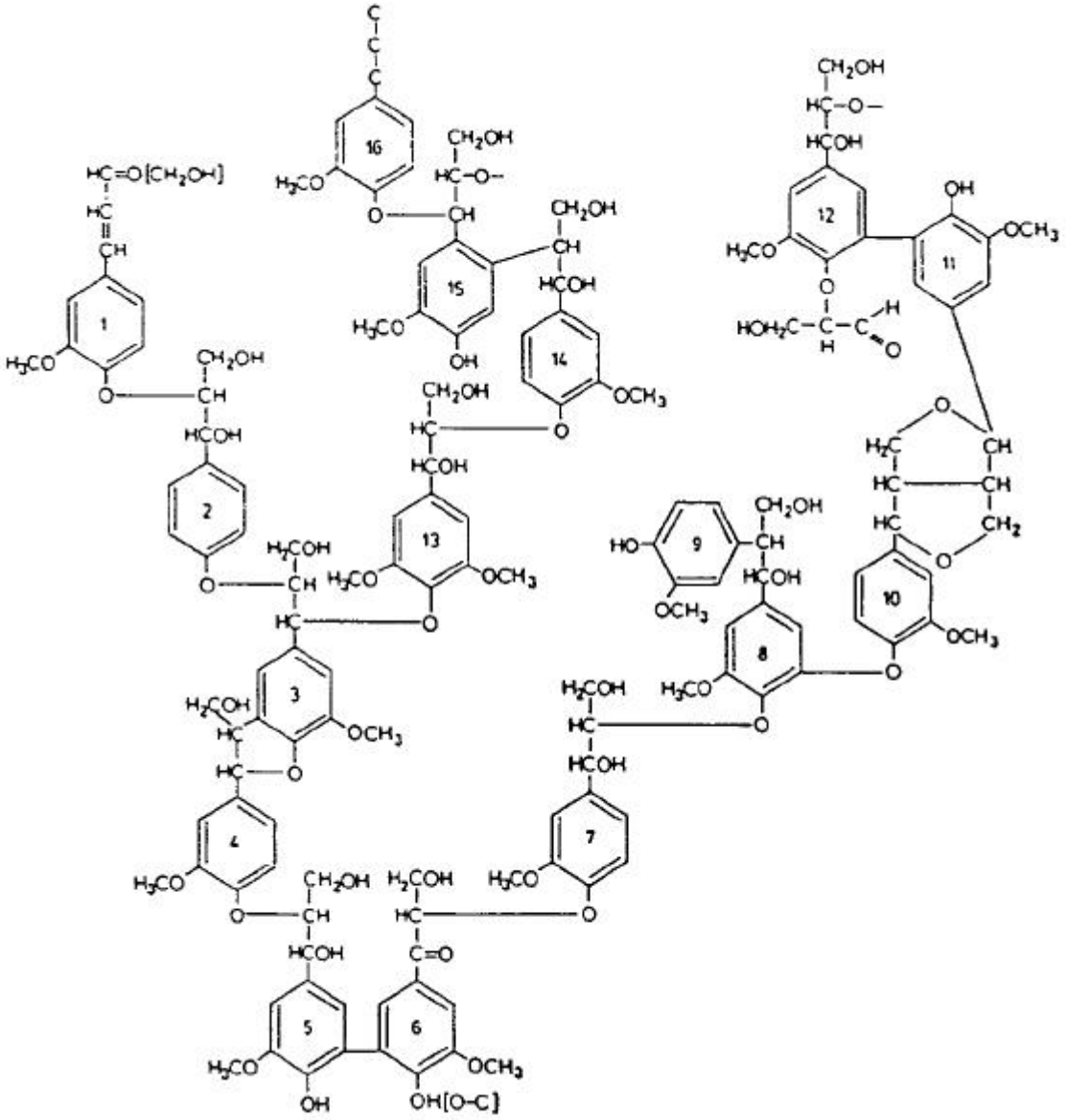

Figure 2.8: Schematic diagram of a representative section of the molecular structure of lignin [14].

Pectin

Pectins can be found in the primary cell wall and represent the major component of the middle lamella. According to Willats *et al*. [15] the very general biochemical definition of pectin is “a group of polysaccharides that are rich in galacturonic acid (GalA)”, highlighting its highly variable chemical structure. The exact biochemical structure is currently not completely understood, but the three major constituents of pectin are homogalacturonan (HGA), rhamnogalacturonan-I

(RG-I) and rhamnogalacturonan-II (RG-II), which are believed to be covalently linked throughout the primary cell wall and middle lamella to form a complex pectin network [15].

HGA is a linear homopolymer of (1→4)-α-linked-D-galacturonic acid and is thought to contain some 100–200 GalA residues [16, 17]. In addition to HGA, an acidic pectic domain consisting of as many as 100 repeats of the disaccharide (1→2)-α-L-rhamnose-(1→4)-α-D-galacturonic acid has been isolated from a wide range of plants and is known as RG-I [18, 19] . RG-I is abundant and heterogeneous and generally thought to be glycosidically attached to HGA domains. In most cases, 20–80% of rhamnose residues in RG-I are substituted at C-4 with side chains in which neutral residues predominate and these can vary in size from a single glycosyl residue to 50 or more, resulting in a large and highly variable family of polysaccharides [18]. The highly branched nature of RG-I has led to it being known as the hairy region of pectin, in contrast to HGA domains which are known as the smooth region [20]. Despite its name, RG-II is not structurally related to RG-I but is a branched pectic domain containing an HGA backbone. RG-II has a backbone of around 9 GalA residues that are (1→4)-α-linked and is substituted by 4 heteropolymeric side chains of known and consistent lengths [19, 21]. The side chains contain eleven different sugars including apiose, aceric acid and 2-keto-3-deoxy-Dmanno- octulosonic acid (KDO) [19, 21]. RG-II appears to be the only major pectic domain that does not have significant structural diversity or modulation of its fine structure [15]. Figure 2.9 presents a highly schematic diagram of the structure of HGA, RG-I and RG-II and lists the major potential variations within their fine structure.

Common nomenclature for pectic substances refers to the amount of methyl esterified galacturonic acid units and involves the following three classifications:

- ≥ 50% high methoxy pectin
- ≤ 50% low methoxy pectin
- ≤ 10% pectic acid / pectate

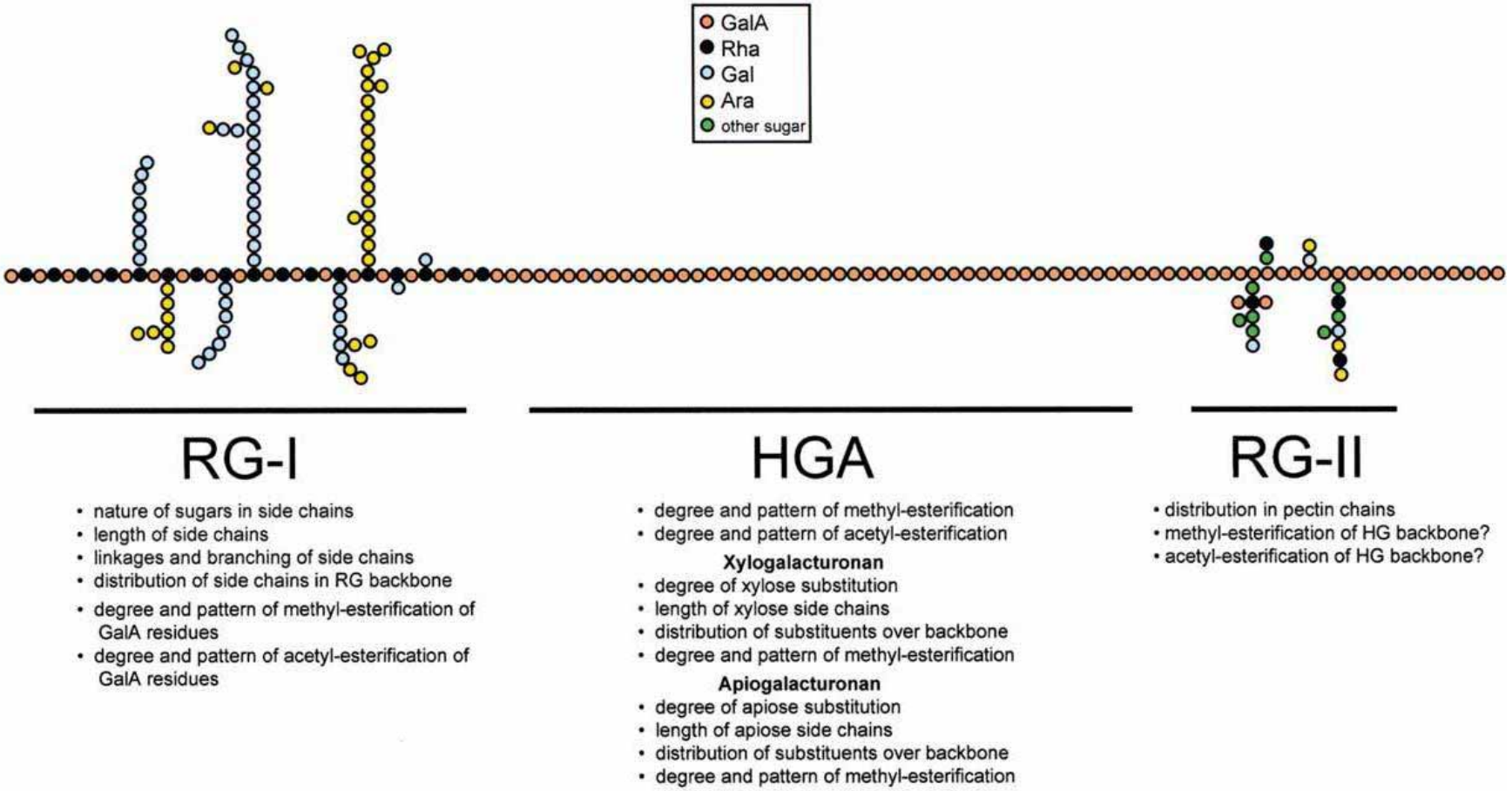

Figure 2.9: Simplified schematic diagram to indicate some of the features of the three major polysaccharide domains of pectin:
homogalacturonan (HGA), rhamnogalacturonan-I (RG-I) and rhamnogalacturonan-II (RG-II). Both RG-I and RG-II are thought to be covalently attached to HGA domains but at present there is no evidence for a direct linkage between RG-I and RG-II. Listed beneath each schematic representation are some of the important ways in which the fine structure of the domains can vary (from [15]).

2.4 Processing of cellulose fibres

All treatments applied to natural fibres for composite applications have the following common goals:

- Improvement of mechanical properties;
- Improvement of composite properties by increasing interfacial strength;
- Reduction of water absorption; and
- Increased uniformity of natural fibres.

The increase of mechanical properties is mainly achieved by removal of mechanically inferior components such as waxes, pectin, hemicellulose and lignin. Other treatments also focus on improvement of the mechanical properties by changing the cellulose fraction structurally. A small microfibril angle and high crystallinity are desirable. The interfacial strength can be improved by the introduction of coupling agents, the creation of bonding sites at the fibre surface or general increase of surface roughness. While any of these treatments may decrease the mechanical properties of the pure natural fibre, the overall aim is to improve the properties of the final composite.

Common industrial applications for these purposes include mercerization in sodium hydroxide solution [5, 22-24], steam explosion [6, 25, 26], extractions with organic solvents and bleaching [5, 27, 28].

Enzymatic retting

The investigation of eco-friendly processing methods is a main point of interest in this work. Enzymes are in use in many industrial applications already, being tailor-made for various applications such as paper and pulp processing, food production and upgrading and textile preparations with good recycling and disposal properties [28-30]. In the context of fibre preparation, the complete or partial removal of non-cellulosic components such as waxes, pectins, hemicelluloses, mineral salts and impurities (eg: machinery and size lubricants) using enzymes is commonly referred to as *Bio-Scouring* or *Bio-Preparation* [29].

Enzymes are proteins for which their function is determined by their complex structure. The catalyzed reaction takes place in a small part of the enzyme called the active site, while the rest of the protein acts as scaffolding. Figure 2.10 shows the molecular structure and the mechanism of enzyme activity. During an enzyme catalyzed reaction, the amino acids around the active site attach to the substrate molecule and hold it in position while the reaction takes place. This makes the enzyme specific for one reaction only, as other molecules will not fit into the active site. Factors affecting the rate of enzyme reaction are temperature, pH level, enzyme concentration and substrate concentration.

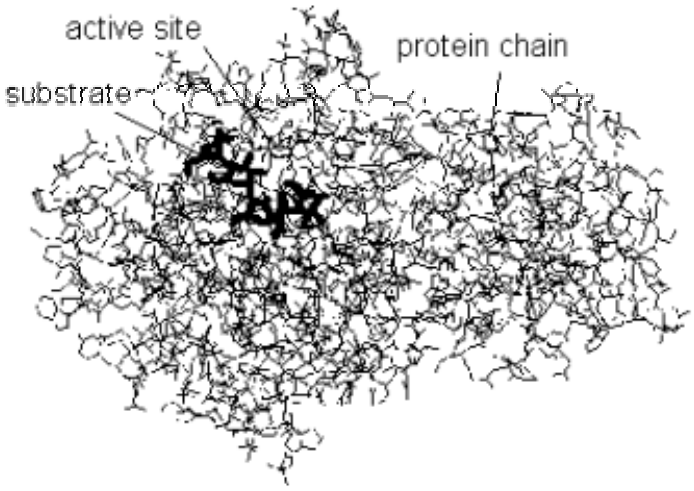

(a)

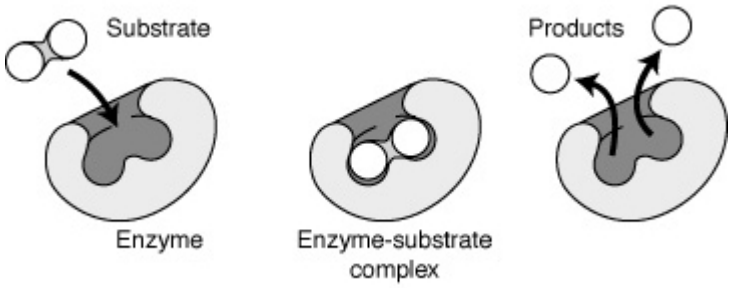

(b)

Figure 2.10: Molecular enzyme structure (a) and mechanism of enzyme activity (b) [31].

Enzymes work best at an optimum temperature. Up to the optimum temperature the reaction rate increases with temperature because the enzyme and substrate molecules both have more kinetic energy and thus collide more often. Also more molecules have sufficient energy to overcome the activation energy of the catalysed reaction. Above the optimum temperature denaturation of the enzyme structure begins as structural bonds are broken down. Due to the above described mechanism of enzyme activity, the enzyme loses its shape and thereby its functionality.

Similarly, an optimum pH exists for each enzyme. The pH affects the charge of the amino acids at the active site; hence, with varying pH the properties of the active site change and the substrate can no longer bind. Additionally at extreme pH values the tertiary structure may change, resulting in enzyme denaturation.

Both enzyme and substrate concentrations can become rate-limiting if supplied in amounts inferior to those necessary for the maximum reaction rate determined by the reaction's kinetics. Further positive or negative influences on enzyme activity can be exerted by coenzymes or inhibitors.

In order to achieve the desired defibrillation in natural fibres, different enzyme systems have been developed and tested [32-36]. It has been found, that the degradation of the pectin layers by pectinases is essential for the enzymatic preparation of technical natural fibres as pectin makes up both the outer covering layers of the fibre and great parts of the interior amorphous layers that connect the fibrils; especially polygalactorunase activity is believed to play a fundamental role during the retting process [33, 37].

Different enzymes are classified according to the major mechanism catalyzing the respective reactions. As all enzymes used for this work exhibit pectolytic activities, these shall be introduced in more detail.

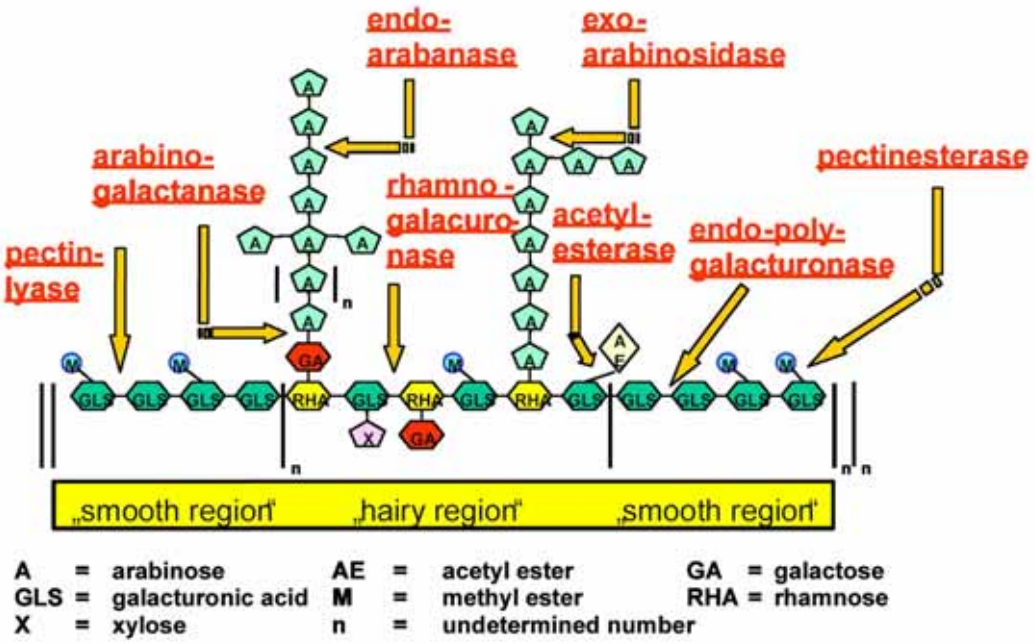

Figure 2.11: Enzymes suitable for pectin degradation and the specific region of attack within the pectin molecule [38].

Figure 2.11 gives an overview of enzymes that attack the pectin molecule in different regions. All enzymes chosen for this work are specific on the main galactose chain, they are polygalactorunase, pectate and pectin layse and pectin esterase:

1. *Polygalacturonases* (PGases) are the pectinolytic enzymes that catalyze the hydrolytic cleavage of the polygalacturonic acid chain with the introduction of water across the oxygen bridge. They are the most extensively studied among the family of pectinolytic enzymes [30]. The PGases involved in the hydrolysis of pectic substances are endo-PGase (E.C. 3.2.1.15) and exo-PGase (E.C. 3.2.1.67). PGases have biological, functional and technical applications in food processing and plant–fungal interactions [30].
2. *Lyases* (or transeliminases) perform non-hydrolytic breakdown of pectates or pectinates, characterized by a trans-eliminative split of the pectic polymer [39]. The lyases break the glycosidic linkages at C-4 and simultaneously eliminate H from C-5, producing a D 4:5 unsaturated

product [30, 40]. Lyases can be classified into following types on the basis of the pattern of action and the substrate acted upon by them.

(I) endopolygalacturonate lyase (EndoPGL, E.C. 4.2.2.2);

(II) exopolygalacturonate lyase (ExoPGL, E.C. 4.2.2.9);

(III) endopolymethylgalacturonate lyase (EndoPMGL, E.C. 4.2.2.10);

(IV) exopolymethylgalacturonate lyase (ExoPMGL).

The reactions catalyzed by lyases can be illustrated as follows [30]:

$$\begin{aligned}&\text{polygalactorunate} \xrightarrow{\text{PGL}} \Delta 4:5 \text{ unsaturated galactorunates}\\ &\text{polymethylgalacturonate} \xrightarrow{\text{PMGL}} \text{unsaturated methyloligogalacturonates}\end{aligned} \qquad (2.1)$$

3. *Pectinesterase* (PE, Pectin pectlylhydrolase, E.C.3.1.1.11), often referred to as pectinmethylesterase, pectase, pectin methoxylase, pectin demethoxylase and pectolipase, is a carboxylic acid esterase and belongs to the hydrolase group of enzymes [41]. It catalyzes the deesterification of methyl ester linkages of galacturonan backbone of pectic substances to release acidic pectins and methanol [42]. The resulting pectin is then acted upon by polygalacturonases and lyases [43]. The mode of action of PE varies according to its origin. Fungal PEs act by a multi-chain mechanism, removing the methyl groups at random. In contrast, plant PEs tend to act either at the non-reducing end or next to a free carboxyl group, and proceed along the molecule by a single chain mechanism [30]. The reaction catalyzed by PE can be represented as follows:

$$\text{pectin} + n\text{H}_2\text{O} \xrightarrow{\text{PE}} \text{pectate} + n\text{C}_2\text{H}_5\text{OH} \qquad (2.2)$$

The main patterns of action as described above are also displayed in Figure 2.12.

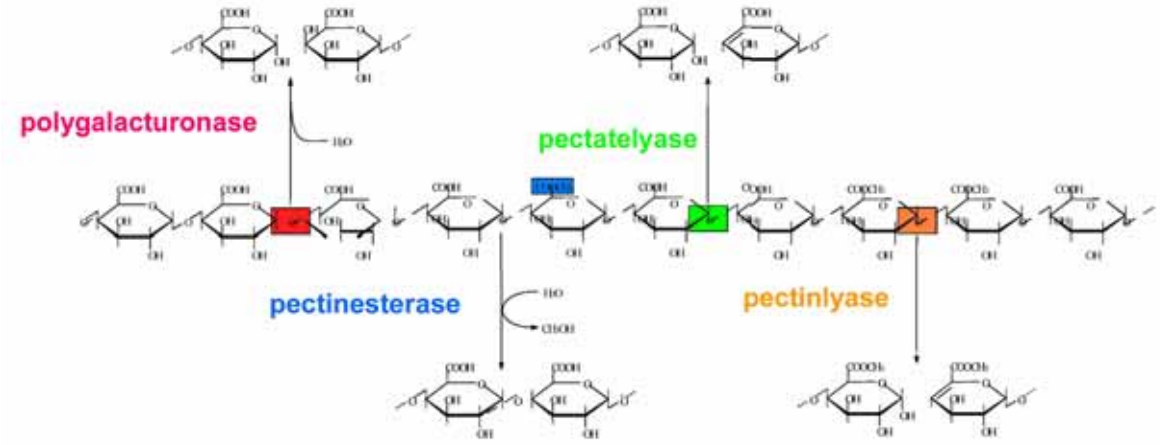

Figure 2.12: Mechanisms of pectin degradation observed for the four different enzyme classes investigated [38]

Assay for enzyme activity

For each enzyme the different activities, *e.g.* with respect to the pectolytic activites as described above, can be assessed by enzyme assays. Although the activity of an enzyme regarding its main activity can usually be found in the accompanying product sheet, it is advisable to carry out independent assays for two reasons. First of all a comparison between different enzymes is only possible if the same activity is given for each enzyme which is not usually the case. Secondly the activity of a specific enzyme can change dramatically with conditions such as pH or temperature and also looses activity with time (*i.e.* several months).

All enzymes used in this work were analysed with respect to pectinesterase and polygalactorunase.

Alkalization

Alkaline treatment is widely applied to cotton and other natural fibres at different concentrations of NaOH for textile applications (mercerization). The effects of alkaline treatment show a strong dependency on concentration, treatment time and temperature as well as shrinkage allowed during treatment, [9]. The fibre structure and hence the mechanical properties of cellulose fibres are influenced by alkaline treatment. Changes in composition [23, 44], crystallinity [24, 44-46], orientation [9, 23], degree of polymerization [45] and type of cellulose [23,

24, 44, 45] have been observed and can lead towards both increase and decrease of the mechanical properties [9, 22-24, 44, 45, 47-51].

Acetylation

The acetylation reaction involves the generation of acetic acid as a by-product which must be removed from the lignocellulosic material before the fibre is used (Figure 2.13). Chemical modification with acetic anhydride involves the introduction of the acetyl group into organic combinations, which contain -OH, -SN, or -NH_2 groups. Through these modifications the cell wall polymers become more hydrophobic [52] and it is consequently applied to enhance hydrophobicity and thereby adhesion with other hydrophobic polymers (eg: thermoplastics), water absorption and biological resistance to decay of the degradable product during use [5, 52, 53].

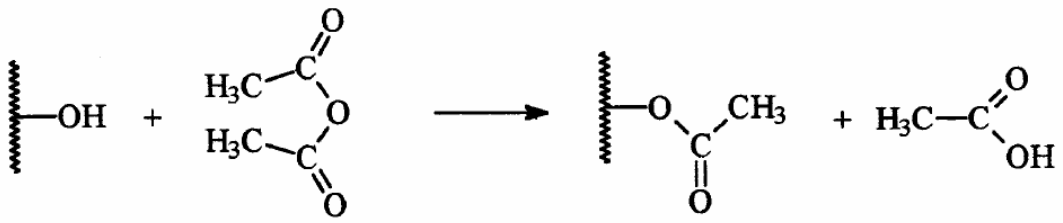

Figure 2.13: Reaction scheme of acetylation [52].

2.5 Analytical methods

Various methods have been applied in order to characterize the treated hemp fibres. For the investigation of fibre structure and fracture behaviour, optical microscopy (OM) and scanning electron microscopy (SEM) have been employed. Both strength and stiffness of treated material can be measured by tensile testing. Fourier Transform Infrared Spectroscopy (FTIR) can serve to give an even deeper insight into the fibres' structure. FTIR allows identification of main components and content and chemical structure (*e. g.* degree of methylesterification and crystallinity of the cellulose regions). In the second part of the project three-point bending tests and dynamic mechanical analysis (DMA) were used to characterise the mechanical properties of the composites. Along with the atomic force

microscopy technique (AFM) employed to identify possible correlations between fibre and composite properties, the more complex techniques FTIR and DMA will be described in greater detail in the following sections.

2.5.1 Fourier Transform Infrared Technique

The basis of Fourier transform infrared (FT-IR) spectroscopy is the two-beam Michelson interferometer as shown schematically in Figure 2.14 A. Broadband infrared radiation is emitted by a thermal source (globar, metal strips, Nernst glower) and falls onto a beam splitter which, in the ideal case, transmits half the radiation and reflects the other half. The reflected half, after traversing a distance *L*, falls onto a fixed mirror M1. The radiation is reflected by M1 and, after traversing back along distance *L*, falls onto the beam splitter again. The transmitted radiation follows a similar path and also traverses distance *L*; however, the mirror M2 of the interferometer can be moved very precisely along the optical axis by an additional distance *x*. Hence, the total path length of the transmitted radiation is 2 (*L* + *x*). On recombination at the beam splitter the two beams possess an optical path difference of D = 2 *x*. Since they are spatially coherent, the two beams interfere on recombination. The beam, modulated by movement of the mirror, leaves the interferometer, passes through the sample cell and is finally focussed on the detector. The signal registered by the detector, the interferogram, is thus the radiation intensity *I* (*x*), measured as a function of the displacement *x* of the moving mirror M2 from the distance *L* (Figure 2.14 B). The mathematical transformation, a Fourier transform, of the interferogram, performed by computer, initially provides a so-called single-beam spectrum. This is compared with a reference spectrum measured without the sample to obtain a spectrum analogous to that measured by conventional dispersive methods (Figure 2.14 C).

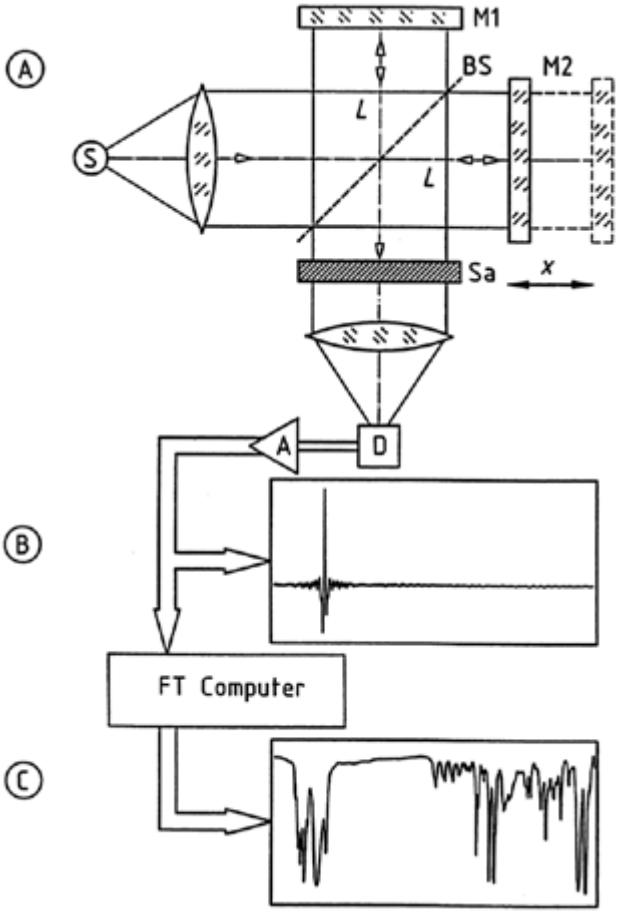

Figure 2.14: Recording of a Fourier transformed interferogram

A) Schematic diagram of a Michelson interferometer;

B) Signal registered by the detector D, the interferogram;

C) Spectrum obtained by Fourier transform (FT) of the interferogram

S = Radiation source; Sa = Sample cell; D = Detector; A = Amplifier; M1 = Fixed mirror; M2 = Movable mirror; BS = Beam splitter; *x* = Mirror displacement

In comparison with conventional spectroscopy, the FT-IR method possesses significant advantages. In an FT-IR spectrometer, all frequencies emitted by the IR source reach the detector simultaneously, which results in a large signal-to-noise ratio advantage over dispersive instruments. Furthermore, the measuring time is only determined by the time required to move the mirror M2 the distance necessary to give the desired resolution. In an FT spectrum, the accuracy of each wavenumber is coupled to the accuracy with which the position of the moving mirror is determined; by using an auxiliary HeNe laser interferometer the position of the mirror can be determined to an accuracy better than 0.005 µm. This means that the wavenumbers of an FT-IR spectrum can be determined with high accuracy (< 0.01 cm^{-1}).

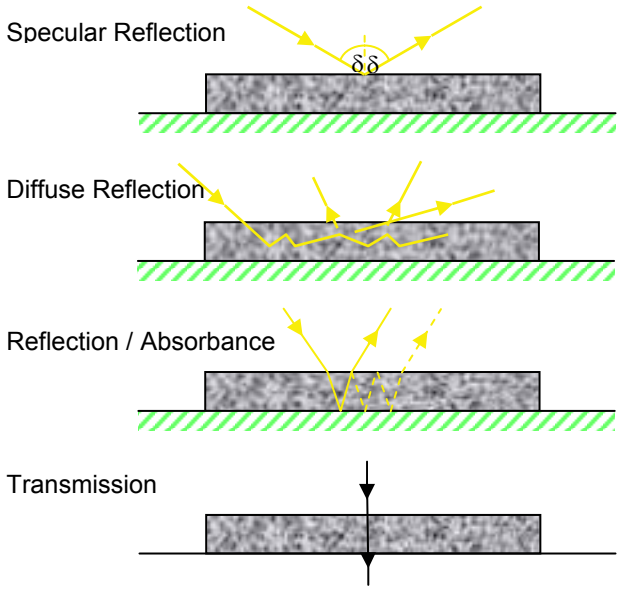

Figure 2.15: Optical diagram for commonly used infrared sampling techniques, [54].

There are several infrared sampling techniques commonly used. Diagrams of these techniques are shown in Figure 2.15.

Transmission spectroscopy was used for all measurements of the submitted work. For this technique solid materials are grinded and afterwards pressed with infrared inactive KBr to form thin pellets. The sample is placed in the beam of the infrared spectrometer, and the intensity of the incident beam is compared with that transmitted by the sample. As the absorption of radiation is a function of transmittance, parameters that can be determined in transmission spectroscopy are the thickness or the concentration of the sample. It is therefore applicable for quantitative analysis.

2.5.2 Dynamic Mechanical Analysis

Dynamic mechanical analysis (DMA) is employed to characterize the elastic behaviour of materials with respect to temperature and frequency. The results from DMA can give information about molecular structure. A dynamic mechanical analyzer consists of two main parts: a unit that applies and measures static or sinusoidal loads and a second unit that controls and measures the sample temperature, Figure 2.16.

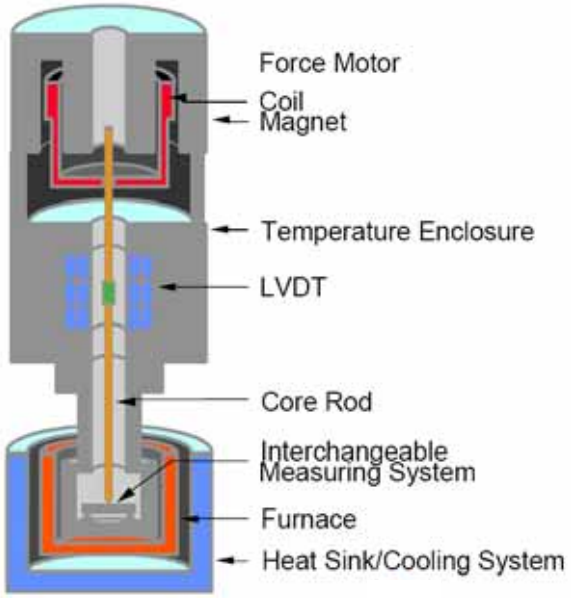

Figure 2.16: Structure of a dynamic mechanical analyzer, [55].

The mechanic response of a material to an externally applied load can be elastic, viscous or viscous-elastic. In the case of elastic behaviour, the application of a load results in an immediate and proportional strain response. A sinusoidal stress therefore results in a sinusoidal strain both in phase with each other (Figure 2.17 (b)). Viscous material on the other hand is defined as behaviour that shows proportionality between stress and strain rate, which is the first derivative of the strain, Figure 2.17 (c). Combination of both materials can be written as a response with phase lag or angle δ. $0 \le \delta \le \pi/2$ limits the phase lag with 0 the elastic and $\pi/2$ the viscous extreme. The resulting equation can be written as:

$$\varepsilon(t) = \varepsilon_0 \sin(\omega t + \delta) \qquad (2.3)$$

Separation into in-phase and out-of-phase strains leads to curves like those in Figure 2.17 (b) and (c), respectively. This can be expressed as a complex strain:

$$\varepsilon^* = \varepsilon' + i\varepsilon'' \qquad (2.4)$$

With equations for stress and strain, these quantities can now be written in terms of a complex elastic modulus for which the real part is known as the storage modulus (E') while the imaginary part is referred to as the loss modulus (E") [56].

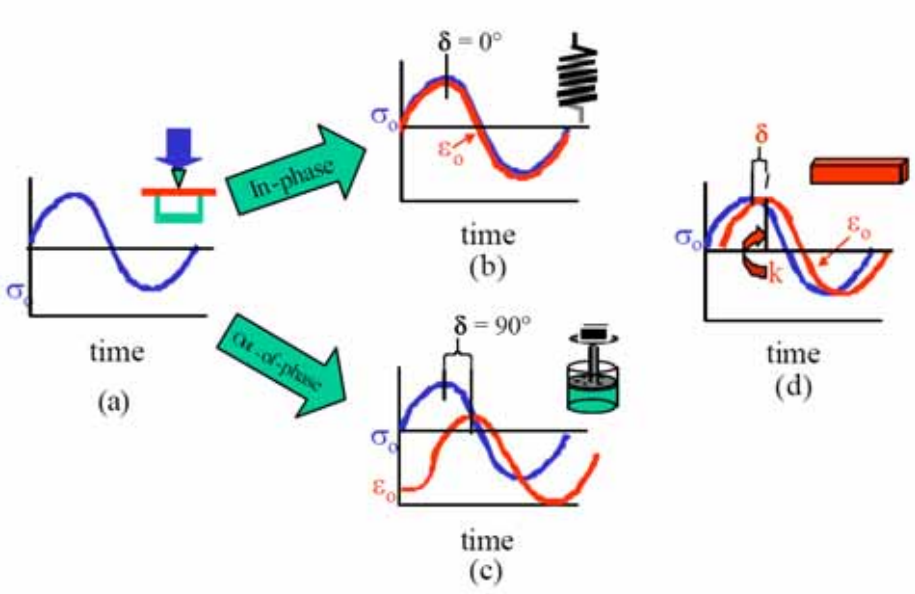

Figure 2.17: Material response to stress, [56].

The ratio of the loss modulus and storage modulus is also the tangent of the phase angle and is called the damping factor:

$$\text{Damping} = \tan\delta = E''/E' \qquad (2.5)$$

Damping is a dimensionless property and is a measure of how well the material can disperse energy [56]. These properties are dependant on frequency, which is why the dynamic tests are conducted at different frequencies as well as over a wide temperature range. The DMA used for this project features a specific program using the superposition of chosen frequencies, so that all frequencies can be measured within one heating cycle. An illustration of the artificial oscillation used is given in Figure 2.18.

The DMA uses the presented basic relations to examine the material's behaviour at different temperatures. As molecular differences and transitions result in detectable peaks or gradient changes in the plots of E', E'' or $\tan\delta$, DMA can be used to detect a wide range of material properties.

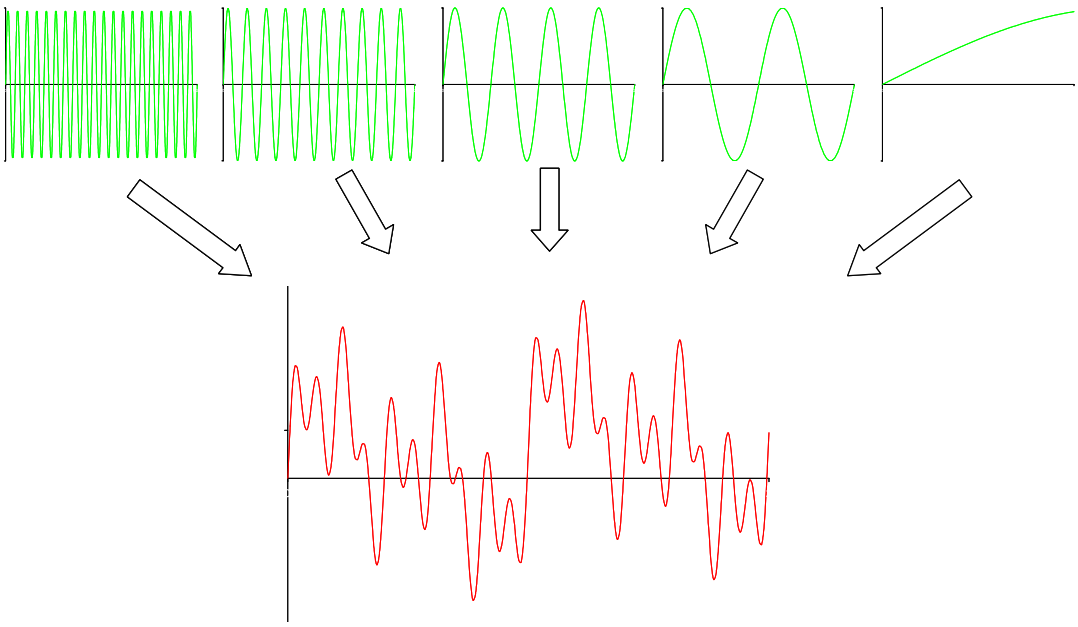

Figure 2.18: Superposition of frequencies (0.1, 1, 2, 5, 10 Hz) for simultaneous testing.

2.5.3 Atomic Force Microscopy

The atomic force microscope (AFM) is known for its high resolution imaging capabilities, facilitating the investigation of single molecules and structures on the molecular level [57]. Moreover, it can be used for sensitive force measurements.

The main part of an AFM is the cantilever with a specialized tip on its end. The AFM tip is able to probe an extremely small interaction area (using a tip radius in the range of 5-50 nanometers), and this gives it a high sensitivity to small forces. The forces can be measured at the cantilever which acts as a soft spring, Figure 2.19. The cantilevers are usually silicon or silicon nitride beams, 100-200 microns long, and allow forces in the pico-Newton range to be measured [57]. The order of magnitude of forces correspond with those that are required to separate receptors from ligands or to break a single hydrogen bond [57].

In AFM imaging modes, the cantilever is usually scanned over the surface to produce a three dimensional image of the surface. In AFM “force spectroscopy” experiments, the cantilever and tip are moved directly towards the sample until they are in contact with it, and then retracted again, while the interaction between the tip and sample is measured. This may then be repeated at different locations

to build up a map of the tip-surface interaction, or can be repeated at the same point to give a full statistical understanding of the interaction.

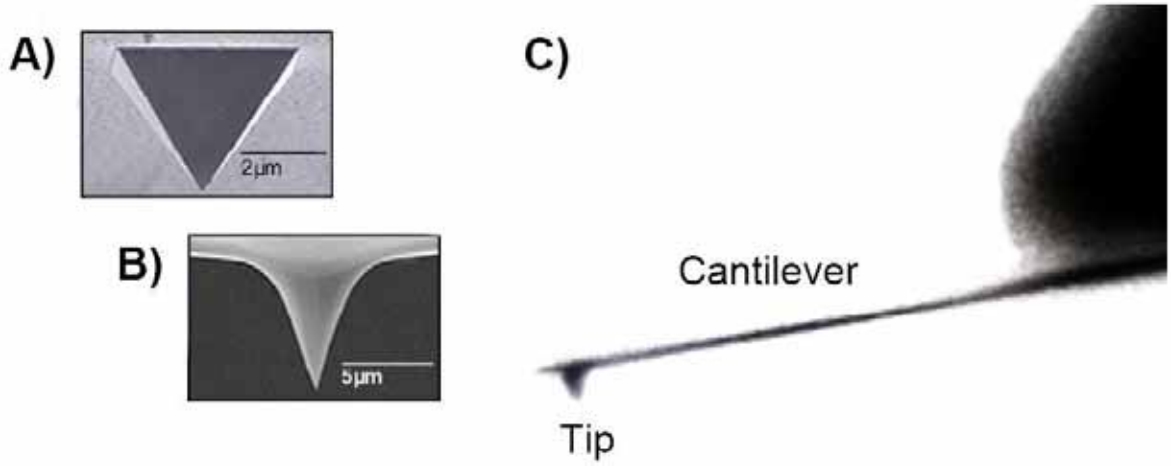

Figure 2.19: Scanning electron microscopy images of typical pyramidal (A) and cone-shaped (B) AFM tips and an optical microscope image of an AFM cantilever and tip (C) [57].

The schematic diagram in Figure 2.20 shows the movement of the cantilever and tip during the force spectroscopy experiment – approaching and then retracting from the sample. The image series reflects different points in the approach and retract cycle, the lateral position of the cantilever is usually constant.

Table 2.4 gives a summary of interactions that have been measured using the atomic force microscope.

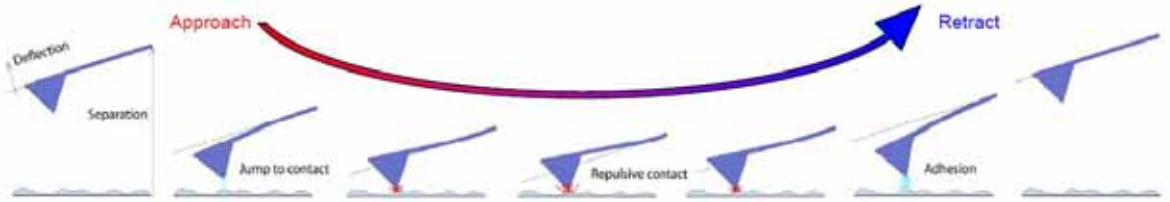

Figure 2.20: Schematic diagram of the vertical tip movement during the approach and retract parts of a force spectroscopy experiment [57]

Approach	
Tip far away (10 - 100 microns)	No interaction
Tip approaching (few microns)	• Electrostatic forces Long-range interactions from adsorbed molecules, e.g. polymer brush
Tip close to surface (nanometers to atomic distances)	• Van der Waals • Capillary forces (in air) • DLVO/screened electrostatics (in aqueous solutions) • Chemical potential • Magnetic • Solvation forces (water layering) 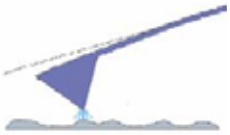
Contact	
Tip indenting sample	• Stiffness (Young's modulus, elastic response) • Viscoelastic response (variable rates or indentation depth) Measurement of active forces (e.g. generated by cells) 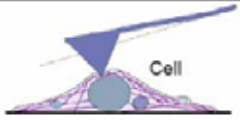
Retract	
Tip lifting off surface (few atomic distances to nanometers)	Adhesion: • Non-specific (including chemical affinity, surface coatings) • Ligand-receptor (e.g. antibody-antigen) • DNA hybridisation (e.g. matched or mismatched pairs) • Cell surface interactions 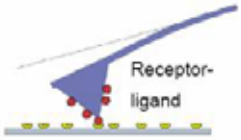
Tip further away (nanometers to hundreds of nanometers)	Stretched molecules between tip and surface: • Protein unfolding, pulling out of membranes • Entropic elasticity • DNA stiffness, structural transitions and "melting" • Other conformational changes in stretched molecules, e.g. chair-to-boat transition in sugar rings Other stretched attachments e.g. membrane tethers formed on cells 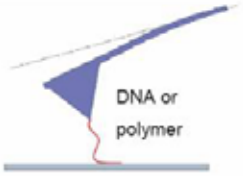
Tip far from surface (1-5 microns)	Connections broken between the tip and surface, no further interaction. Adhesion strength can be measured between attached molecules and the surface when the attachments break.

Table 2.4: Overview of some of the interactions measured at different points during a force spectroscopy cycle.

The results recorded during AFM spectroscopy are usually displayed as force curves, plotting the height position of the cantilever during the spectroscopic cycle on the x-axis and the corresponding interaction force on the y-axis.

However, the force curve does not represent the raw data. Three steps are necessary to convert the raw data into the height position and interaction force values plotted in the force curves. In order to understand the employed conversions, a basic knowledge of the actually performed measurements within the AFM are necessary and shall be given before the summarizing the data manipulation:

As the cantilever is moved towards and from the surface, its deflection can be measured by an optical beam deflection setup which delivers a proportional electrical signal (in Volts, as the signal from the photodiode). The example shown in Figure 2.21 (a) reflects a typical interaction for an uncoated cantilever in air approaching a hard, incompressible hydrophilic surface such as glass or mica. Approach (red) and retract (blue) curves are both plotted on the same axes. As the cantilever approaches the surface, initially the forces are too small to give a measurable deflection of the cantilever, and the cantilever remains in its undisturbed position. At some tip-sample distance, the attractive forces (usually Van der Waals, and capillary forces in air) overcome the cantilever spring constant and the tip jumps into contact with the surface. Once the tip is in contact with the sample, it remains on the surface as the separation between the base of the cantilever and the sample decreases further, causing a deflection of the cantilever and an increase in the repulsive contact force. As the cantilever is retracted from the surface, often the tip remains in contact with the surface due to some adhesion and the cantilever is deflected downwards.

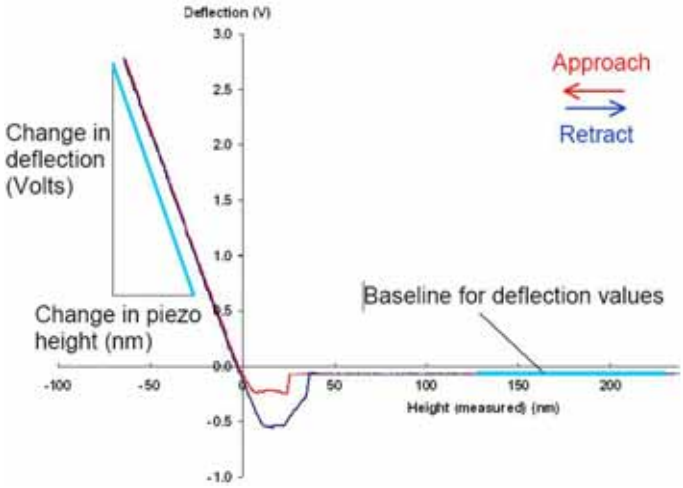

(a)

Plot of approach (red) and retract (blue) curves in water. The gradient chosen for sensitivity measurements and the baseline offset for the deflection are both marked on this plot.

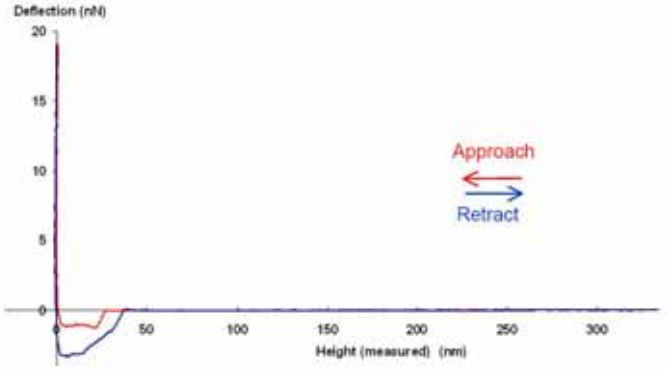

(b)

Force-separation (corrected height) plot (force curve) for the data shown in (a).

Figure 2.21: Originally recorded and converted data (force curve) [57].

The calibration and conversion steps involved in the preparation of force curves are as follows:

- Calibration of cantilever deflection (y-axis)

The deflection of the cantilever spring is directly proportional to the tip-sample interaction force, but there are two measurements required to convert the photodetector signal into a quantitative value of force. The first stage is to calibrate the distance that the cantilever actually deflects for a certain measured change in

photodetector voltage. This value depends on type of cantilever, but also on the optical path of the AFM detection laser, and will be slightly different each time the cantilever is mounted in the instrument. Once the deflection of the cantilever is known as a distance, *x*, the spring constant, *k*, is needed to convert this value into a force *F*, using the well-known Hooke's law:

$$k \cdot x = F \qquad (2.6)$$

A force curve between a plain cantilever tip and a bare hard substrate is used to determine the sensitivity of the experimental setup. This is a measurement of the deflection of the tip in nanometers for a given movement of the detection laser on the photodetector. The repulsive contact region, where the deflection rises steeply upwards, is linear for a hard surface and tip. Therefore the software can easily determine the factor for converting Volts into nanometers. This measurement can then be used for calibrating the applied forces when the samples of interest are investigated.

When the cantilever is far from the surface, the interaction forces are virtually zero (the flat part of the curve on the right hand side in Figure 4). This offset (which may be due to the initial settings of the equipment, or to thermal drift) should be subtracted from all the deflection data in order to calculate the true interaction force. The baseline value is also marked in Figure 4.

- Cantilever spring constant calibration (y-axis)

For quantitative force measurement, the spring constant of the cantilever must be calibrated, so that the nanometers deflection of the cantilever can be converted into actual force values. There are various different ways of calibrating spring constants of cantilevers, *e.g.* calculation from the cantilever geometry, measurement using a reference cantilever, measurement using the thermal noise method.

The latter calibration method, which was employed in this work, is based on fluctuations in the environment (in air or fluid) that constantly provide small force impulses, as can be seen for example in the diffusion of small particles (Brownian motion). Soft cantilevers are susceptible to thermal fluctuations, and the AFM can be used to measure and analyse the movements. The thermal noise spectrum is a

plot of the cantilever fluctuations as a function of frequency; on average the greatest amplitude will be seen around the cantilever resonance frequency. An example is shown in Figure 2.22.

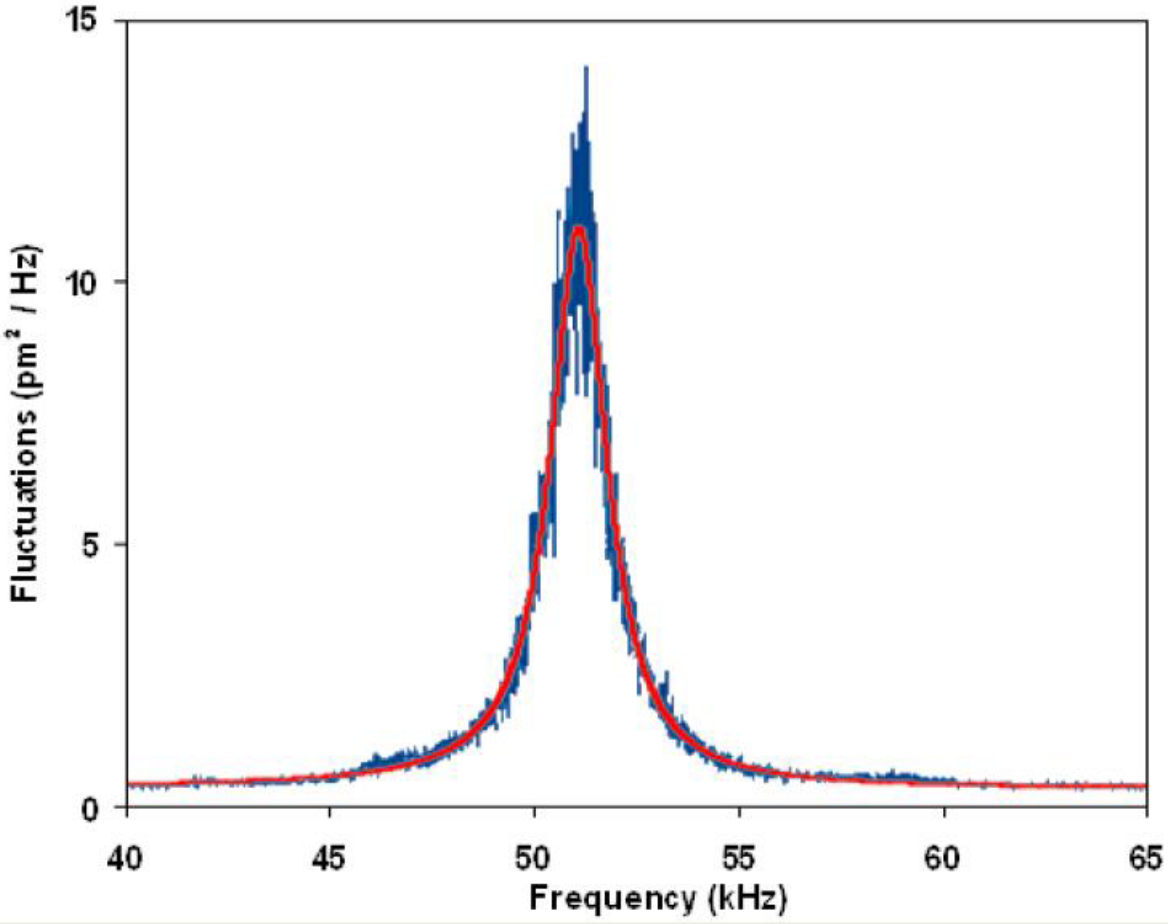

Figure 2.22: Thermal noise measurement of a contact mode cantilever in air. The blue line represents the measured resonance peak with the Lorentz fit (red) [57].

The amplitude of the fluctuations for a given temperature depends only on the spring constant of the cantilever [58]. The thermal resonance curve can therefore be fitted to a Lorentz function, which allows calculation of the spring constant. This method has the advantage that it can be done in-situ with software analysis.

When the deflection of the cantilever is known as a distance in units of length then this is simply converted to a value of force. The deflection (in meters) is multiplied by the by the spring constant of the cantilever (in N/m) to give a force in Newtons.

- Calculation of tip-sample separation (x-axis)

So far, all the conversion has been in the y-axis, or deflection/force values. However, there is also a conversion needed for the height, or x-axis values. The change in piezo height has been used for the distance between the tip and the sample, but in fact this must be corrected for the deflection of the cantilever. If the cantilever deflects towards the sample, for example, then the separation between the tip and the surface will be less than expected from the piezo position alone. Since the cantilever deflection and position are available in the same units, this can be easily corrected by subtracting the cantilever deflection from the piezo height. This conversion leads to the gradient of the steep upwards part of the curve becoming vertical. Once the tip is in contact with the surface, the tip-sample separation remains at zero while the force is increased by the cantilever pushing towards the surface. An example of the final converted curve is shown in Figure 2.21 (b). Here the x-axis is plotted as the actual tip-sample separation, rather than the piezo movement and the deflection values are now displayed in units of force.

Atomic force microscopy as tool for fibre and composite characterization

As already described in Chapter 2.1 one of the main objectives of the treatments of natural fibres prior to composite preparation is the enhancement of fibre-matrix compatibility and consequently the strength of the fibre-matrix interface. The interfacial strength is greatly reduced by the different polarity of cellulose and most thermoplastics [59]; while the latter are non-polar, cellulose is generally polar due to the presence of hydroxyl groups. Several routines, such as silanization [49, 59, 60] or acetylation [52, 53, 59-63], have been developed and successfully employed to overcome this problem by reducing the number of polar groups on the fibre surface. However, the assessment of the effect of such treatments on interfacial bond strength has so far only been measured by single fibre pull-out tests and mechanical characterization of the final composite properties (*e.g.* flexural or tensile strength and fracture surface morphology). It would be highly desirable to develop a technique that could directly correlate fibre surface properties to final composite properties so that we can develop a better

understanding of the factors that control the interfacial strength and hence help to optimise fibre treatments so the true potential of natural fibres might be realised.

The AFM represents a versatile ensemble of techniques that are highly suitable for the characterization of natural fibres. Information regarding intermolecular forces, nano-mechanical properties, and surface wetting characteristics can be obtained through the analysis of the appropriate regions of the force curve.

When AFM is conducted under atmospheric conditions, a liquid bridge may form between the tip and sample due to capillary condensation, resulting in a meniscus force that dominates the observed adhesion [64-69]. Due to the extremely sharp geometry of AFM tips, with nominal radii on the order of 10's of nm, the thickness of the liquid bridge is 10's of molecular layers and represents an extremely local assessment of the wettability of the surface. In the absence of a liquid bridge, the adhesion between the tip and sample will be affected by the surface energy of the tip and substrate, primarily through attractive van der Waals interactions between the two materials [70, 71]. Therefore, under atmospheric conditions, it is expected that the AFM adhesion force result from a combination of these two phenomena.

A number of studies indicate that the AFM adhesion force has the power to discriminate between hydrophilic and hydrophobic substrates [64-70, 72]. Recent research was able to relate AFM adhesion on a wide variety of substrates to the surface energy of highly differentiating calibration substrates [73].

In this work variations in the adhesion between the AFM tip and substrate are used to estimate the adhesion force experienced after various fibre treatments and the results of these measurements will be analyzed in the context of the "classical" methods of analysis described above.

3 Experimental

3.1 Enzyme assays

The enzyme assays were carried out according to methods supplied by AB enzymes for pectinesterase and polygalactorunase activity.

Pectinesterase activity [74]

1 PE is defined as the amount of enzyme, which sets free 1 µval acid under the given conditions.

Principle

The method is based on the titration of COOH-groups released during the decomposition of pectin with 0.025M NaOH at constant pH. Application of 0.55% pectin solution leads to a linear decomposition curve for a consumption of up to 1.0 ml 0.025 M NaOH during 3 minutes.

Reagents

- 2 M NaCl solution
- Substrate solution

9.50 g pectin were elutridated in 25 ml ethanol absolut and 800 ml hot deionised water added under continuous stirring. The solution was then stirred for 15 minutes at constant RPM and left in fridge at 10 °C overnight. It was then topped up to 1000 ml with deionised water and 200 ml 2 M NaCl solution. Finally another 600 ml of deionised water was added. The pH was then adjusted with 5 M NaOH.

Method

The samples were dissolved in the range 0.1-3.3 PE ml^{-1} in order to remain within the linear measurement range.

Before starting the analysis the pH-electrode was calibrated in calibration solutions of pH 4, 7 or 10 depending on which two values bracketed the pH of the respective buffer solution of the sample.

In a beaker, 22.5 ml substrate solution was then temperated at 30°C for 5 minutes. The solution was constantly agitated and the pH electrode was immersed.

2.5 ml of sample were then added and the pH adjusted to 4.5 (or 8) within one minute using 0.025 M NaOH. After successful adjustment the reaction time was started and the pH was kept constant for the next 6 minutes by adding NaOH, noting usage after 3 and 6 minutes. Usage (per 3 minutes) should not be under 0.2 ml and should not exceed 1.0 ml to ensure linearity and uniform measurement conditions. The consumption after 3 and 6 minutes was compared and checked for linearity. For a deviation above 10% the enzyme quantity was reduced, if no change in pH was measured the enzyme quantity was increased by a factor of 20.

Evaluation

Pectinesterase activity is defined as the released acid per time and sample weight and consequently the general equation for calculation of PE units is

$$PE \cdot g^{-1} = \frac{val.releasedCOOH \cdot 1000}{time[\text{min}] \cdot weighed\ sample[mg]} \qquad (3.1)$$

1 ml 0.025 M NaOH contains 0.025 mmol NaOH (25 µmol NaOH) which corresponds to 25 µval-COOH.

$$PE \cdot g^{-1} = \frac{usageNaOH[ml] \cdot 25 \cdot 1000}{time[\text{min}] \cdot weighed\ sample[mg]} \qquad (3.2)$$

The procedure was repeated at least five times for each type of enzyme solution.

Spectrophotometric determination of polygalacturonase activity [75]

Polygalacturonase activity is determined as the amount of enzyme which sets free 1µmol galactose by decomposition of potassium pectate within 1 minute at 40°C under standard conditions. The commonly found units and abbreviations corresponding to 1µmol galactose

PGP	Unit of photometric PG-activity
PGP*mg^{-1}	activity concentration
PGU	Unit of PGase activity determined by viscosimetry

PGU / mg = 10 * PGP /mg

Principle

The reducing sugars produced by decomposition of potassium pectate are being transformed by p-hydroxy-benzoic acid-hydrazid into bisbenzol-hydrazin-anions, which are measured photometrically at 412nm.

Reagents

p-hydroxy-benzoic acid-hydrazid was supplied ready by the Department of Plant and Microbiology

- Buffer: Each enzyme was tested in a buffer solution close to its optimum activity pH
- Substrate solution (0.7%): 0.7 g potassium pectate was weighed into a beaker and dissolved in 100 ml boiling deionised water.
- Enzyme solution: Solutions with buffer were prepared so that extinction difference equalled 0.2-0.8 OD.
- Galactose solution: 0.2g galactose were dissolved in 100ml buffer solution

Determination of molar coefficient of extinction

Main value: 250µl buffer solution + 650 µl PAHBAH-solution + 100 µl galactose (concentration x)

Blank value: 350 µl buffer solution + 650 µl PAHBAH solution

After development for 15 minutes at 80°C, the values were measured photometrically at 412nm. The coefficient of extinction was calculated as gradient of extinction differences depending on galactose concentration.

Method

For the determination of the main value 250 µl substrate solution and 100 µl enzyme solution were mixed. After an incubation time of 10 min at 40°C the reaction was stopped by adding 650 µl PAHBAH reagent. Colour development was carried out at 80°C for 15 min and each sample measured photometrically at 412 nm. The absolute extinction was ensured to be below 1 OD in order to keep all samples in the measurement range of the photospectrometer. If a sample

reached a higher absolute extinction the amount of enzyme was reduced accordingly.

For the determination of the blank value 250 µl of substrate solution was mixed with 650 µl PAHBAH reagent and 100 µl enzyme solution was subsequently added. The colour development and measurement was carried out as for the main value.

Scheme of PGU assay:

Step of analysis	Reagent	Main Value	Blank value
basic solution	substrate	250 µl	250 µl
	PAHBAH	↓	650 µl
	enzyme	100 µl	100 µl
		↓	
reaction		10 min at 40°C	
		↓	
stop of reaction	PAHBAH	650 µl	↓
		↓	
colour reaction		15 min at 80°C	
		↓	
measurement		photometry at 412nm	

Evaluation

Calculation of molar coefficient of extinction

$$\varepsilon = \frac{E_{\text{Galactose}}}{c * d} \qquad (3.3)$$

Calculation of activity

$$PGP/mg = \frac{\Delta E \cdot V}{\varepsilon \cdot d \cdot v \cdot t \cdot c} \quad (3.4)$$

The fixed parameters can be summarized as a constant

$$K_1 = \frac{V}{\varepsilon \cdot d \cdot v \cdot t} = 314.8059 \quad (3.5)$$

The final equation for the calculation of PGP can then be written as

$$PGP/mg = \frac{\Delta E}{c} K_1 \quad (3.6)$$

In order to compare PGP with a viscosimetrically determined PGU, a factor of 10 can be applied to obtain an approximation.

$$PGU/mg = 10 \cdot PGP/mg \quad (3.7)$$

All samples were measured in duplicate and after colour development each sample was again halved and thus measured photometrically in duplicate.

3.2 Fibre preparation

3.2.1 Enzyme treatments

The systems and pure enzyme preparations used in this work, were supplied by Novozymes Australia and AB enzymes, Germany.

The enzyme solutions Pectinex® Ultra SP-l, Scourzyme L and BioPrep 3000 (all Novozymes) are commercial enzyme systems tailored for the bio-scouring of cotton fabrics (Scourzyme/BioPrep) [28, 29, 76, 77] and maceration of fruit pulp (Pectinex) [78, 79]. While the first two are essentially an alkaline pectate lyase preparation [76, 77], Pectinex is a polygalactorunase [78]. However, all three enzyme solutions were deliberately designed to feature side activites such other pectinase, hemicellulase or cellulase.

The enzyme provided by AB enzymes on the other hands are essentially pure preparations as listed in Table 3.1.

As introduced in Chapter 2.4, all enzyme solutions possess an optimum temperature at which they have the highest reaction rate. The temperatures are given in Table 3.1. Treatments were always carried out at the optimum temperature which was kept constant by a temperature-controlled water bath. In

order to also maintain a constant optimum pH buffer solutions were used to dissolve and use the enzymes at their optimum pH. The enzymes had to be dissolved and diluted to ensure as much as possible an equal specific activity of each solution as determined by the enzyme assays. As polygalacturonase has been identified as the key component in retting of natural fibres [37], the respective activity (PGU) was used as basis for these dilutions. However, this was only possible for enzymes sharing a common activity and the commercial enzyme mixtures with multiple side activities (BioPrep and Scourzyme) were diluted 1:10 according to their main activity ratio of 300:3000 APSU [76, 77]. The dilutions used are given in Table 3.2. These solutions were then used as a concentrated basis for all other experiments.

Table 3.1: List of enzyme used in this work

Enzyme	**Classification**	**Reaction conditions**		**Supplier**
		pH	Temp.	
Rohament PL	macerizing endo-polygalacturonase	4.5	25 °C	AB enzymes [80]
Rohapect PTE	Pectin lyase	4.5	40 °C	AB enzymes [81]
Rohapect MPE	Pectin methylesterase	5.8	45°C	AB enzymes [82]
EL 2005023	non-macerizing endo-polygalacturonase	4.5	25°C	AB enzymes [83]
Pectinex Ultra SP-L	polygalacturonase	4.5	36 °C	Novozymes [78]
Scourzyme L	alkaline pectate lyase	8.0	60 °C	Novozymes [77]
Bioprep 3000	alkaline pectate lyase	8.0	60 °C	Novozymes [76]

Table 3.2: Dilutions used to produce the basic solutions for the experiments.

Enzyme	*g or ml per 100ml solution*	*pH of buffer solution*
EDTA	0.5 g	4.5
Pectinex	10 ml	4.5
Scourzyme	10 ml	8.0
BioPrep	1 ml	8.0
PL	10.870 g	4.5
EL	0.1586 g	4.5
MPE	0.2381	4.5
PTE	12.85 g	5.8

All treatments were carried out in sealable plastic bags using 50 ml solution to treat approximately 2 g of fibre. At the end of the treatment the enzymes were thermally deactivated in hot water (90-100°C). Most of the enzyme solution was then drained off carefully. Afterwards holes were made into the plastic bags with a thick needle and the fibres were washed with water several times by filling the bags and leaving them to empty via the holes. Subsequently, the wet fibres were transferred onto flexible absorbent paper and pre-dried on suction filter. In a final step the fibres were dried overnight at 60°C in a convection oven. Table 3.3 gives a summary of all enzymatic treatments carried out for this part of the project.

Table 3.3: List of experiments carried out to evaluate the effectiveness of enzymatic treatment on hemp fibre.

Sample No.	Duration [hrs]	Concentration [%]	Buffer pH 4.5	Buffer 5.8	EDTA	Pectinex	Scourzyme	BioPrep	PL	EL	MPE	PTE
1	1		X									
2	1			X								
3	1				X							
4	1	0.5				X						
5	1	5				X						
6	1	0.5					X					
7	1	5					X					
8	1	0.5						X				
9	1	5						X				
10	1	0.5							X			
11	1	5							X			
12	1	0.5								X		
13	1	5								X		
14	1	0.5									X	
15	1	5									X	
16	1	0.5										X
17	1	5										X
18	3.5		X									
19	3.5			X								
20	3.5				X							
21	3.5	0.5				X						
22	3.5	5				X						
23	3.5	0.5					X					
24	3.5	5					X					
25	3.5	0.5						X				
26	3.5	5						X				
27	3.5	0.5							X			
28	3.5	5							X			
29	3.5	0.5								X		
30	3.5	5								X		
31	3.5	0.5									X	
32	3.5	5									X	
33	3.5	0.5										X
34	3.5	5										X
35	6		X									
36	6			X								
37	6				X							

Table 3.3: List of experiments carried out to evaluate the effectiveness of enzymatic treatment on hemp fibre.

Sample No.	Duration [hrs]	Concentration [%]	Buffer pH 4.5	Buffer 5.8	EDTA	Pectinex	Scourzyme	BioPrep	PL	EL	MPE	PTE
38	6	0.5				X						
39	6	5				X						
40	6	0.5					X					
41	6	5					X					
42	6	0.5						X				
43	6	5						X				
44	6	0.5							X			
45	6	5							X			
46	6	0.5								X		
47	6	5								X		
48	6	0.5									X	
49	6	5									X	
50	6	0.5										X
51	6	5										X
52	24		X									
53	24			X								
54	24				X							
55	24	0.5				X						
56	24	5				X						
57	24	10				X						
58	24	0.5					X					
59	24	5					X					
60	24	10					X					
61	24	0.5						X				
62	24	5						X				
63	24	10						X				
64	24	0.5							X			
65	24	5							X			
66	24	10							X			
67	24	0.5								X		
68	24	5								X		
69	24	10								X		
70	24	0.5									X	
71	24	5									X	
72	24	10									X	
73	24	0.5										X
74	24	5										X

Table 3.3: List of experiments carried out to evaluate the effectiveness of enzymatic treatment on hemp fibre.

Sample No.	Duration [hrs]	Concentration [%]	Buffer pH 4.5	Buffer 5.8	EDTA	Pectinex	Scourzyme	BioPrep	PL	EL	MPE	PTE
75	24	10										X
76	24	5							X	X		
77	24	5							X		X	
78	24	5							X			X
79	24	5								X		
80	24	5								X	X	
81	24	5								X		X
82	24	5									X	
83	24	5									X	X
84	24	5										X
85	24	5							X	X	X	
86	24	5								X	X	X
87	24	5							X		X	X
88	24	5							X	X		X
89	24	5							X	X	X	X
90	24+(2)	5				(X)			X			
91	24+(2)	5				(X)				X		
92	24+(2)	5				(X)					X	
93	24+(2)	5				(X)						X
94	24+(2)	5				(X)			X	X		
95	24+(2)	5				(X)			X		X	
96	24+(2)	5				(X)			X			X
97	24+(2)	5				(X)				X		
98	24+(2)	5				(X)				X	X	
99	24+(2)	5				(X)				X		X
100	24+(2)	5				(X)					X	
101	24+(2)	5				(X)					X	X
102	24+(2)	5				(X)						X
103	24+(2)	5				(X)			X	X	X	
104	24+(2)	5				(X)				X	X	X
105	24+(2)	5				(X)			X		X	X
106	24+(2)	5				(X)			X	X		X
107	24+(2)	5				(X)			X	X	X	X
108	24	0.5			X	X						
109	24	5			X	X						

3.2.2 Fibre treatments used for AFM analysis

Buffer treatment

Fibres were treated in pH 4.5 buffer solution for 24 hrs. After washing to obtain a pH of 7, the fibres were dried overnight in a convection oven at 60°C.

Enzyme treatment

Fibres were treated as described in Chapter 3.2.1, but only Pectinex was used at a concentration of 5% for 3.5 hours.

Alkaline treatment

25 g of fibre was washed in water and subsequently immersed in 500 ml 10wt.% NaOH at 40°C. The fibres were stirred after 10 and 20 minutes to allow for a more homogeneous treatment. After 30 minutes the treatment was terminated by washing the fibre under tap water until a pH of 7 was reached. The fibres were left to stand in water for another 30 minutes to allow residual NaOH to dissolve and after an additional pH check were dried overnight in a convection oven at 60°C.

Acetylation

Acetylation was performed on fibre previously treated by the alkaline procedure described above. Fibre and glassware were dried overnight in a 60^{o}C oven to remove residual moisture. Approximately 10 g of fibre was added to a flask with 100 ml of acetic anhydride. The flask was fitted with a condenser, and the system incubated at 100^{o}C in a hot oil bath for two hours. The fibres were then washed thoroughly three times with acetone and a final wash with iso-propyl alcohol. The fibres were dried overnight in a convection oven at 60°C.

3.3 Methods of analysis

3.3.1 Visual evaluation

All samples were subjected to a preliminary examination by more or less subjective means such as change in colour, texture, relative level of defibrillation and other conspicuous features.

3.3.2 FTIR analysis

For the FTIR analysis a Shimadzu FTIR-8201PC (Chemistry Department, University of Canterbury) was used in transmission mode. The first difficulty encountered in the attempt to employ transmission mode was the preparation of a suitably homogenous disc.

The infrared inactive potassium bromide (KBr) was used as the base material. ∅10 mm discs were prepared using about 200 mg of KBr per disc blended with fibre material at a ratio of 100:1 (*i.e.* 2 mg fibre material per sample). A homogeneous disc was then formed by pressing the mixture for 1 minute in a 12 ton press. The applied pressure was kept constant by measuring the achieved deformation of the press but not measured directly.

As investigated by Faix and Böttcher [84], a small particle size is important to minimize non-linearities in the absorbances of the different components. Furthermore a reduction of particle size provides better dispersion of the fibre, thus preventing favoured measurement on fibre surfaces.

The breakdown of hemp into small particles is not an easily accomplished task due to the flexibility of the fibre. Therefore, different procedures were developed and tested. The best and fastest method was employed for the preparation of the FTIR discs afterwards. For the fibre breakdown metal sieves for geological purposes were implemented. A small amount of fibre material was carefully rubbed by applying light pressure over a sieve with 100 micron mesh. The screened particles were collected on white paper and subjected to another grinding/sieving step over a 45 micron mesh. For fibre treatments that caused embrittlement of the hemp this method was easily applied without further modifications. The breakdown of the more flexible fibre samples proved difficult without the application of force onto the mesh of the sieves. Hence, these samples were immersed in liquid nitrogen for about two seconds before grinding them. If necessary the freezing was repeated to collect enough fine fibre material. Between fibre batches the sieves were cleaned thoroughly and dried with a hair dryer. 2 mg of fibre “flour” was then intimately mixed with 200 mg of KBr with a small mortar and pestle and immediately pressed into a disc applying pressure for two minutes. Even though the KBr was dried beforehand and stored in a desiccator, the

prepared samples exhibited residual water from moisture present in the fibre material or KBr as shown by background spectra taken of pure KBR discs. To minimize the influence of water, the discs were dried in a vacuum oven at 50°C overnight. Following the drying they were then analysed as fast as possible without further storage. To account for the changes in moisture content during the analysis of the whole series, new background spectra were taken every 4 samples and only spectra with possibly small noise were accepted. Otherwise a new background was taken and the sample was re-measured.

For the measurements a resolution of 4 cm^{-1} and a total of 16 scans per sample were used to obtain spectra in the mid-infrared area from 400 to 4000 cm^{-1}. To minimize the noise to signal ratio, Happ apodization was employed as recommended by the instrument's manual. The recorded spectra were saved in .txt file format and then imported into excel for further analysis.

In order to enable an easier comparison, all spectra were automatically baseline corrected by the best-fit algorithm of the software package Peakfit V4.12. As a last step of pre-processing all spectra were additionally normalized and for some parts of the analysis a deconvolution was carried out in Peakfit based on the second derivative of the spectrum.

3.3.3 Atomic Force Microscopy

AFM measurements were carried out on a Digital Instruments Dimension 3100 with a Nanoscope IIIa controller in contact mode. All measurements were made under standard environments (temperature of 21^{o}C and relative humidity of ~60%). Oxidation sharpened contact mode tips with triangular Si_3N_4 cantilevers (Veeco DNP-S20) were used. The force constant of the cantilevers was determined from the power spectral density of thermal noise of the cantilever. The tips had nominal radii of 20$\pm$5 nm, as determined from field emission scanning electron microscope images, and spring constants of 0.12 N/m. After contacting the surface a scan of the topography was made and subsequently force curves were measured on the same area, collecting two force curves on 20 areas spaced at 100 nm intervals.

3.3.4 SEM analysis

For the investigation under the scanning electron microscope the fibre samples were arranged on sample holders with carbon tape surface and afterwards gold coated to achieve electrical conductivity.

For the gold coating, a Polaron Specimen Coating Unit (E5100 Series II Cool Sputter) was used. At a voltage of 1.2 kV the samples were coated three times for 2.5 minutes under 45° from opposite directions and perpendicular to the carbon surface. A current of 35 mA was manually adjusted via the pressure of the argon atmosphere inside the sample compartment. After coating the samples were stored in a desiccator.

For the SEM analysis a JEOL JSM-6100 SEM microscope was operated at an accelerating voltage of 4 keV.

3.3.5 Tensile testing

The tensile properties of the untreated and treated fibres were tested according to ASTM standard D3822-01 [85]. A Perkin Elmer Diamond DMA, Figure 3.1 (a), was used in static mode for the tensile testing of single fibres.

In order to provide a means of handling fragile fibre samples and protecting the fibre ends in the clamps to minimize failure at the grips, a tabbing technique following Annex 1 of the ASTM standard D3822-01 was employed. Sample holders made of drawing paper were prepared by punching the paper and afterwards trimming the adjacent area as shown in Figure 3.1 (b) to approximately 2 mm and 10 mm. Circular holes lead to some variation in gage length as the specimen may be not perfectly centred over the punched hole. On the other hand the use of a hole-puncher provided for uniform holes of 5.5 mm in diameter as opposed to hand-cut rectangular holes, thus resulting in comparable variance while greatly reducing the sample preparation time. The diameter of 5.5 mm deviated from the recommended gage length of 10 mm in the ASTM standard as the latter was too long for the fibres exposed to more aggressive treatments.

(a) Diamond DMA, [86]

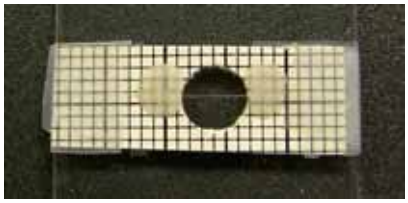

(b) sample holder

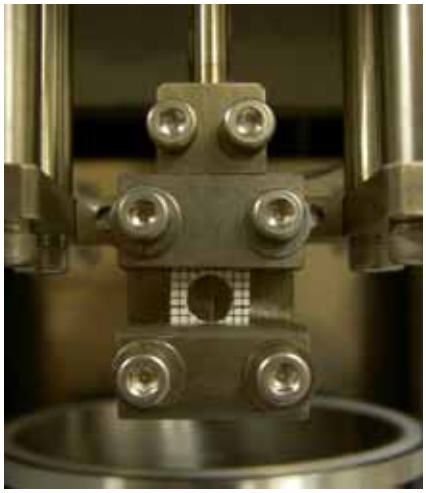

(c) installed sample

Figure 3.1: Equipment and set-up used for tensile tests

The tailored sample holders were then taped onto microscope slides to prevent deflection during mounting of the fibres. As the treatments carried out on the different samples accounted for more or less deformation of the fibres, the mounting could not be carried out as described in the standard, which proposes placing a drop of resin on each side of the hole and then positioning the fibre in the resin. In order to straighten a bent fibre before fixing it in the resin, a reversed method was applied. In a first step one end of the fibre was attached to a small piece of adhesive tape and glued to the sample holder facing the centre of the hole. Using tweezers the second end of the fibre was then likewise glued to another small piece of adhesive tape and aligned on the opposite side of the hole without applying tension to the fibre but guaranteeing a straight gage area. Both strips of tape were carefully placed at a distance of at least 3 mm from the hole so that in the next step a small amount of resin could be applied onto the fibre ends. Each drop of resin was applied touching the edge of the hole in order to account

for the predefined gage length. The mounting resin (Lecoset 7007) was left to cure until completely hardened.

The determination of fibre diameter for the calculation of stress was then carried out with an Olympus reflected light microscope equipped with digital camera and connected to a PC. After locating the thinnest part of each fibre sample at a magnification of 5 times, images were then collected at a magnification of 20 times. The diameters were then measured directly from the images by a manually placing a straight line across the fibre using an image analysis package (Figure 3.2). If a more rectangular cross-section could be observed for fibre bundles, the shortest and longest side was measured rather

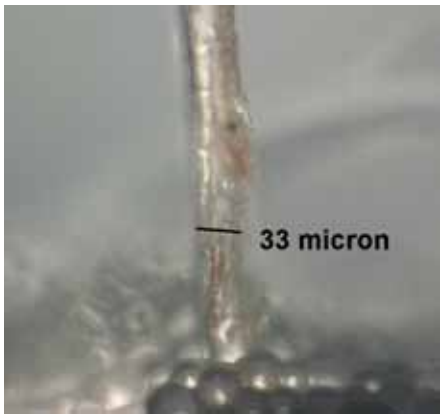

Figure 3.2: Measurement of diameter close to resin fixture

than a “diameter”.

For testing on the Diamond DMA the machine was adjusted to a gage length just over the sample length so that the sample holder could be carefully clamped on the resin as shown in Figure 3.1 (c). One side of the paper was then carefully cut with a pair of scissors. As the upper probe can be moved easily during clamping, resulting in tension being applied to the fibre after cutting the sample holder completely, a close inspection as to signs of applied tension was necessary before cutting the second part of the paper. If in doubt the probe was lowered up to 0.1mm to release tension and then the second paper reinforcement was cut.

The stress-strain curves were recorded at constant rate of extension. Following the ASTM standard a rate of extension of 50 micron/min (~10% of initial specimen length per minute) was chosen. The results were exported as Excel files and the

appropriate stresses and elongations were calculated assuming circular or, where applicable, rectangular cross-sections.

Considering the strong dependency of the tensile properties on fibre diameter and the large spread of diameter within each fibre batch, a test series for the determination of the clamp error (fibre share that is pulled out of the clamp corrupting the calculation of the elongation at break) was not carried out. The necessary number of specimens for the elimination of such influences would have exceeded the usefulness of the correction. This corruption needs to be considered for quantitative comparisons with external data, but does not interfere with the qualitative comparison carried out between the samples of this work. Clamping defects for similar gage lengths were calculated by Mieck *et al*. [87], and found to be approx. 0.2 mm for green and 0.15 mm for retted flax at a total length change of 0.285 mm.

3.3.6 3-Point bend testing of hemp-epoxy composites

Flexural properties were measured for hemp fibre-epoxy composites. The epoxy resin used in this work was EpoFix (Struers A/S, Denmark) [88, 89]. Twenty samples were prepared for each batch of fibres tested. The dimensions of the samples were 2 mm x 13 mm x 55 mm in accordance with ASTM Standard 790 [90]. Hemp fibre was cut into segments ~5mm in length and 0.5 g of fibres were then mixed with enough resin to achieve a thorough wetting of the fibre material. To help the wetting and ensure a uniform distribution of the fibres within the sample, the mixture was thoroughly kneaded between the fingers and pulled apart into small lumps to prevent clogging. Each sample was prepared near net shape in a mould assembled from plexiglass pieces as shown in Figure 3.3. The resin was left to cure overnight. Additionally, the samples were conditioned at 50°C for at least 15 hours to relieve residual stresses before they were released from the mould. Finally, overlapping edges were ground away on an abrasive belt.

The dimensions of each sample were measured with a sliding calliper and the weight was determined in order to identify the fibre weight fraction:

$$0.5\text{ g fibre} + \text{weight}_{resin} = \text{weight}_{sample}$$

$$W_{fiber} = \frac{0.5\text{ g fiber}}{\text{weight}_{sample}} \qquad (3.8)$$

The 3-point bend tests were carried out according to ASTM Standard D790-00 Procedure B with a support span of 40 mm and a crosshead speed of 13 mm/min. The latter was calculated as follows:

$$R = \frac{ZL^2}{6d} \qquad (3.9)$$

where:

R = rate of crosshead motion, mm/min,

L = support span, mm (40 mm)

d = depth of beam, mm (≈ 2 mm)

Z = rate of straining of the outer fibre, mm/mm/min. Z shall be equal to 0.01 (Procedure A) or 0.10 (Procedure B).

The decision to carry out the tests according to Procedure B was based on maximum strain measured, which exceeded the maximum of 5% for the slower crosshead motion of Procedure A.

The flexural properties where calculated as follows [90]:

- Flexural stress (σ_f):

$$\sigma_f = \frac{3PL}{2bd^2} \qquad (3.10)$$

- Flexural strain (ε_f)

$$\varepsilon_f = \frac{6Dd}{L^2} \qquad (3.11)$$

- Tangent modulus of elasticity

$$E_B = \frac{L^3m}{4bd^3} \qquad (3.12)$$

where,

σ = stress in the outer fibre at midpoint, MPa

ε = strain in the outer surface, mm/mm

E_B = modulus of elasticity in bending, MPa

D = maximum deflection in the centre of the beam, mm

P = load at a given point on the load-deflection curve, N

L = support span, mm

b = width of beam tested, mm

d = depth of beam tested, mm

m = slope of the tangent to the initial straight-line portion of the load-deflection curve, N/mm of deflection

For the calculation of average values samples which fractured away from the line of load transmission were discarded.

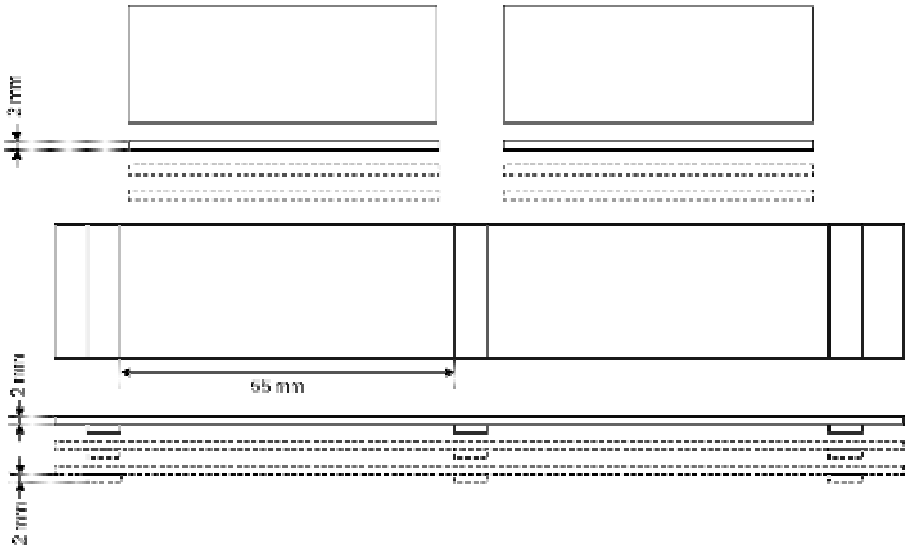

(1)

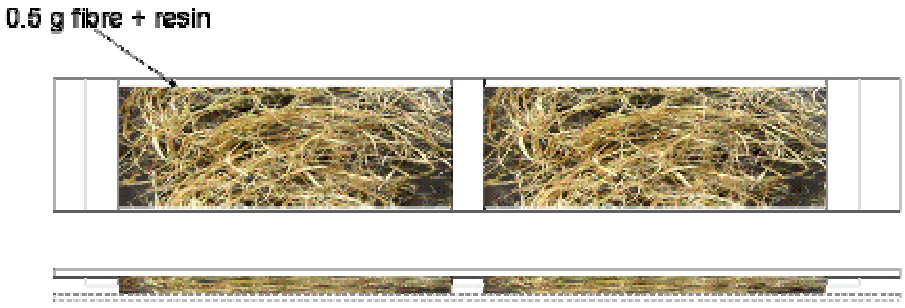

(2)

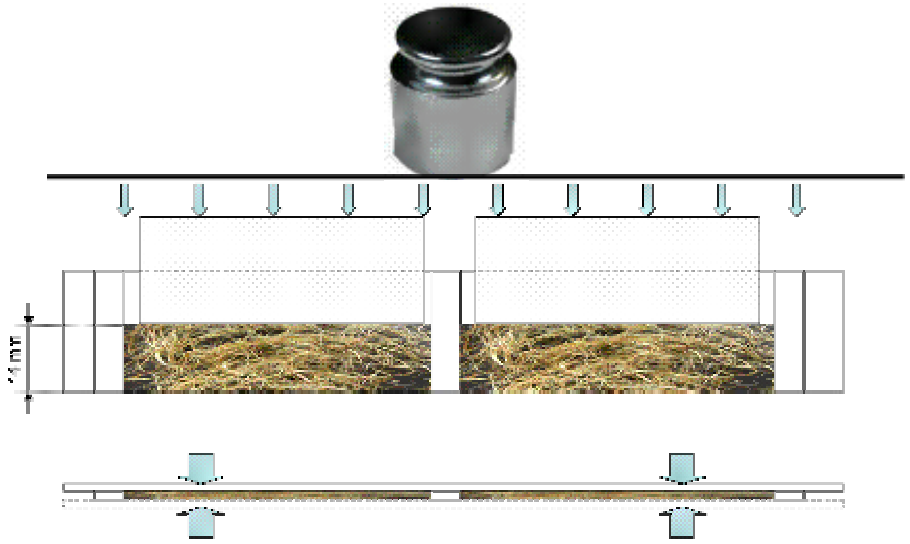

(3)

Figure 3.3: Manufacturing route for 3-point-bending samples.

3.3.7 Dynamic Mechanical Analysis

The dynamic mechanical measurements were carried out with a Perkin Elmer Diamond Dynamic Mechanical Analyzer in 3-Point Bend mode using the same sample preparation and dimensions as described above for 3-point bending.

DMA tests were generally carried out between room temperature (25-30°C) and 130°C. Initially, test runs were performed from -100°C to 175°C with pure epoxy and a composite sample to check for any additional molecular transitions. No significant peaks were observed, however the higher temperature did lead to degradation and release of gaseous components. A heating rate of 2°C/min was used for all tests. Five frequencies (0.1, 1, 2, 5, 10 Hz) were superimposed and tested simultaneously as described in Chapter 2.5.2.

The recorded data was stored in Excel-files and summaries with maximum damping, storage modulus, loss modulus and the respective temperatures were compiled using a visual basic macro.

3.3.8 Correlation analysis

The correlation coefficient indicates the strength and direction of a linear relationship between two random variables. In general statistical usage, correlation or co-relation refers to the departure of two variables from independence, although correlation does not imply causality. In this broad sense there are several coefficients, measuring the degree of correlation, adapted to the nature of the given data. Thus, a number of different coefficients are used for different situations.

Pearson's product-moment coefficient

The correlation $\rho_{X,Y}$ between two random variables X and Y with expected values μ_X and μ_Y and standard deviations σ_X and σ_Y is defined as:

$$\rho_{X,Y} = \frac{\operatorname{cov}(Y,Y)}{\sigma_X \sigma_Y} = \frac{E((X-\mu_X)(Y-\mu_Y))}{\sigma_X \sigma_Y} \qquad (3.13)$$

where E is the expected value of the variable and cov means covariance. Since $\mu_X = E(X)$, $\sigma_{X^2} = E(X^2) - E^2(X)$ and likewise for Y, we may also write

$$\rho_{X,Y} = \frac{E(XY) - E(X)E(Y)}{\sqrt{E(X^2) - E^2(x)}\sqrt{E(Y^2) - E^2(Y)}} \qquad (3.14)$$

The correlation cannot exceed 1 in absolute value. A positive value indicates a positive relationship between the two variables. Accordingly, a negative correlation is found for variables exhibiting a negatively linear relationship. The closer the coefficient is to either −1 or 1, the stronger the correlation between the variables. Correlations of values between 0 and 1 are illustrated in Figure 3.4.

If the variables are independent then the correlation is 0, but the converse is not true because the correlation coefficient detects only linear dependencies between two variables.

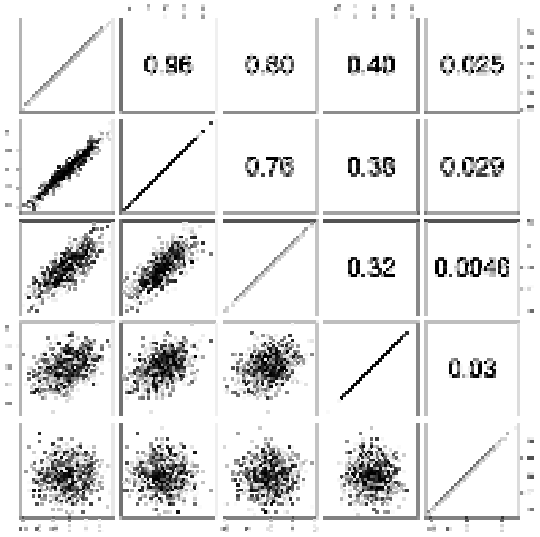

Figure 3.4: Simple example of linear correlation.

1000 pairs of normally distributed numbers are plotted against one another in each panel (bottom left), and the corresponding correlation coefficient shown (top right). Along the diagonal, each set of numbers is plotted against itself, defining a line with correlation +1. Five sets of numbers were used, resulting in 15 pairwise plots.

For a series of n measurements of X and Y written as x_i and y_i where i = 1, 2, ..., n, the Pearson product-moment correlation coefficient can be used to estimate the correlation of X and Y . The Pearson coefficient is also known as the "sample correlation coefficient". It is especially important that X and Y are both normally distributed. The Pearson correlation coefficient is then the best estimate of the correlation of X and Y. The Pearson correlation coefficient is written:

$$r_{xy} = \frac{\sum(x_i - \bar{x})(y_i - \bar{y})}{(n-1)s_x s_y} \qquad (3.15)$$

where $\bar{x}$ and $\bar{y}$ are the sample means of x_i and y_i, s_x and s_y are the sample standard deviations of x_i and y_i and the sum is from i = 1 to n. This can be rewritten as

$$r_{xy} = \frac{n\sum x_i y_i - \sum x_i \sum y_i}{\sqrt{n\sum x_i^2 - (\sum x_i)^2}\sqrt{n\sum y_i^2 - (\sum y_i)^2}} \qquad (3.16)$$

Although the above formula appears to be a trivial calculation, it is notorious for its numerical instability (see below for the alternative Spearman's ρ).

The sample correlation coefficient is the fraction of the variance in y_i that is accounted for by a linear fit of x_i to y_i. This is written

$$r_{xy}^2 = 1 - \frac{\sigma_{y|x}^2}{\sigma_y^2} \qquad (3.17)$$

where $\sigma_{y|x}^2$ is the square of the error of a linear fit of y_i to x_i by the equation y = a + bx.

$$\sigma_{y|x}^2 = \sum_{i=1}^{n}(y_i - a - bx_i)^2 \qquad (3.18)$$

and σ_y^2 is just the variance of y

$$\sigma_y^2 = \sum_{i=1}^{n}(y_i - \bar{y})^2 \qquad (3.19)$$

Since the sample correlation coefficient is symmetric in x_i and y_i, we will get the same value for a fit of x_i to y_i:

$$r_{xy}^2 = 1 - \frac{\sigma_{x|y}^2}{\sigma_x^2} \qquad (3.20)$$

Just as the above described sample correlation coefficient is the fraction of variance accounted for by the fit of a 1-dimensional linear submanifold to a set of 2-dimensional vectors (x_i, y_i), so a correlation coefficient for a fit of an m-dimensional linear submanifold to a set of n-dimensional vectors can be defined. For example, if a plane z = a + bx + cy is fitted to a set of data (x_i, y_i, z_i) then the correlation coefficient of z to x and y is

$$r^2 = 1 - \frac{\sigma^2_{z|yx}}{\sigma^2_z} \qquad (3.21)$$

Pearson's correlation coefficient is a parametric statistic, and it may be less useful if the underlying assumption of normality is violated. Non-parametric correlation methods, such as Spearman's ρ and Kendall's τ may be useful when distributions are not normal; they are a little less powerful than parametric methods if the assumptions underlying the latter are met, but are less likely to give distorted results when the assumptions fail.

Spearman's rank correlation coefficient

Spearman's rank correlation coefficient, often denoted by the Greek letter ρ (rho), is a non-parametric measure of correlation – that is, it assesses how well an arbitrary monotonic function could describe the relationship between two variables, without making any assumptions about the frequency distribution of the variables. Unlike the Pearson product-moment correlation coefficient, it does not require the assumption that the relationship between the variables is linear, nor does it require the variables to be measured on interval scales; it can be used for variables measured at the ordinal level.

In principle, ρ is simply a special case of the Pearson product-moment coefficient in which the data are converted to ranks before calculating the coefficient. In practice, however, a simpler procedure is normally used to calculate ρ. The raw scores are converted to ranks, and the differences D between the ranks of each observation on the two variables are calculated. ρ is then given by:

$$\rho = 1 - \frac{6\sum D^2}{N(N^2 - 1)} \qquad (3.22)$$

where

D = the difference between the ranks of corresponding values of X and Y, and

N = the number of pairs of values.

For this project, the software package SPSS version 13 was used to calculate the correlations explained above. The data was inserted without further manipulation as presented in the respective sections of Chapter 4. The variables

were classified as metrical or ordinal as appropriate according to the type of data obtained.

4 Results and discussion

4.1 Enzyme activities

The enzyme activities pectinesterase and polygalacturonase were measured and calculated as described in Chapter 3.1. The results for each enzyme are listed in Table 4.1. Additionally, the calibration curve for the spectrophotometrical determination of polygalacturonase activity is shown in Figure 4.1.

Table 4.1: Enzyme activities

Enzyme	PE/g	PGU/mg
Pectinex	274	46
BioPrep	- / -	52
Scourzyme	- / -	9
PL	- / -	25
EL	- / -	(- / -)
PTE	- / -	- / -
MPE	487	- / -

The values for PL, EL, Pectinex (PGU) and MPE (PE) can be compared with the information given on the respective data sheets. It can be seen that all commercial enzyme mixtures exhibit side activities. These are at least pectinesterase for Pectinex, characterized as polygalacturonase, and polygalacturonase for the pectate lyases BioPrep and Scourzyme. The values for PL, Pectinex and MPE all lie within a maximum deviation of a factor 2 from the values given on the respective data sheets.

However, 0 PGU/mg was detected for EL although the value should be of the same order of magnitude as the other enzyme solutions. As the PGU values obtained for Pectinex and PL correspond well with the information given by the manufacturers, the applied method was validated in general. The low PGU value

for EL might have been caused by an error during the measurements although all experiments were carried out in duplicate. The “blank” solution itself exhibited a higher extinction than most others, which might have been caused by an additional, uncontrolled ingredient or a repeated pipette handling error during the mixing of the blank sample. A second calculation was carried out with the extinction of the blank value of the bio-chemically similar enzyme PL. A PGU value close to the information supplied by the manufacturer was obtained. The method used for this project is only applied in small-scale assays, while the viscometrical determination of PGU is more commonly found on data sheets, *i.e.* professional enzyme assays (cf. data sheets in the Appendix). The dilution of EL for this project was chosen according to the value supplied by the manufacturer AB enzymes, because of the likely error or corruption during the assay and a certainly higher correlation between the measurements of PL and EL at AB enzymes. As will be presented in the following chapters, the retting efficiency of EL was very low even after a treatment time of 24 hours and doubled concentration, thus the enzyme could not have exhibited satisfying retting efficiency, even if it had been diluted to a lower concentration as intended.

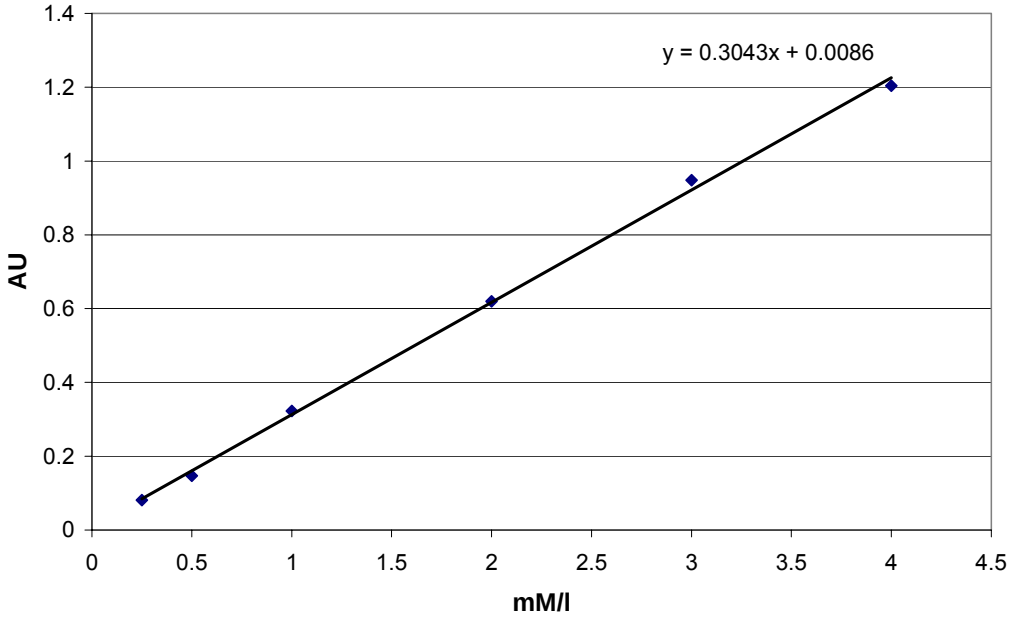

Figure 4.1: Galactose standard for spectrophotometrical measurements of polygalacturonase activity.

4.2 Effects of treatment on hemp properties

4.2.1 Visual evaluation

A visual evaluation of all samples after drying gave very similar results for most of the enzymes used. The fibre material remained coarse and felt hard. Only treatment with Pectinex achieved a noticeable fibre separation and continued softening with longer treatment times. Along with increasing fibre separation, the colour of the fibres changed from a yellow-brownish colour towards a light beige. Combinative treatments yielded comparative results only with a subsequent application of Pectinex and showed defibrillation according to the duration of Pectinex activity and a lighter colour. A collection of samples was evaluated again by an unbiased person to reduce the subjectivity and the same observations were made. These visual observations are summarized in Table 4.2 and pictures of the samples are shown in Figure 4.2.

Table 4.2: Summary of visually observed properties following various enzymatic treatments.

Enzyme	*Colour*	*Texture*
Buffer 4.5 6 hrs		Medium
Buffer 4.5 24 hrs		Medium
EDTA 24 hrs		Medium
PL 24 hrs		Medium
EL 24 hrs		Medium
MPE 24 hrs		Medium
PTE 24 hrs		Soft
Scourzyme 24 hrs		Hard
BioPrep 24 hrs		Hard
Pectinex 1 hr	Slightly lighter	Medium
Pectinex 3.5 hrs	Lighter	Soft
Pectinex 24 hrs	Lighter	Soft
Combi (PL,EL,MPE,PTE 24 hrs+ 2 hrs Pectinex)	Lighter	Soft

Since none of the treatments except Pectinex yielded fibres that were noticeably changed in their appearance (in comparison to control samples treated in the respective buffer solutions), 24 hr treatments were chosen for further analysis. Additionally, a combinative treatment first using all of the enzymes supplied by AB and followed by a short Pectinex treatment was included for further analysis. As Pectinex has been found to weaken hemp fibre considerably after 12 hours under the same conditions in an earlier project [91], the fibres treated for both 1 and 3.5 hours were selected.

Figure 4.2: Pictures of samples after treatments, all enzyme concentrations 5%.

(a) Buffer pH 4.5 24 hrs

(b) EDTA 24 hrs

(c) Pectinex 1 hr

(d) Pectinex 3.5 hrs

(e) Pectinex 24 hrs

(f) Scourzyme 24 hrs

Figure 4.2: Pictures of samples after treatments, all enzyme concentrations 5%.

(g) BioPrep 24 hrs

(h) PL 24 hrs

(i) EL 24 hrs

(j) MPE 24 hrs

(k) PTE 24 hrs

(l) Combi (EL, PL, MPE, PTE 24hrs, Pectinex 2 hrs)

4.2.2 FTIR analysis

The recorded FTIR spectra, pre-processed as described in Chapter 3.3.2, are compiled in Figure 4.4. The spectra appear quite similar for all samples. In order to elucidate the main differences between the spectra, more detailed diagrams of the respective regions are given in Figure 4.5. Where not otherwise stated, Table 4.3 was used as reference for the assignment of the observed peaks.

The first spectral difference observable is in the region between 1600 and 1800 cm^{-1} (Figure 4.5 a). The differing peaks are at about 1740 and 1630 cm^{-1}. These reflect the states of carboxylic groups; the (methyl-esterified) carboxyl groups absorb in the region of 1749 cm^{-1} and the absorbance at 1605-1630 cm^{-1} is caused by the ionized COO^- groups [92-98]. The following ratio has therefore been used as a measure for the degree of esterification [94, 99]:

$$DM = \frac{a_{1749cm^{-1}}}{a_{1630cm^{-1}} + a_{1749cm^{-1}}} \qquad (4.1)$$

Also, these two peaks are the two most prominent when it comes to differences between spectra of pectic substances and are therefore the most suitable for analysis when overlapping contributions of other substances are present. The development of the above-mentioned peaks depending on the degree of methylesterification is illustrated in Figure 4.3.

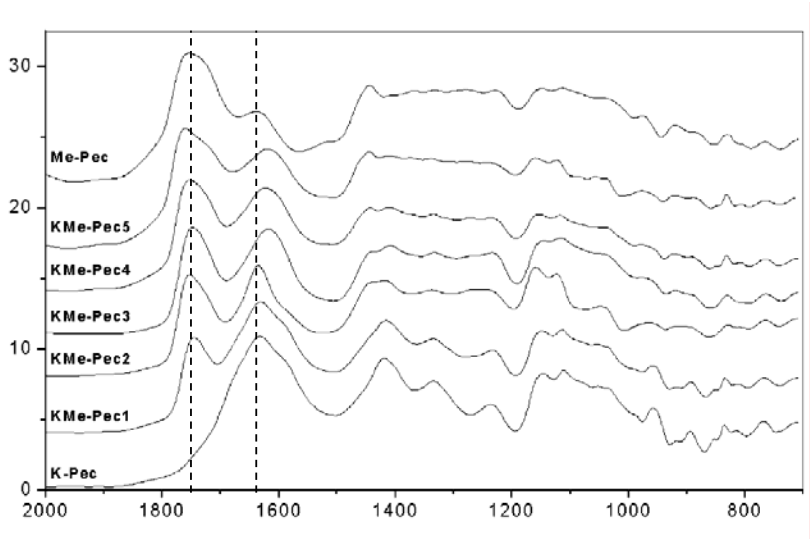

Figure 4.3: FT-IR spectra of pectic substances with decreasing degrees of methylesterification (DM)
(Me-Pec DM=90%, K-Pec DM = 0%. From Synytsya *et al*. [92].)

Table 4.3: Assignment of peak wavenumbers [100].

Wavenumber (cm^{-1}) range of maxima	Band origin (assignment) with comments	Spruce MWL reference [72]	Spruce cellulose	Spruce holo-cellulose
3645–3620	Free OH [73]		[64]	
3560	Absorbed water weakly bound [66]		[64]	
3460–3412	O—H stretch [72]	3412		
3570–3450	Valence vibration of H bonded OH-groups (intramolecular)		[63]	
3455–3410	O(2)H···O(6) intramolecular in cellulose [67]		[64]	
3375–3340	O(3)H···O(5) intramolecular in cellulose [67,68]		[64]	3375
				3343
3310–3230	O(6)H···O(3) intermolecular in cellulose [66–68]		[64]	3280
3400–3200	Valence vibration of hydrogen bonded OH-groups		[63]	
3000–2842	C—H stretch in methyl and methylene groups [72] methoxyl C—H stretching [74]	3000		
2840–2835		2937		
		2879		
		2840		
2981–2933	Asymmetric CH_2 valence vibration		[63]	
2980–2835	CH_2, CH_2OH [66–70,73], in cellulose from C6 [75]		[64]	2902
2940–2850	Symmetric CH_2 valence vibration		[63]	2902
1730–1725	C=O valence vibration of acetyl- or COOH-groups		[63]	1738
1738–1709	C=O stretch in unconjugated ketones, carbonyls and in ester groups (frequently of carbohydrate origin); conjugated aldehydes and carboxylic acids absorb around and below 1700 cm^{-1} [72]	1722		1738
1675–1655	C=O stretch; in conjugated *p*-substituted aryl ketones; strong electronegative substituents lower the wavenumber [72]	1663		
1635	Adsorbed water		[63]	1635
1605–1593	Aromatic skeletal vibrations plus C=O stretch; S > G; G condensed > G etherified [72]	1596		
1515–1505	Aromatic skeletal vibrations; G > S [72]	1510		
1470–1455	CH_2 of pyran ring symmetric scissoring; OH plane deformation vibration		[63]	1454
1470–1460	C—H deformations; asymmetric in $—CH_3$ and $—CH_2—$ [72]	1464		
~ 1460	Asymmetric C—H bending from methoxyl group [72]			
1435	HOC bending [76]			
1430	HOC in plane bending of alcohol groups [77]			

Wavenumber (cm^{-1}) range of maxima	Band origin (assignment) with comments	Spruce MWL reference [72]	Spruce cellulose	Spruce holo-cellulose
1430–1422	Aromatic skeletal vibrations combined with C—H in plane deformation [72]	1423		
1430–1416	CH_2 scissoring		[63]	1430
1375–1374	CH deformation vibration		[63]	1373
1370–1365	Aliphatic C—H stretch in CH_3; not in O—Me [72]	1367		
~ 1368	symmetric C—H bending from methoxyl group [74]			
1365–1335	OH plane deformation vibration		[63]	1337
1330–1325	Phenolic OH: S ring plus G ring condensed; (i.e. G ring substituted in pos. 5) [72]	1326		
1317–1315	CH_2 rocking vibration		[63]	1318
1282–1277	CH - deformation		[63]	1280
1270–1266	G ring plus C=O stretch [72]	1269		
1235–1225	OH plane deformation, also COOH		[63]	
1230–1221	C—C plus C—O plus C=O stretch: G condensed > G etherified [72]	1221		
1205–1200	OH plane deformation		[63]	1201
1162–1125	C—O—C asymmetric valence vibration		[63]	1163
1140	Aromatic C—H in plane deformation: typical for G units; whereby G condensed > G etherified [72]	1140		
1120–1115	Asymmetric in-phase ring stretching, C—C and C—O stretching according to [65,71,77,78]			1110
1110–1107	Ring asymmetric valence vibration		[63]	1110
1086	C—O deformation in secondary alcohols and aliphatic ethers [72]	1086		
1060–1015	C—O valence vibration [63] mainly from C3–O3H [77]		[63]	1060
1060				1034
1047–1004	C_{alky}–O ether vibrations, methoxyl and b-O-4 [79] C_{alky}–O ether vibrations in guaiacol [80]			
1040–1030				
1035–1030	Aromatic C—H in plane deformation, G > S; plus C—O deformation in primary alcohols; plus C=O stretch (unconj.) [63,72,77]	1032		1034
996–985	C—O valence vibration		[63]	995
930–925	Pyran ring vibration		[63]	
925–915	C—H out-of-plane; aromatic [72]	919		
895–892	Anomere C-groups, C_1-H deformation, ring valence vibration		[63]	897
858–853	C—H out-of-plane in position 2, 5 and 6 of G units	858		
805	Due to glucomannan [81]			809
800	Pyran vibration		[63]	
715	Rocking vibration CH_2 [82]; in cellulose Ig [83]			712
670	C—OH out-of-plane bending mode [71]			667

Wavenumbers (cm^{-1}) of bands that are visible only as a shoulder are written in italics. The wavenumber ranges for bands given in the first column were assigned to cellulose (fourth column) by Fengel [63] and Fengel and Ludwig [64] referring to [65–71]

[63] D. Fengel, M. Ludwig, Das Papier 45 (2) (1991) 45–51.
[64] D. Fengel, Holzforschung 47 (1993) 103–108.
[65] K. Tashiro, M. Kobayashi, Polymer 32 (8) (1991) 1516–1526.
[66] E.P. Kalutskaya, S.S. Gusev, Polym. Sci. U.S.S.R. 22 (1981) 550– 556.
[67] N.V. Ivanova, E.A. Korolenko, E.V. Korolik, R.G. Zbankov, Zurnal Prikladnoj Spektroskopii 51 (1989) 301–306.
[68] C.Y. Liang, R.H. Marchessault, J. Polym. Sci. 37 (1959) 385–395.
[69] H.J. Hediger, Infrarotspektroskopie. Grundlagen, Anwendungen, Interpretation, Akadem. Verlagsges., Frankfurt/Main, 1971.
[70] L.J. Bellamy, The Infra-red Spectra of Complex Molecules, Chapman & Hall, London, 1975.
[71] C.Y. Liang, R.H. Marchessault, J. Polym. Sci. 39 (1959) 269–278.
[72] O. Faix, Holzforschung 45 (Suppl) (1991) 21–27.
[73] V.P. Panov, R.G. Zbankov, from D. Fengel, Proceedings of Cellucon Conference, 1993, Lund Sweden, 1988, pp. 75–84.
[74] W.E. Collier, V.F. Kalasinsky, T.P. Schultz, Holzforschung 51 (1997) 167–168.
[75] D. Fengel, in Proceedings of Cellucon Conference, 1993, pp. 75– 84.
[76] B. Hinterstoisser, M. A˙ kerholm, L. Salme´n, Carbohydrate Res. 334 (2001) 27–37.
[77] Y. Mare´chal, H. Chanzy, J. Mol Struct. 523 (2000) 183–196.
[78] H. Staudinger, E. Dreher, A.A. Ekenstam, Berichte der deutschen chemischen Gesellschaft 69 (1936) 1099–1100.
[79] W.E. Collier, T.P. Schultz, V.F. Kalasinsky, Holzforschung 46 (6) (1992) 523–528.
[80] L.P. Gol'man, V.M. Reznikow, Khim. Ispol'z. Lignina, 1974, pp. 140–148.
[81] R.H. Marchessault, Pure Appl. Chem. 5 (1962) 107–129.

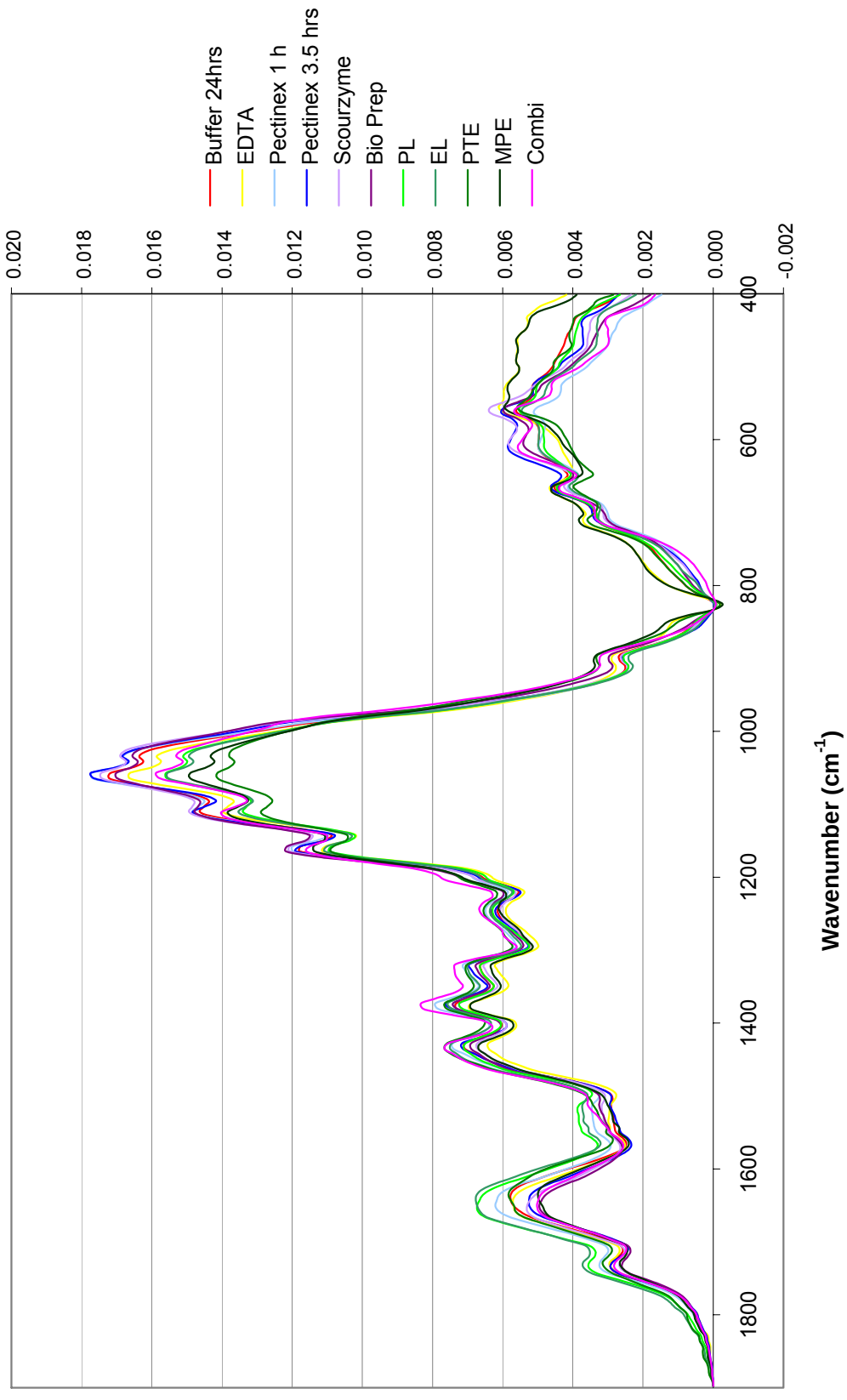

Figure 4.4: FTIR spectra of fibre samples after enzyme treatments, 400 – 1900 cm^{-1}.

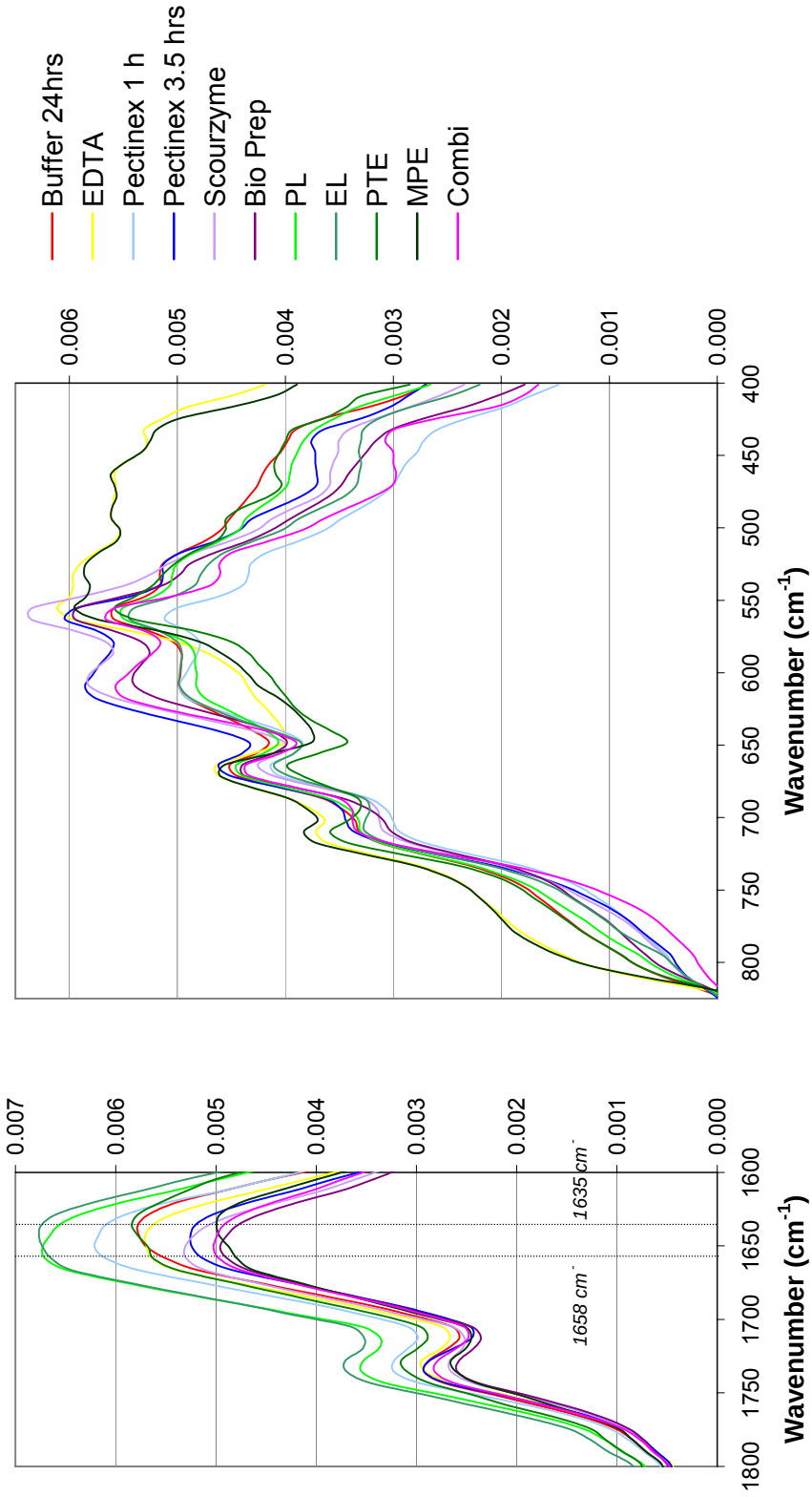

Figure 4.5: FTIR spectra magnified in the regions of greatest variation between enzymes.

As there are overlapping peaks in the neighbourhood of the examined peaks the spectra were analyzed using Peak Fit 4.11. The baseline-corrected and normalized spectra were fitted by single peaks using the second derivative. An example of the resulting fits is given in Figure 4.6. If necessary, neighbouring peaks of low intensity were deleted from the first set of peaks and the fit iterated again in order to achieve comparable area percentages for the selected peaks. Using the area of the peaks near 1605 and 1749 cm^{-1} the ratio as given in equation (4.1) was calculated. The results are displayed in Figure 4.7.

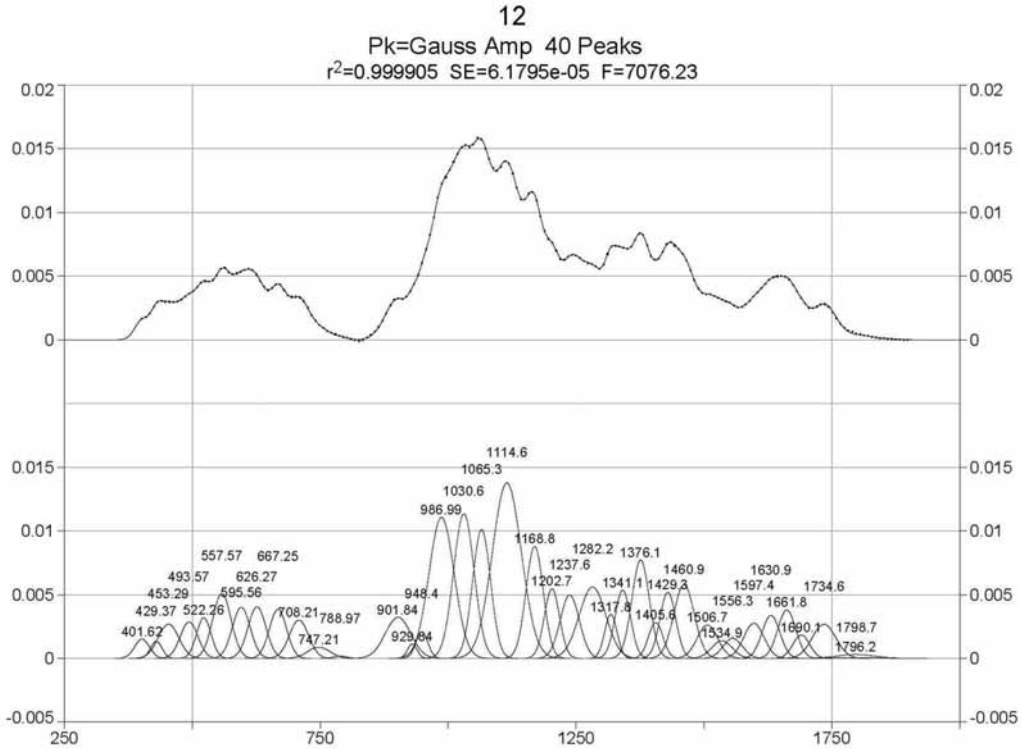

Figure 4.6: Second derivative peak fit of an FT-IR spectrum

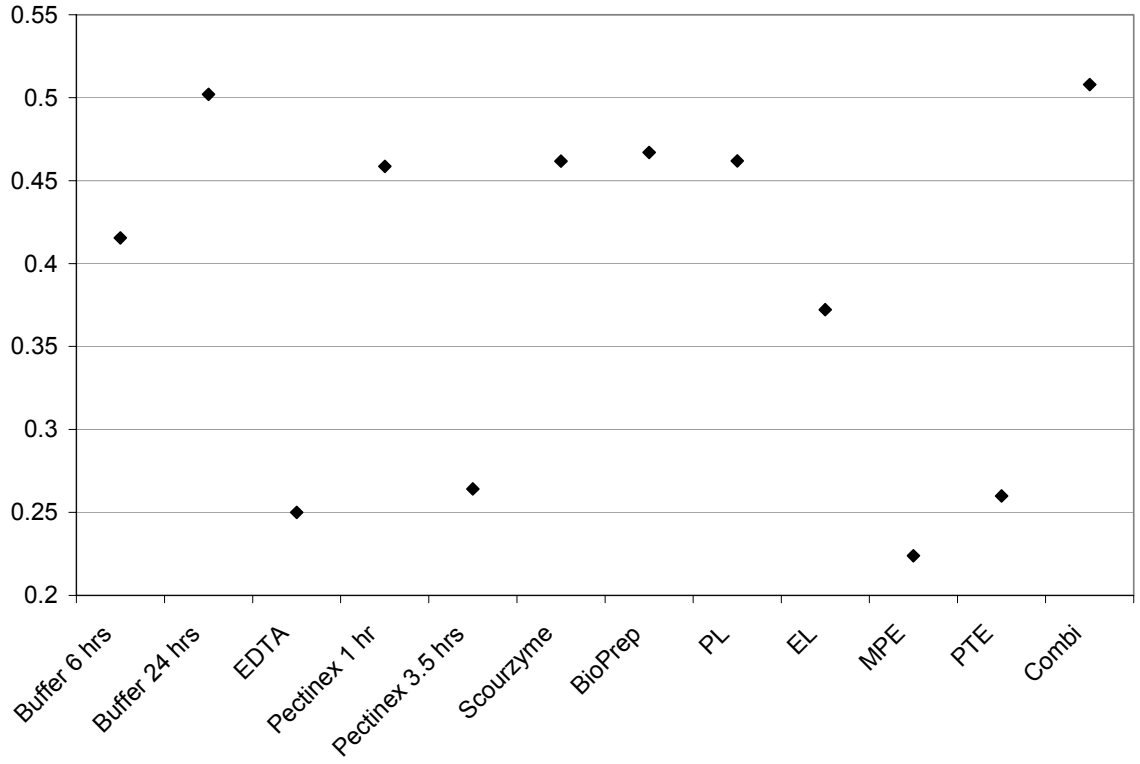

Figure 4.7: Degree of methylesterification of the samples after treatments.

It can be seen that four samples show a distinctly lower DM than all other. This can be explained by looking at the respective mechanisms of action:

- EDTA: removal of Ca^{2+} ions and solution of pectin
- Pectinex: Polygalacturonase complex with PE side activity
- MPE: Pectin methyl esterase – removal of methylester group (cf. p. 22, Figure 2.12)
- PTE: Pectin lyase – splitting of pectin molecule attacking mainly methylesterified galactose rings (cf. p. 22, Figure 2.12)

Of these four the MPE and PTE activities are easily explained by their respective activities.

EDTA can be used for extraction of pectic fractions (usually at 100°C, *e.g.* [101]) and is known to change the tertiary structure of pectin by removing calcium ions binding the pectin chains together via carboxylic groups of non- or low-

methyl-esterified galacturan blocks [102, 103]. The remaining COO^- groups are likely to stay ionized in slightly alkaline solution as is formed by EDTA. The following neutralization with water might still leave enough carbonyl groups balanced in their ionized state to cause the carbonyl absorbance to increase in comparison to the carboxyl absorbance, thus decreasing the DM ratio (without actually influencing the methylesterification of pectin). Additionally, the extraction of pectin caused by the EDTA treatment can lead to a decrease in both pectin peaks with a preferred removal of the less structurally bound methylesterified parts [103]. Disturbing effects of neighbouring peaks from other polysaccharides might also influence the measured DM, but Manrique *et al*. [95] showed that the used ratio does not interfere with other cell wall polysaccharides and does not require extraction of pectin.

The decrease in DM caused by Pectinex is a logical consequence of the enzyme's activity. Although it is classified as polygalacturonase, it was found to exhibit a strong methyl esterase side activity during the enzyme assays carried out in the scope of this work. The side activity for this commercial enzyme solution is useful as polygalacturonase does not usually attack methylesterified galactose blocks and would normally need to be used in conjunction or after a treatment with methyl pectin esterase (like Rohapect MPE) [104].

The spectra of MPE, EDTA and partly PTE treated fibres clearly show some differences from the other spectra, especially around 700, 600 and 550-400 cm^{-1} (Figure 4.5 (b)). Unfortunately, this region of the IR spectrum is not commonly studied for the characterization of cell wall polysaccharides which usually focuses on the 'fingerprint' regions around the 850-1200 cm^{-1} range, characteristic peaks up to about 1900 cm^{-1} and broad absorbencies around 3000 cm^{-1} [92-99, 105]. Thus, the peaks in the above region are only rarely listed in the literature and thus no definite assignments have been made. Therefore, it is interesting to note that treatments with EDTA, PTE and MPE resulted in differences in spectra although no detailed interpretation can be made at this point.

Another aspect commonly examined when dealing with FT-IR spectra of natural fibres is the degree of crystallinity. The infrared crystallinity of natural fibres is

commonly determined by the calculation of two absorbance ratios. Nelson and O'Connor [106] suggested the ratio of the absorbencies at 1372 and 2900 cm^{-1} to determine the level of crystallinity or crystallinity index (CrI):

$$CrI = \frac{a_{1372cm^{-1}}}{a_{2900cm^{-1}}} \qquad (4.2)$$

An illustration of the respective baseline corrections carried out during the calculation of the index is given in Figure 4.8 (a). A second index employed in this context is the Lateral Order Index (LOI) given by:

$$LOI = \frac{a_{1429cm^{-1}}}{a_{893cm^{-1}}} \qquad (4.3)$$

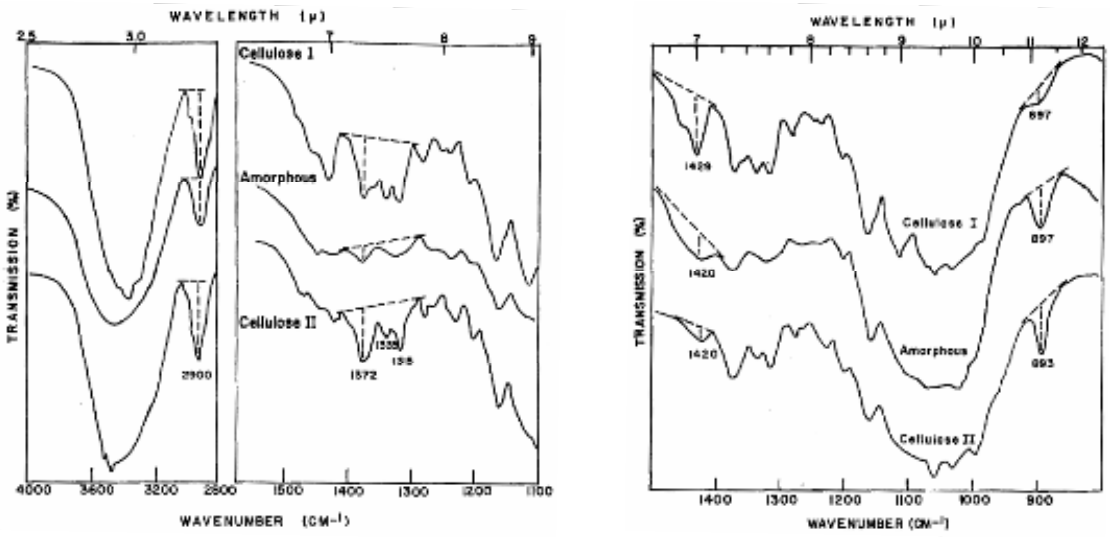

(a) Crystallinity Index (CrI) a_{1372}/a_{2900} (b) Lateral order index (LOI) a_{1429}/a_{893}

Figure 4.8: Baseline corrections for the determination of CrI and LOI according to Nelson and Connor [106].

The baseline-corrected absorption peaks at 1430 and 897 cm^{-1} correspond to the sensitive absorption frequencies of crystalline and amorphous cellulose structures, respectively (see Figure 4.8 (b)) [24, 35, 107]. The LOI describes the order of crystallinity rather than the amount of crystalline cellulose relative to the amorphous components. However, the LOI is only of limited significance for the case of alkaline-treated fibres since amorphous and Type II cellulose produce a similar spectra [107].

The results of the calculations are displayed in Figure 4.9. It can be seen that a treatment in buffer solution for 24 hours increases the CrI by approximately 0.1. All treatments except for the combinative treatment yielded similar crystallinity indices. The combinative treatment yielded a value of 0.64, which is 0.2 above the average observed for the other isolated 24 hr treatments involving PL, EL, PTE or MPE. This appears to be due to the application of Pectinex since it was observed that an isolated Pectinex treatment of only 1 or 3.5 hrs yielded a CrI similar to the average observed after 24 hr treatments involving PL, EL, PTE or MPE. Using the CrI for the control sample treated in a buffer solution for 6 hrs as a basis, the corresponding CrI for the isolated Pectinex treatment is approximately 0.2. This value corresponds well with the CrI increase after an additional Pectinex treatment in case of the combinative treatment.

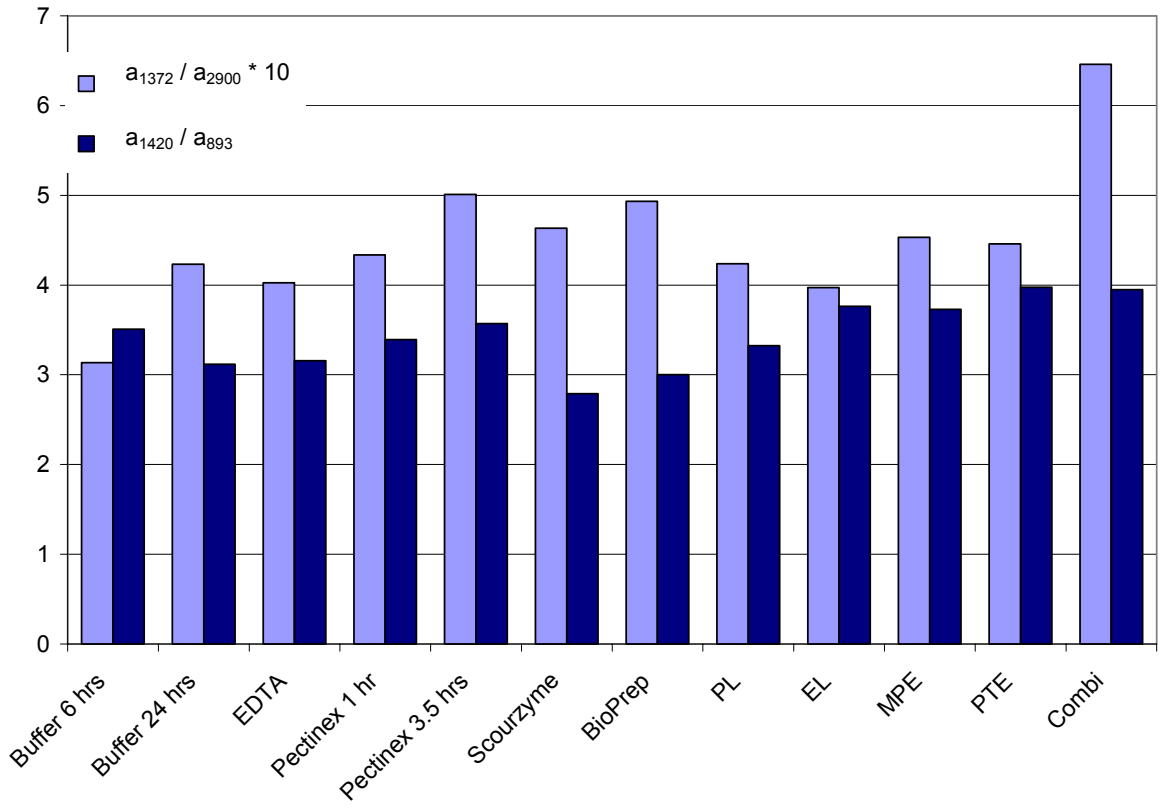

Figure 4.9: Infrared crystallinity and lateral order index.

The LOI shows similar changes. A drop in lateral order can be observed with increased buffer treatment duration. This is probably due to swelling and disturbance of the structure in the slightly acidic environment. Pectinex treatment results in an increase in LOI with treatment duration, however, the absolute values

stay in the region of the 6 hrs buffer treated sample. EDTA does not affect the lateral order when compared with the 24 hr buffer treatment. Scourzyme and BioPrep lower the index by 10% and 4%, respectively. All other enzymes increase LOI with the maximum increase of 27% observed for PTE and the combinative treatments.

4.2.3 Tensile testing

Tensile testing was carried out as described in Chapter 3.3.5. Generally speaking, the Diamond Dynamic Mechanical Analyzer and the self-made sample holders used for the tests were suitable. However, difficulties arose from the freely movable DMA probe during the testing of weak fibres. During clamping of the jaws on the resin, the probe could easily be displaced, thus resulting in a pretension being applied to the sample holder. In the subsequent cutting of the reinforcing tab of paper, the pretension was transferred to the fibre and a vibration of the upper probe was caused by the release of tension. Strong, ductile fibres endured these movements of the probe. Pretension could mostly be detected while cutting the first paper side. In this case the probe could be moved downwards to release tension before cutting the sample holder completely.

A number of samples were additionally destroyed by an internal error in the DMA. A broken coil caused the probe to move uncontrollably at the beginning of new tests rupturing the specimen before any data could be collected. Unfortunately, the machine could not be repaired and up to 60% of the specimens were lost due to this fault.

For those samples successfully installed in the DMA, the tensile tests resulted in fracture within in the gage length. Only on rare occasions was the fibre being pulled out of the resin, or fracture at the resin fixture observed. Due to the small number of breaks at the resin, the samples fractured were considered successful, complying with the guidelines given by the ASTM standard, [85].

A main source of corruption as far as the absolute values recorded in this work are concerned, is the clamp error of the used setup. The clamp errors calculated for the gage length of 5 mm by Mieck and Reussmann [87], were found to make

up a considerable part of the total length change recorded. Calibration curves for flax and hemp are shown in Figure 4.10. In this work, the clamping error has been ignored due to the short length of the hemp fibres and large number of measurements needed for the calibration. The results presented in this chapter should therefore be used for qualitative comparisons only. The relative comparisons made here proved sufficient for the purposes of this study since the mechanical properties measured lie within the range of values reported in the literature (*e.g.* [35]).

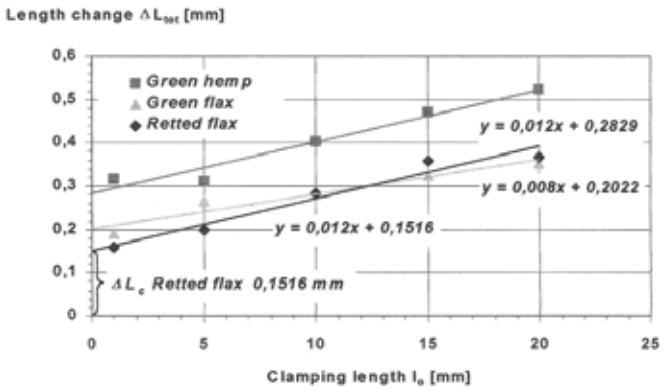

Figure 4.10: Total length change ΔL_{tot} = f (clamping length) [87].

The stress-strain curves recorded exhibit the typical properties reported for natural fibres. The curves are characterised by mostly brittle fracture although ductile fracture was also observed. They show a small degree of strain hardening and in some cases the fracture of single fibres within the bundle can be observed. The mechanical properties presented below were calculated as shown for the stress-strain curve example in Figure 4.11.

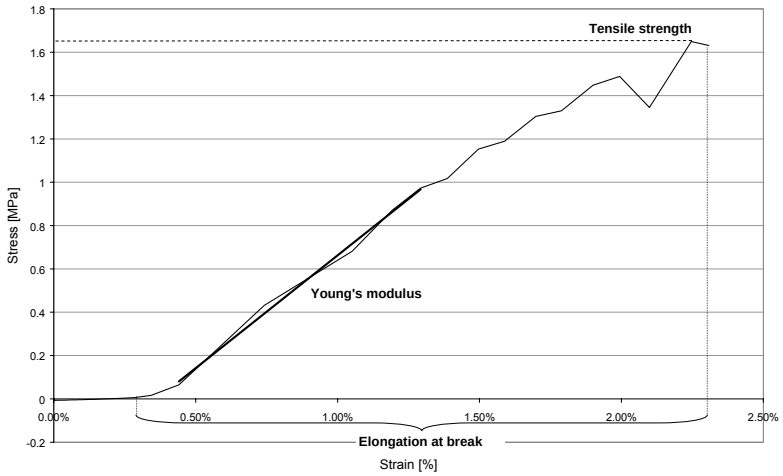

Figure 4.11: Determination of various tensile properties from DMA.

The overall results show typical distributions of mechanical properties dependant on fibre (bundle) diameter [87]. Figure 4.12 illustrates the observed increase in the Young's modulus with decreasing diameter. Although the gradient varied from sample to sample, a general increase of mechanical properties with decreasing diameter was always observed.

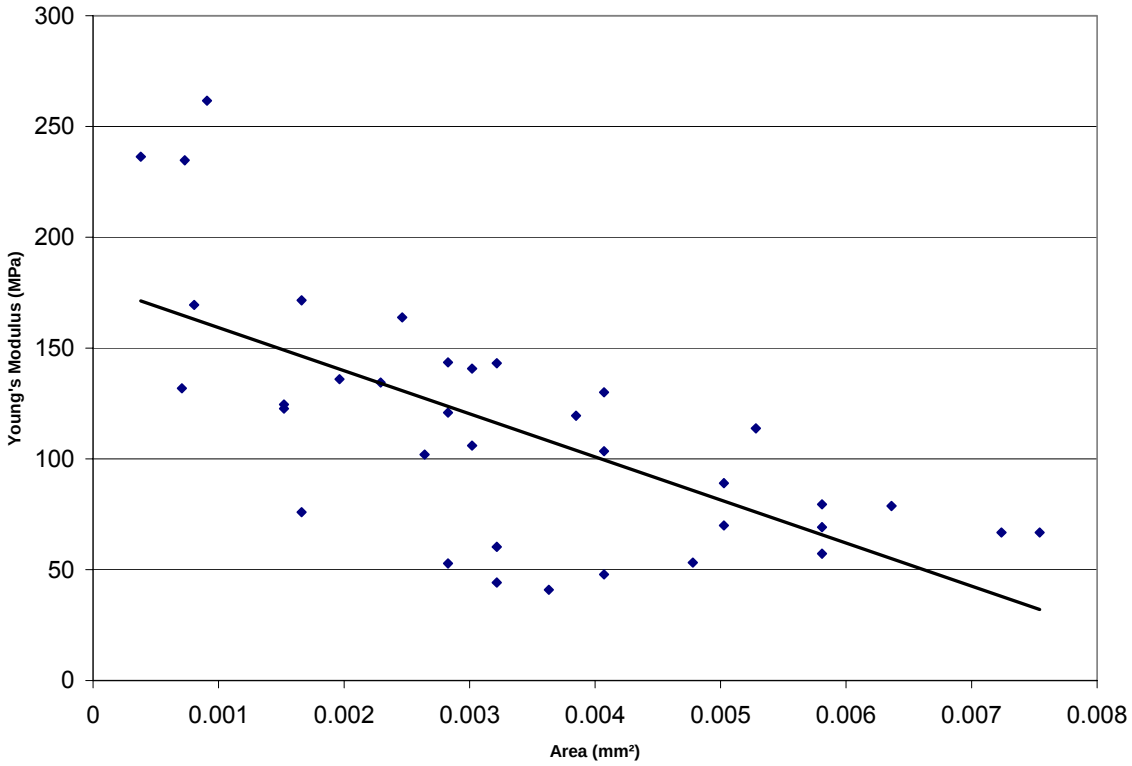

Figure 4.12: Relationship between cross-sectional area and Young's modulus.

The results recorded during single fibre tests on the DMA were analyzed with an Excel macro that was written specifically to process the data written by the DMA. The macro code with screenshots can be found in Table A 2. It collects all data files from one directory and filters the data so that the initial probe movement as slack in the system is being removed is deleted. Elongation at break, Young's modulus and tensile strength can be calculated. A user form can be used to insert the geometrical information of the tested fibre. Before each dataset (cross-sectional area, elongation at break, Young's modulus and tensile strength) is stored in a summary file, the graph that is used to calculate the Young's modulus can be viewed to visually evaluate the correctness of the fitted function and make final adjustments.

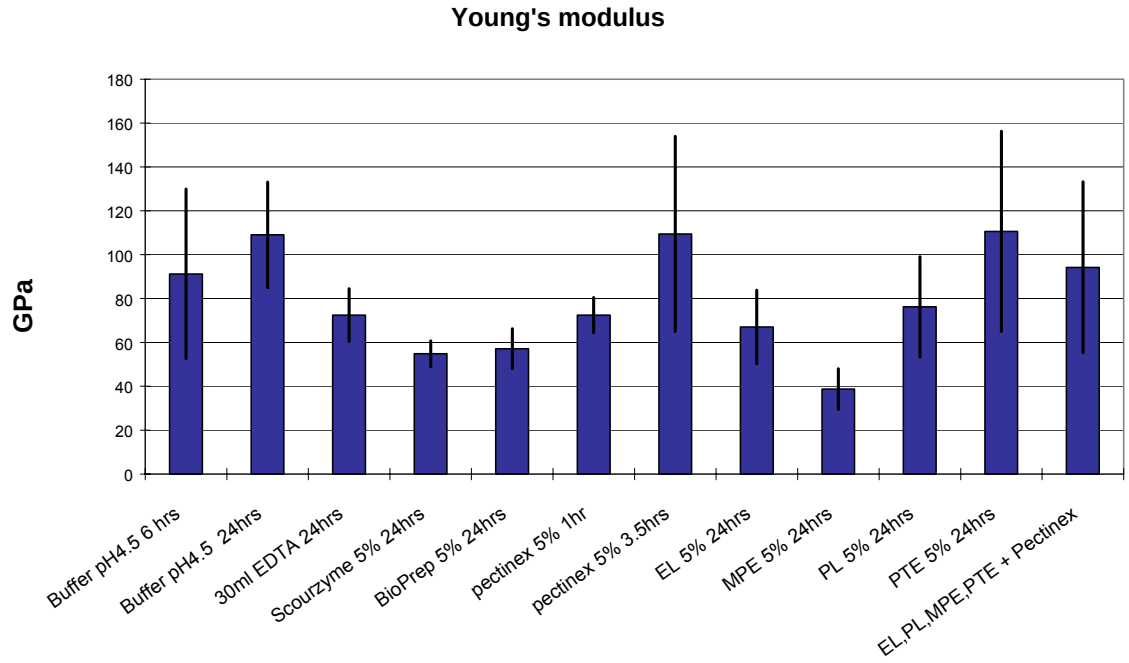

(a)

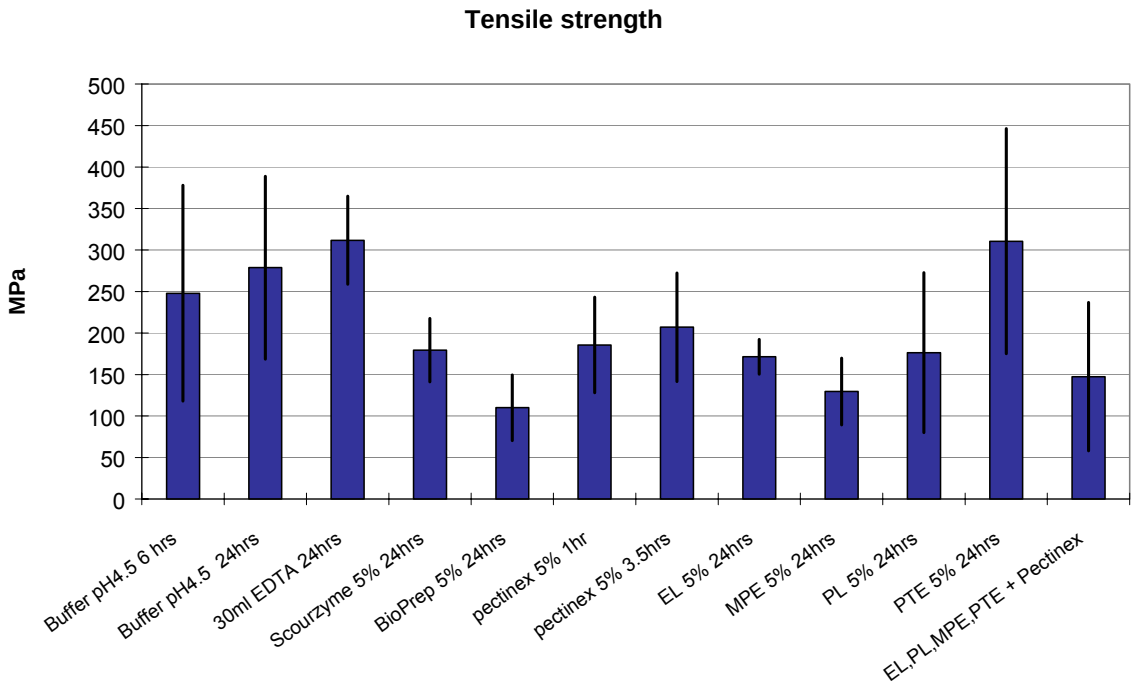

(b)

Figure 4.13: Young's modulus, tensile strength, elongation at break and respective cross-sections of fibres as determined by single fibre tensile tests.

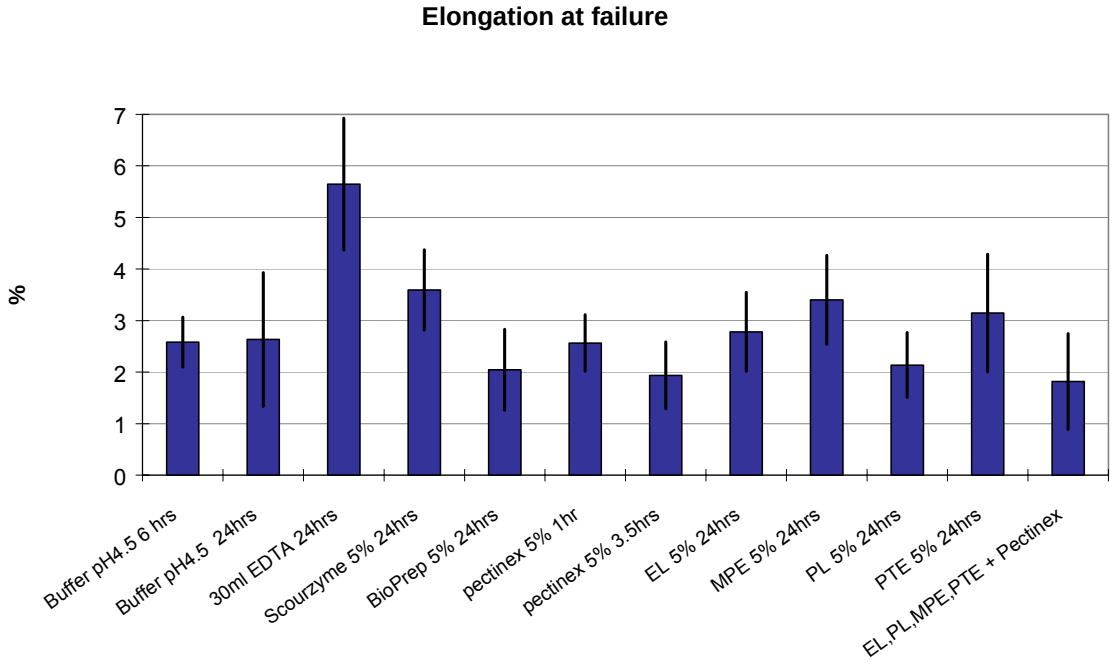

(c)

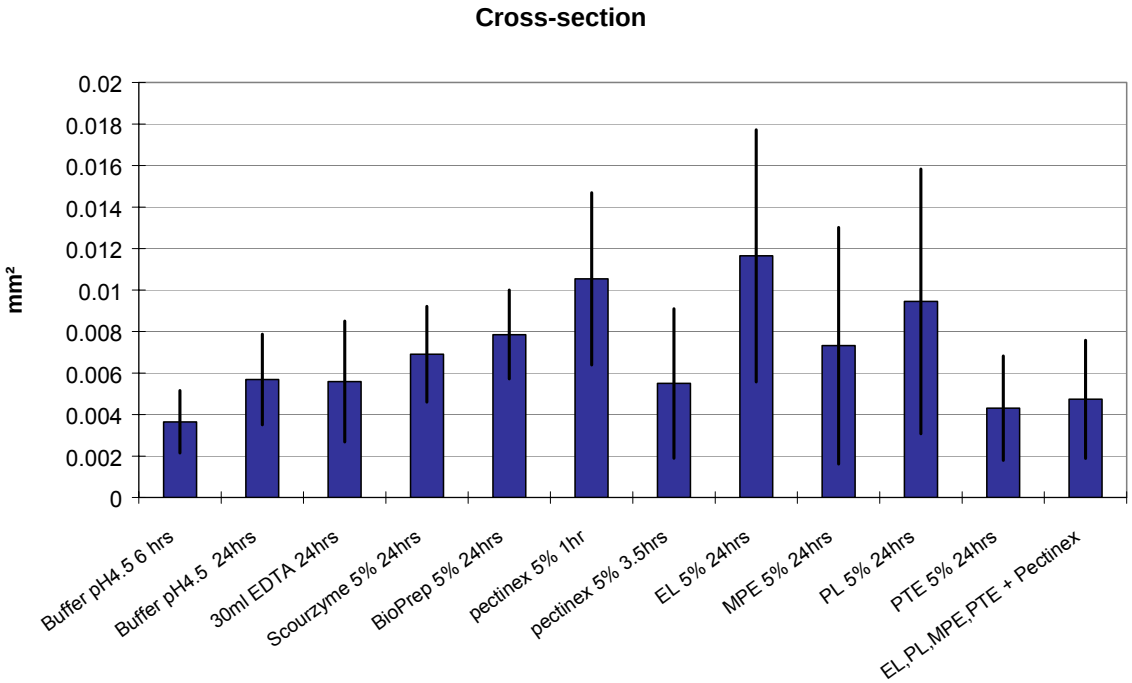

(d)

Figure 4.13 cont'd: Young's modulus, tensile strength, elongation at break, and respective cross-sections of fibres as determined by single fibre tensile tests.

Figure 4.13 gives an overview of the average mechanical properties recorded for the selected sample batches. Due to the reasons outlined above the variances shown in the same graphs are high for some samples, but general trends can still be observed and compared with results reported in the literature.

EDTA treatment resulted in a greatly increased elongation at break of 5.5%. Also, a slight loss of stiffness and increase of tensile strength could be observed. It is interesting to note that Stuart *et al*. [108] examined flax after 3 hours of treatment in EDTA and did not find any significant change in fibre properties.

The commercial enzyme solutions Pectinex, Scourzyme and BioPrep can also be compared to the literature as they can easily be identified by their name. In the present results for Scourzyme and BioPrep treatment, the stiffness was reduced by 50% and tensile strength by a third and half, respectively. The elongation at break was increased for Scourzyme and decreased after application of BioPrep. Shanks *et al*. [35] and Dreyer *et al*. [109] applied Scourzyme and BioPrep to hemp fibre and found comparable values for both Young's modulus and tensile strength. Shanks *et al* reported equal changes in stiffness and strength after 24 hours treatment duration. Elongation at break on the other hand was not reported to change with either treatment duration or concentration. Dreyer *et al*. only stated the strength measured after 2 hrs treatment in BioPrep but their reduction of tensile strength by one third does also correspond well with the reduction by 50% after 24 hours. Pectinex has also been used by Stuart *et al*. [108] but no significant changes in strength and stiffness were observed. In comparison to the results obtained for 6 hrs treatment in buffer solution, Pectinex lowered the fibres' stiffness initially after a 1 hr treatment but after a 3.5 hr treatment stiffness was increased by 20 GPa to 110 GPa, although with a larger variance. Tensile strength increased slightly after 3.5 hours and elongation at break was reduced by 0.5% in comparison to 6 hrs in the buffer solution or a 1 hr Pectinex treatment.

The enzyme solutions EL, MPE and PL all yielded weakened fibre material. MPE produced the weakest fibres with a reduction of Young's modulus from 110 GPa (24 hrs buffer) to 40 GPa and tensile strength to 130 MPa (24 hrs buffer 280 MPa). Only PTE led to improvement of mechanical properties as characterized by tensile testing. It should be noted though, that the results were split evenly into two

groups, one at a high level and one at the level of the other AB enzyme solutions. Taking into account the variances of each value, the fibre properties remained greatly unchanged in comparison to the buffer solution.

After combinative treatment with all AB enzyme solutions and a subsequent Pectinex treatment the fibres' stiffness remained at the level observed for buffer and Pectinex treatment (90-110GPa), while the strength was reduced to approximately 50%. Elongation at break was reduced to 1.8% close to the value of 1.9% recorded after 3.5 hrs Pectinex treatment.

4.2.4 Scanning Electron Microscopy of single fibres

SEM is a spatially very limited method of analysis and therefore micrographs cannot represent the morphology of an entire fibre batch. The fibres shown in Figure 4.14 are specimens analyzed after tensile testing. Consequently, the sections shown on the left of Figure 4.14 (magnification x100) are all fractured samples rather than random fibre ends. While carrying out microscopic analysis care was taken to choose representative parts of the fibre, especially for the higher magnifications.

The visual analysis presented in Chapter 4.2.1 already suggested a far superior defibrillation achieved by Pectinex treatment. This is also the most prominent difference when comparing Figure 4.14 (d) with all other micrographs. The fibre bundle is separated from the end and even where several fibrils are still bound together they can be distinguished easily. Magnified by 1000 the fibre looks clean and no adherent residues can be observed. The shorter 3.5 hr treatment shows the beginning of defibrillation but fibres are still in a thicker bundle and show residual interfibrillar material. Most other fibres do not show greatly improved defibrillation in comparison to the control sample Figure 4.14 (a).

Scourzyme, BioPrep and MPE seem to have yielded a cleaner fibre bundle surface without separating the fibres sufficiently. In the case of Scourzyme and BioPrep this might be the reason for the harder texture observed in Chapter 4.2.1. PTE on the other hand (Figure 4.14 (i)) was found to be softer than most other fibres. The left micrograph shows a thick layer of amorphous material covering the

fibre bundle. As this is in contrast to both Scourzyme and BioPrep treated fibres, this layer might contribute to the increased softness found during inspection of the fibres' texture.

The enzyme solutions PL and EL did not result in effective fibre separation either, but an increased surface roughness could be observed on the respective fibre bundles.

While the microfibrils were not sufficiently separated in the experiments carried out in the scope of this project, the enzyme solution PL was reported to be effective in the retting of flax stems [37]. The observed retting efficiency in the cited work might however not be comparable to the conditions examined here. While Zhang *et al*. [37] observed the release of flax fibres from stems the hemp material used in this work was pre-retted. The experiments presented in this thesis did therefore investigate the next retting step.

Applied in combination, the enzyme solutions did not achieve a sufficient degree of retting either. The surface roughness observed above was increased though and a beginning removal of parts of the covering layer can be observed. The bent parts of the fibre shown on the micrograph Figure 4.14 (k) are most likely no result of the enzyme treatment but originate from DMA probe movements directly after fibre fracture during the tensile test.

For a later correlation analysis the following classifications were introduced:

- Defibrillation
    - 1 = no defibrillation
    - 2 = separation of fibre bundles
    - 3 = separation of fibrils
- Surface cleanliness
    - 1 = no covering layer visible
    - 2 = fibre partly covered
    - 3 = covering layer
    - 4 = covered bundle with released flakes of covering layer

The samples were classified as follows:

Table 4.4: Classification of samples according to morphology as observed by SEM.

Treatment	Defibrillation	Surface Cleanliness
Buffer 24 hrs	1	3
EDTA 24 hrs	2	2
Pectinex 3.5 hrs	2	2-3
Pectinex 24 hrs	3	1
Scourzyme 24 hrs	1	3
BioPrep 24 hrs	1	3
PL 24 hrs	2	3
EL 24 hrs	1	3
PTE 24 hrs	1	3
MPE 24 hrs	1	2
Combi 24 hrs	2	4

Figure 4.14: Scanning electron micrographs of hemp fibres after various treatments.

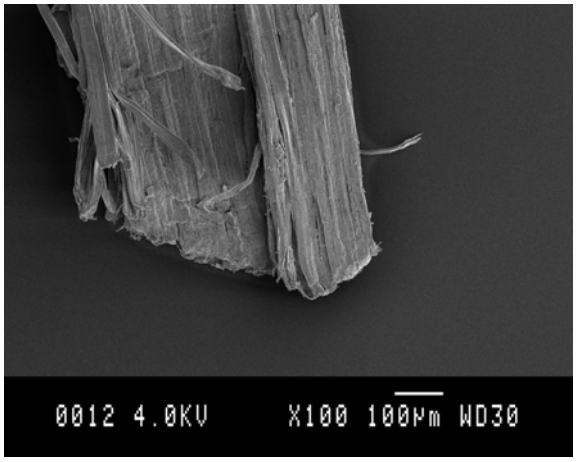

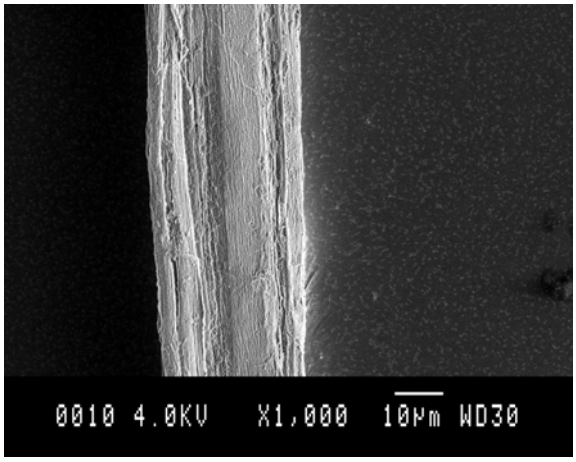

(a) Buffer 24 hrs

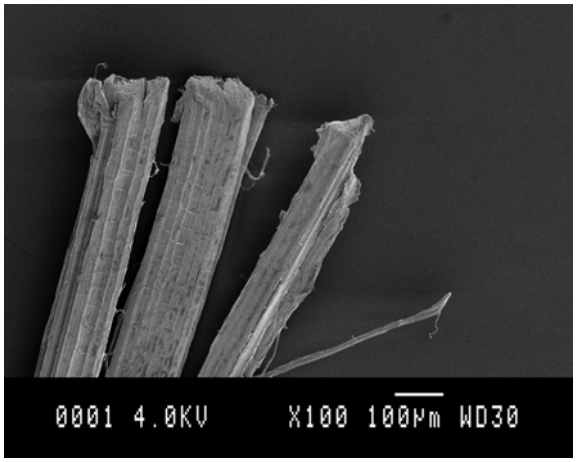

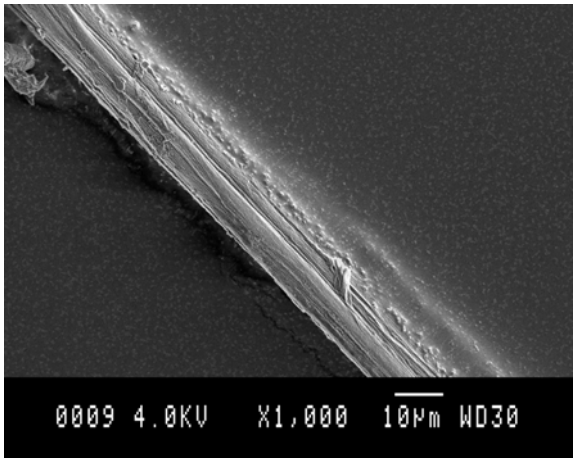

(b) EDTA 24 hrs

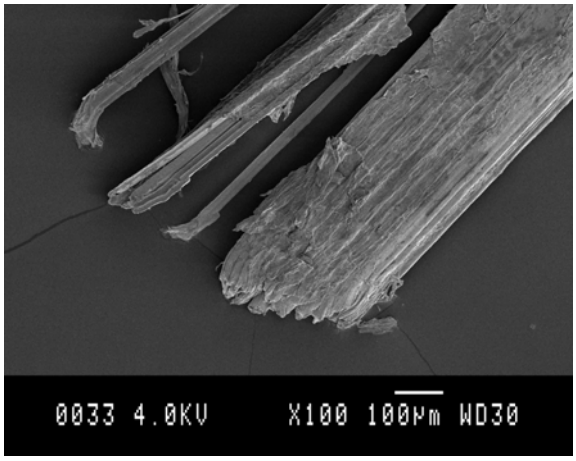

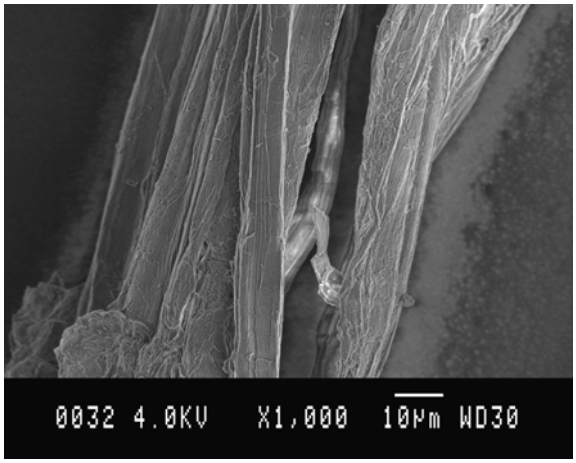

(c) Pectinex

Figure 4.14: Scanning electron micrographs of hemp fibres after various treatments.

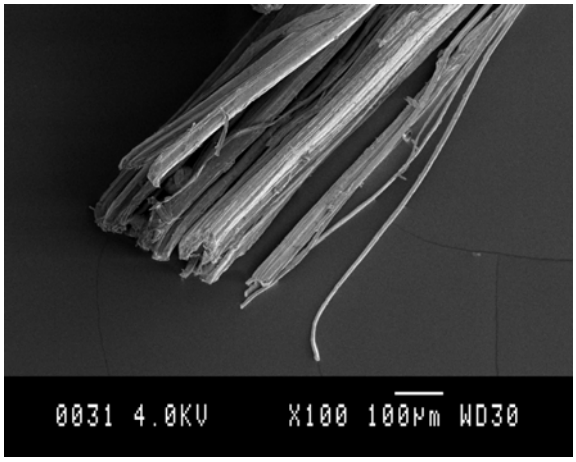

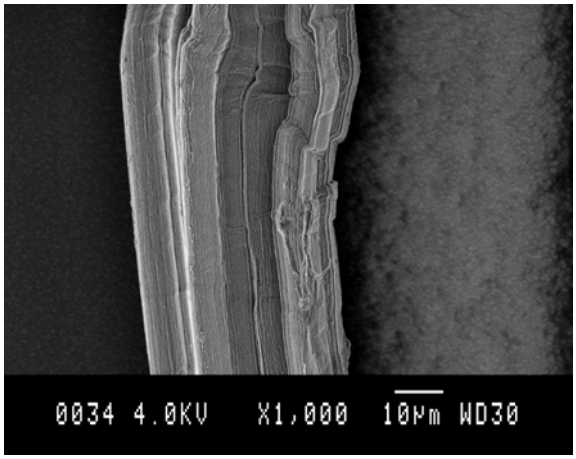

(d) Pectinex 24 hrs

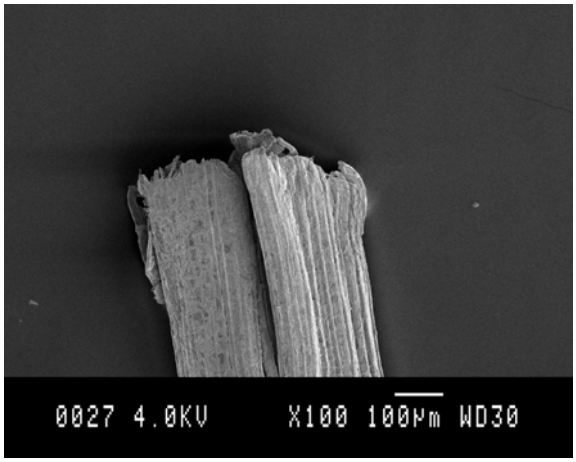

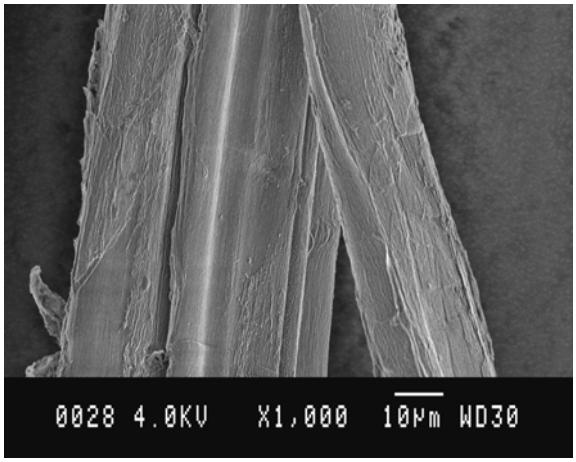

(e) Scourzyme 24 hrs

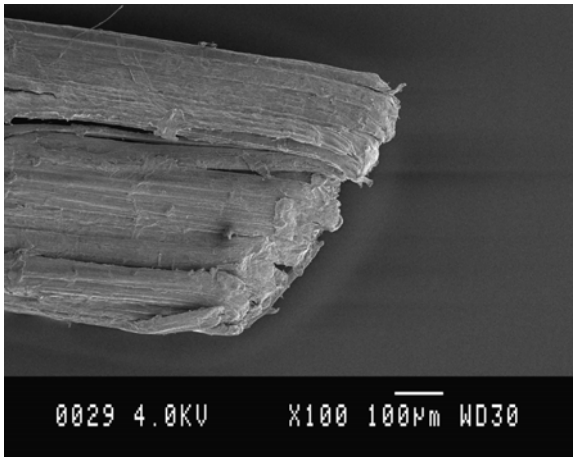

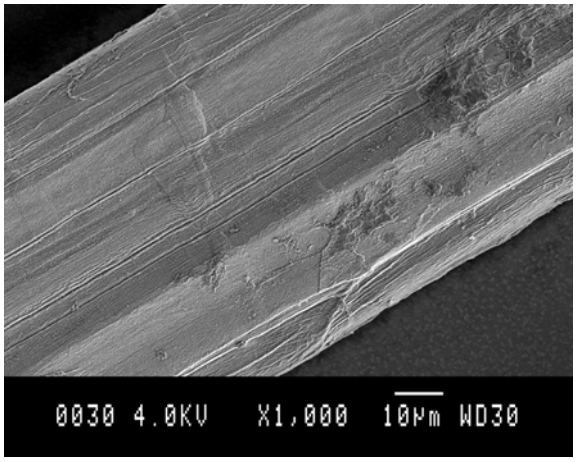

(f) BioPrep 24 hrs

Figure 4.14: Scanning electron micrographs of hemp fibres after various treatments.

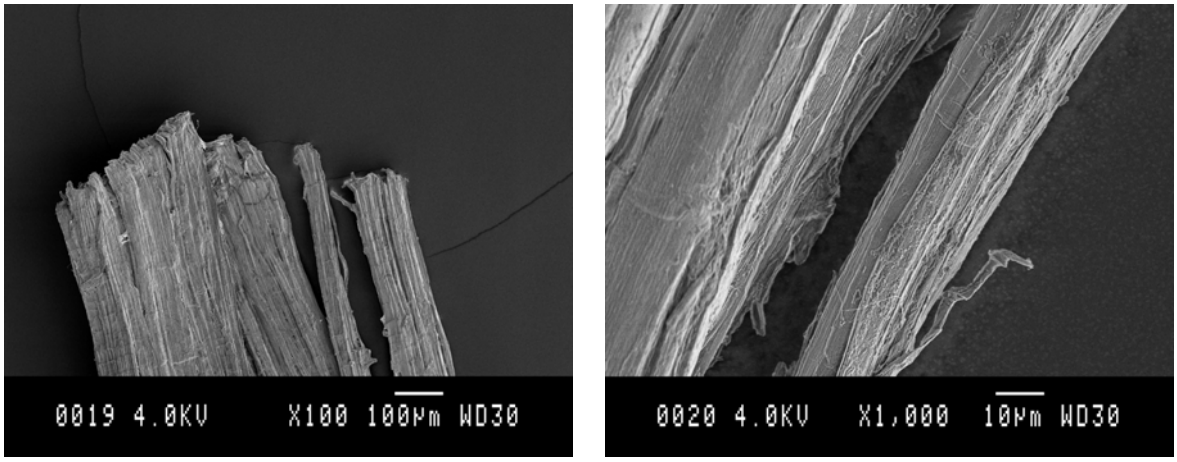

(g) PL 24 hrs

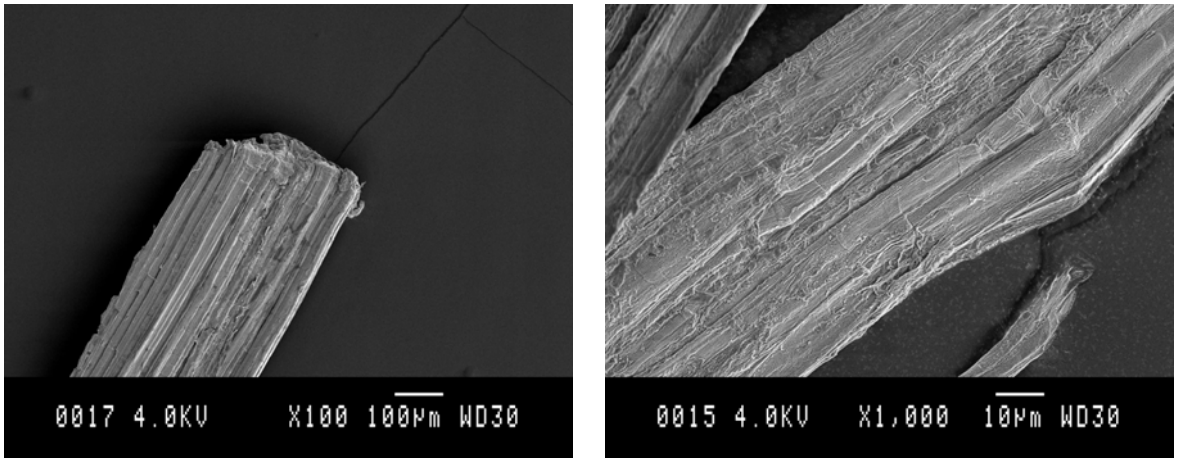

(h) EL 24 hrs

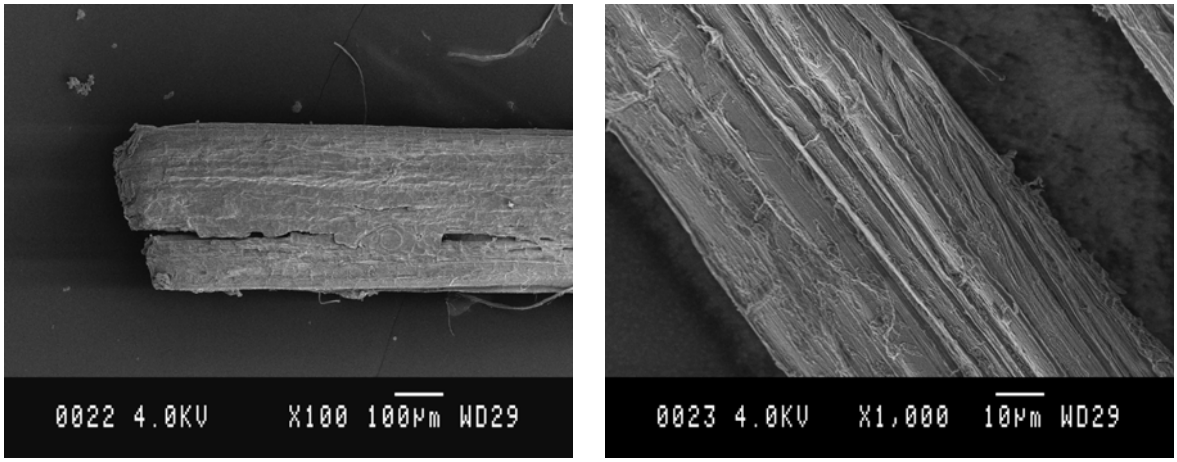

(i) PTE 24 hrs

Figure 4.14: Scanning electron micrographs of hemp fibres after various treatments.

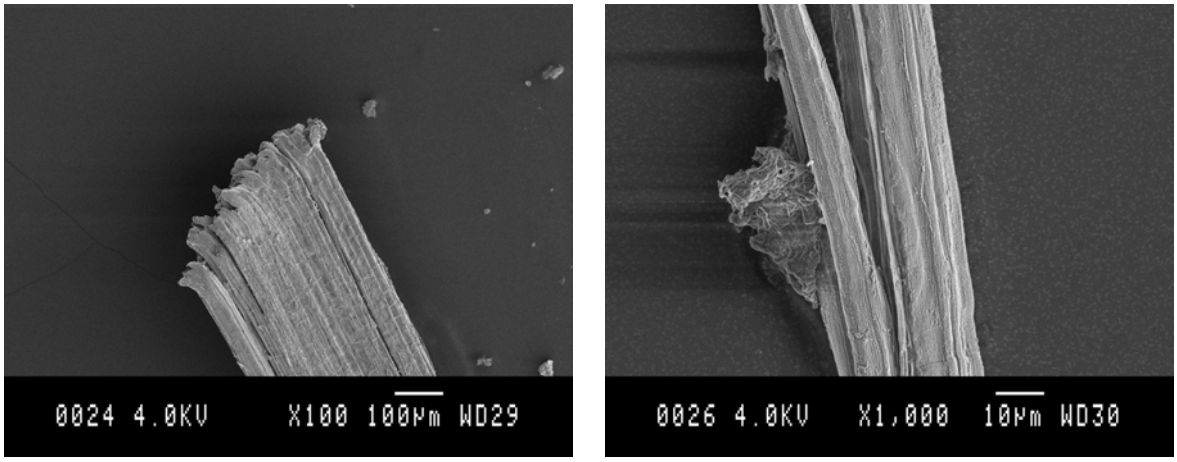

(j) MPE 24 hrs

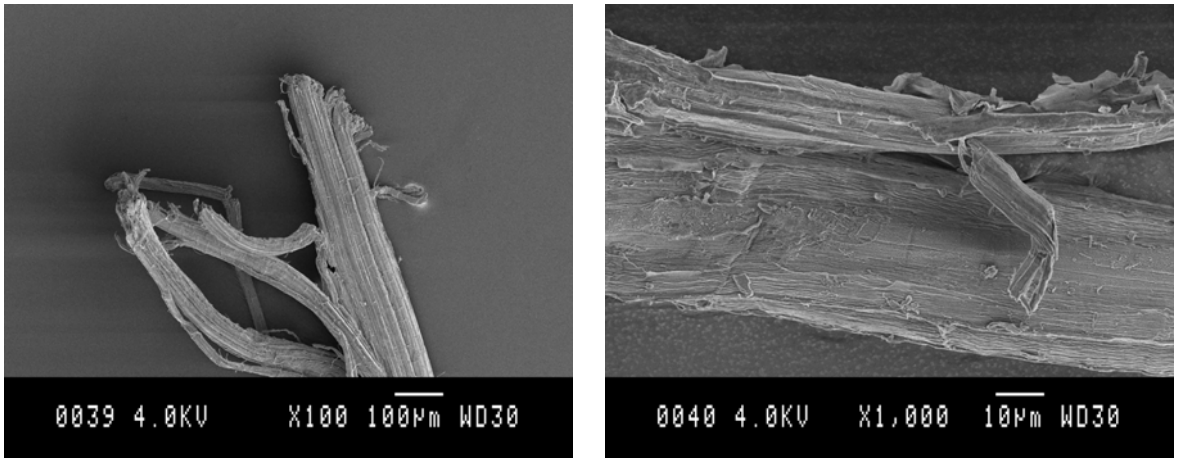

(k) Combinative treatment 24 + 2 hrs

4.2.5 Correlation analysis

The results from correlation analysis carried out in SPSS release 13.0 are listed in Table 4.5 and Table 4.6 at the end of this chapter. The relationship between each pair of variables is also visualized in the scatter plot matrix in Figure 4.15. All correlations significant to the level of 0.05 or 0.01 are coloured for easier orientation. Fields with a green background mark insignificant correlations that represent data concerning the enzyme mixtures, *e.g.* hours (duration of treatment), or enzyme activities and their respective application times which are inherently

correlated. Yellow shading indicates correlations found between variables of discrete values from subjective evaluations, such as texture, colour, Pectinex (duration of Pectinex application), surface and defibrillation. The correlations found for these variables have all been described in the respective chapters (*e.g.* Pectinex treatments increase defibrillation, surface cleanliness, softness and lighter colour).

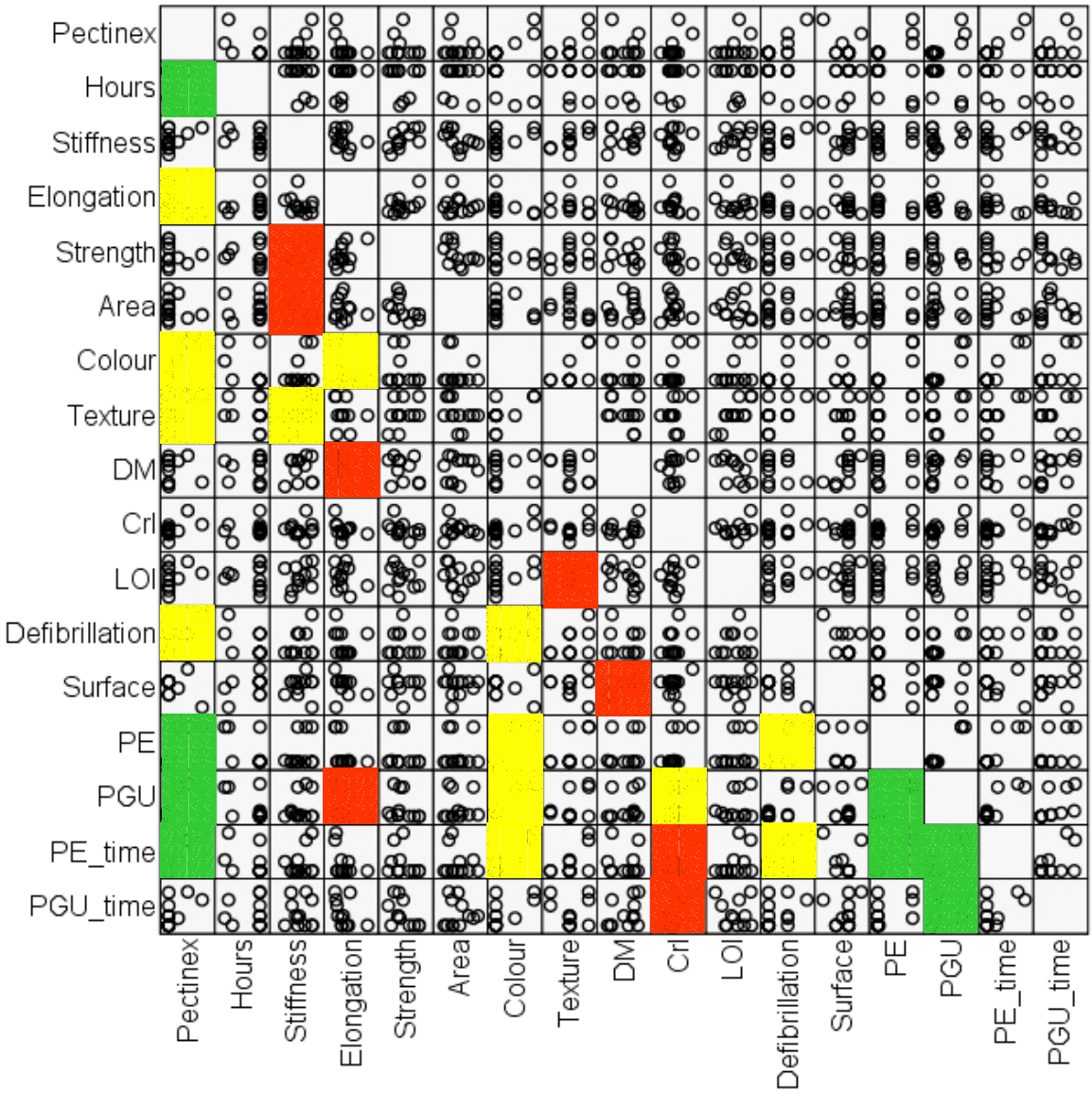

Figure 4.15: Scatter plots of analyzed data pairs.

All significant correlations are coloured and thereby classified into correlations between variables previously defined as mutually dependant (green), correlations between subjectively determined variables (yellow) and correlations between objectively determined numerical variables (red).

The correlations marked with a red box are of greater importance as they represent the relationships between numerical variables which are less easy to detect. An example is the correlation between stiffness, strength and cross-sectional area that has already been mentioned in Chapter 4.2.3. A 3D plot of the data shown in Figure 4.16 allows an even clearer appreciation of how the tensile properties increase with decreasing fibre diameter.

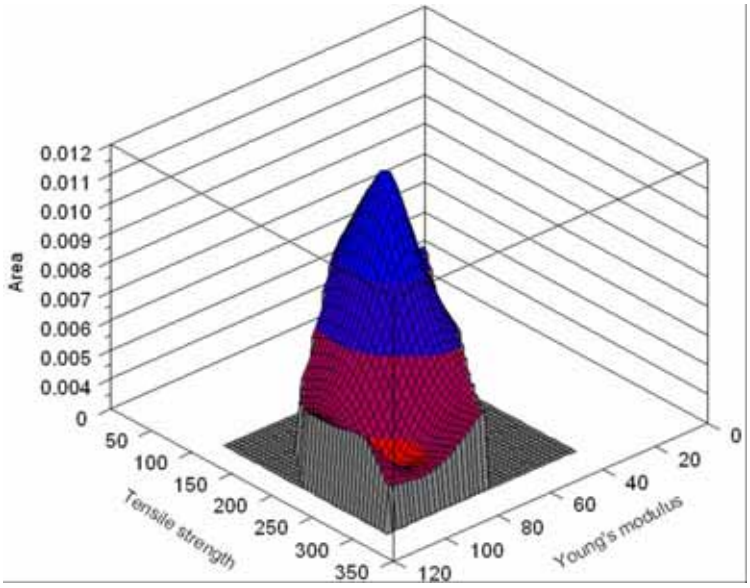

Figure 4.16: 3D plot of stiffness and tensile strength as a function of fibre cross sectional area.

In the fourth column of Figure 4.15, a correlation is marked between elongation at break and both PGU and DM. Both correlations are plotted in Figure 4.17. It can be seen that, with the exception of Scourzyme, the enzyme solutions with higher polygalacturonase lead to fibres with a lower elongation at break, especially after longer treatment durations. Additionally, the elongation at break generally decreases with increasing DM.

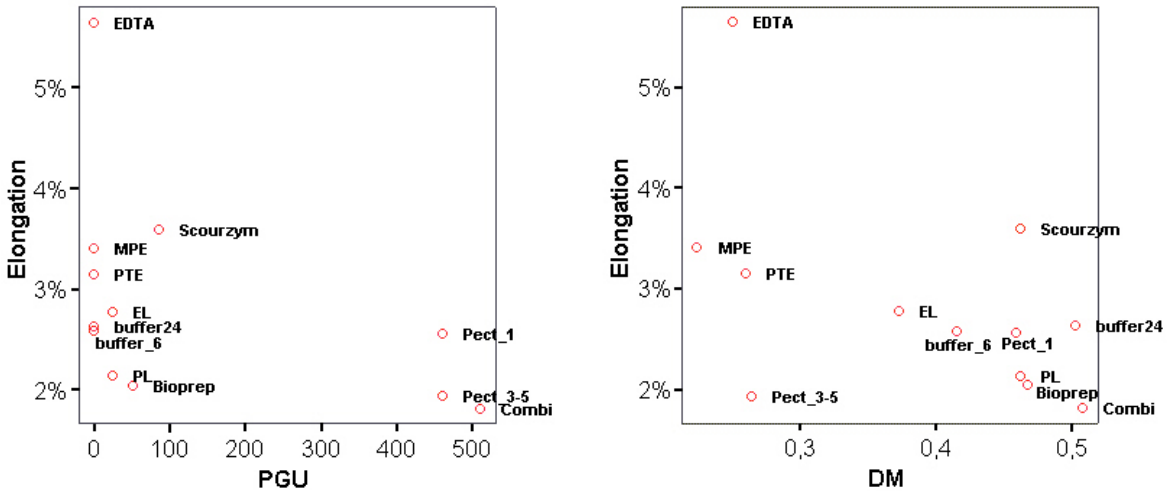

(a) (b)

Figure 4.17: Plot of elongation at break versus polygalacturonase activity.

Correlations have also been identified between the crystallinity index and both PE and PGU activity. PE_time – CrI correlation was found to be 0.612 (Spearman), while the PGU – CrI correlation equals 0.733 for linear (Pearson's) and 0.679 for Spearman correlation. Accordingly, the plot in Figure 4.18 illustrates the increasing crystallinity for higher polygalacturonase activity (a) and the weaker correlation with pectinesterase activity (b).

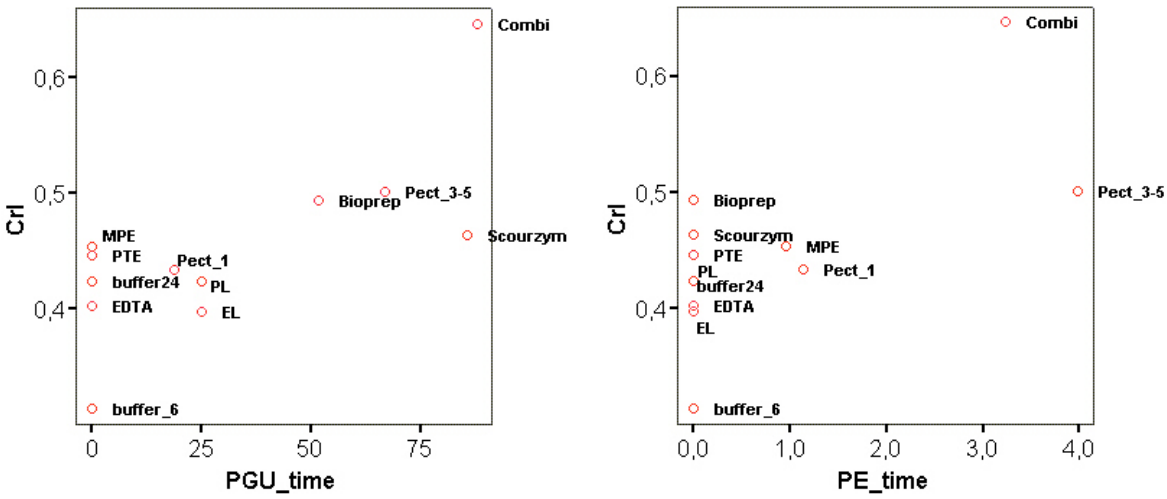

(a) (b)

Figure 4.18: Correlation of crystallinity index with the (a) polygalacturonase and (b) pectinesterase activities.

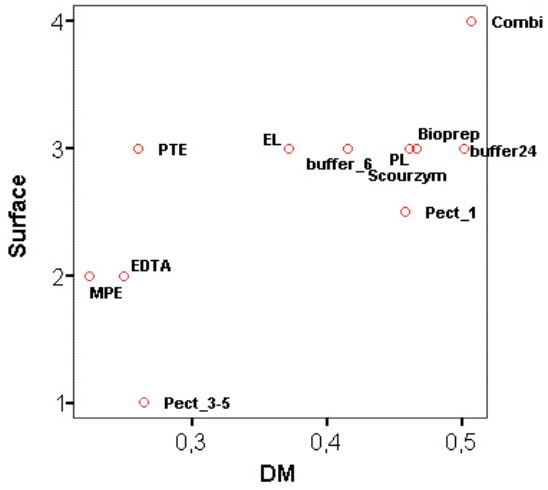

Figure 4.19: Plot of surface properties versus degree of methylesterification.

Another interesting correlation revealed by SPSS is shown in Figure 4.19. Apparently, surface cleanliness improves with decreasing DM. This observation could be related to the spatial distribution of the different kinds of pectic substances. The non- or low-esterified fractions form calcium bridges both within molecules and with other polysaccharides and these bridges have been reported to form a strengthening part of the cell wall structure and are found predominantly between the microfibrils [15, 102, 103, 110]. As has been mentioned before, a decrease in DM can be caused by a preferred degradation of the outer, higher esterified pectic substances. This degradation would lead to a removal of the covering outer layer, uncovering and eventually releasing the microfibrils from their bundle.

The last relation worth noting is the correlation between LOI and texture. As can be seen in Figure 4.20, the softness of the fibre increases with the lateral order index. Unfortunately, texture is an ordinal variable determined subjectively so that a more detailed analysis of this interesting correlation will prove difficult without additional numerical objective data.

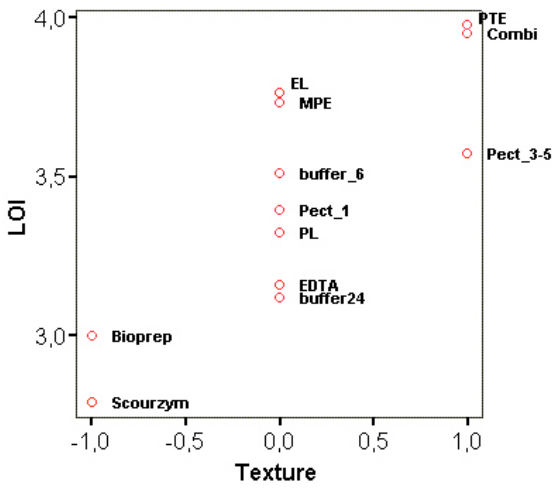

Figure 4.20: Plot of LOI versus texture.

Correlations

		Pectinex	Hours	Stiffness	Elongation	Strength	Area	Colour	Texture	DM	CrI	LOI	Defibrillation	Surface	PE	PGU	PE_time	PGU_time
Pectinex	Pearson's correlation	1	-0.536	0.440	-0.435	-0.150	-0.187	,954(**)	,604(*)	-0.088	0.573	0.308	,815(**)	-0.408	,877(**)	,865(**)	,965(**)	0.552
	Significance		0.073	0.153	0.157	0.641	0.562	0.000	0.038	0.785	0.052	0.330	0.001	0.188	0.000	0.000	0.000	0.063
	N	12	12	12	12	12	12	12	12	12	12	12	12	12	12	12	12	12
Hours	Pearson's correlation	-0.536	1	-0.274	0.285	-0.055	0.021	-0.471	-0.224	0.033	0.220	-0.074	-0.480	0.526	-,604(*)	-0.548	-0.421	0.013
	Significance	0.073		0.388	0.370	0.864	0.948	0.122	0.484	0.920	0.493	0.820	0.114	0.079	0.037	0.065	0.173	0.969
	N	12	12	12	12	12	12	12	12	12	12	12	12	12	12	12	12	12
Stiffness	Pearson's correlation	0.440	-0.274	1	-0.295	,618(*)	-0.534	0.401	,708(*)	0.046	0.081	0.326	0.328	0.107	0.310	0.267	0.332	-0.055
	Significance	0.153	0.388		0.352	0.032	0.074	0.197	0.010	0.887	0.802	0.301	0.297	0.740	0.326	0.402	0.291	0.865
	N	12	12	12	12	12	12	12	12	12	12	12	12	12	12	12	12	12
Elongation	Pearson's correlation	-0.435	0.285	-0.295	1	0.517	-0.121	-0.462	-0.207	-0.514	-0.371	-0.258	-0.143	-0.308	-0.431	-0.454	-0.427	-0.398
	Significance	0.157	0.370	0.352		0.085	0.708	0.130	0.518	0.088	0.235	0.419	0.659	0.330	0.162	0.138	0.166	0.200
	N	12	12	12	12	12	12	12	12	12	12	12	12	12	12	12	12	12
Strength	Pearson's correlation	-0.150	-0.055	,618(*)	0.517	1	-0.500	-0.217	0.342	-0.319	-0.447	0.022	0.014	-0.098	-0.228	-0.293	-0.259	-0.539
	Significance	0.641	0.864	0.032	0.085		0.098	0.497	0.277	0.312	0.145	0.945	0.965	0.762	0.477	0.356	0.416	0.070
	N	12	12	12	12	12	12	12	12	12	12	12	12	12	12	12	12	12
Area	Pearson's correlation	-0.187	0.021	-0.534	-0.121	-0.500	1	-0.165	-0.384	0.192	-0.128	-0.130	-0.015	-0.093	-0.001	0.018	-0.215	0.006
	Significance	0.562	0.948	0.074	0.708	0.098		0.608	0.218	0.549	0.691	0.688	0.964	0.774	0.998	0.955	0.502	0.985
	N	12	12	12	12	12	12	12	12	12	12	12	12	12	12	12	12	12
Colour	Pearson's correlation	,954(**)	-0.471	0.401	-0.462	-0.217	-0.165	1	,614(*)	0.071	,696(*)	0.374	,765(**)	-0.248	,950(**)	,951(**)	,963(**)	,594(*)
	Significance	0.000	0.122	0.197	0.130	0.497	0.608		0.034	0.825	0.012	0.231	0.004	0.436	0.000	0.000	0.000	0.042
	N	12	12	12	12	12	12	12	12	12	12	12	12	12	12	12	12	12
Texture	Pearson's correlation	,604(*)	-0.224	,708(*)	-0.207	0.342	-0.384	,614(*)	1	-0.358	0.321	,815(**)	0.504	-0.147	0.527	0.455	,629(*)	-0.052
	Significance	0.038	0.484	0.010	0.518	0.277	0.218	0.034		0.254	0.309	0.001	0.095	0.648	0.078	0.137	0.028	0.872
	N	12	12	12	12	12	12	12	12	12	12	12	12	12	12	12	12	12
DM	Pearson's correlation	-0.088	0.033	0.046	-0.514	-0.319	0.192	0.071	-0.358	1	0.204	-0.372	-0.145	,648(*)	0.119	0.203	-0.106	0.387
	Significance	0.785	0.920	0.887	0.088	0.312	0.549	0.825	0.254		0.525	0.234	0.654	0.023	0.713	0.528	0.744	0.214
	N	12	12	12	12	12	12	12	12	12	12	12	12	12	12	12	12	12
CrI	Pearson's correlation	0.573	0.220	0.081	-0.371	-0.447	-0.128	,696(*)	0.321	0.204	1	0.234	0.358	0.152	,592(*)	,651(*)	,682(*)	,733(**)
	Significance	0.052	0.493	0.802	0.235	0.145	0.691	0.012	0.309	0.525		0.464	0.254	0.636	0.043	0.022	0.015	0.007
	N	12	12	12	12	12	12	12	12	12	12	12	12	12	12	12	12	12
LOI	Pearson's correlation	0.308	-0.074	0.326	-0.258	0.022	-0.130	0.374	,815(**)	-0.372	0.234	1	0.117	0.084	0.322	0.260	0.414	-0.146
	Significance	0.330	0.820	0.301	0.419	0.945	0.688	0.231	0.001	0.234	0.464		0.718	0.795	0.307	0.415	0.181	0.650
	N	12	12	12	12	12	12	12	12	12	12	12	12	12	12	12	12	12
Defibrillation	Pearson's correlation	,815(**)	-0.480	0.328	-0.143	0.014	-0.015	,765(**)	0.504	-0.145	0.358	0.117	1	-0.548	,743(**)	,717(**)	,744(**)	0.333
	Significance	0.001	0.114	0.297	0.659	0.965	0.964	0.004	0.095	0.654	0.254	0.718		0.065	0.006	0.009	0.006	0.290
	N	12	12	12	12	12	12	12	12	12	12	12	12	12	12	12	12	12
Surface	Pearson's correlation	-0.408	0.526	0.107	-0.308	-0.098	-0.093	-0.248	-0.147	,648(*)	0.152	0.084	-0.548	1	-0.335	-0.252	-0.356	0.194
	Significance	0.188	0.079	0.740	0.330	0.762	0.774	0.436	0.648	0.023	0.636	0.795	0.065		0.286	0.429	0.256	0.546
	N	12	12	12	12	12	12	12	12	12	12	12	12	12	12	12	12	12
PE	Pearson's correlation	,877(**)	-,604(*)	0.310	-0.431	-0.228	-0.001	,950(**)	0.527	0.119	,592(*)	0.322	,743(**)	-0.335	1	,989(**)	,874(**)	0.483
	Significance	0.000	0.037	0.326	0.162	0.477	0.998	0.000	0.078	0.713	0.043	0.307	0.006	0.286		0.000	0.000	0.111
	N	12	12	12	12	12	12	12	12	12	12	12	12	12	12	12	12	12
PGU	Pearson's correlation	,865(**)	-0.548	0.267	-0.454	-0.293	0.018	,951(**)	0.455	0.203	,651(*)	0.260	,717(**)	-0.252	,989(**)	1	,863(**)	,596(*)
	Significance	0.000	0.065	0.402	0.138	0.356	0.955	0.000	0.137	0.528	0.022	0.415	0.009	0.429	0.000		0.000	0.041
	N	12	12	12	12	12	12	12	12	12	12	12	12	12	12	12	12	12
PE_time	Pearson's correlation	,965(**)	-0.421	0.332	-0.427	-0.259	-0.215	,963(**)	,629(*)	-0.106	,682(*)	0.414	,744(**)	-0.356	,874(**)	,863(**)	1	0.554
	Significance	0.000	0.173	0.291	0.166	0.416	0.502	0.000	0.028	0.744	0.015	0.181	0.006	0.256	0.000	0.000		0.061
	N	12	12	12	12	12	12	12	12	12	12	12	12	12	12	12	12	12
PGU_time	Pearson's correlation	0.552	0.013	-0.055	-0.398	-0.539	0.006	,594(*)	-0.052	0.387	,733(**)	-0.146	0.333	0.194	0.483	,596(*)	0.554	1
	Significance	0.063	0.969	0.865	0.200	0.070	0.985	0.042	0.872	0.214	0.007	0.650	0.290	0.546	0.111	0.041	0.061	
	N	12	12	12	12	12	12	12	12	12	12	12	12	12	12	12	12	12

*. The correlation is significant to the level of 0.05

**. The correlation is significant to the level of 0.01

Table 4.5: Pearson's correlation

Correlations

		Pectinex	Hours	Stiffness	Elongation	Strength	Area	Colour	Texture	DM	CrI	LOI	Defibrillation	Surface	PE	PGU	PE_time	PGU_time
Pectinex	Coefficient of correlation	1.000	-,602(*)	0.358	-,661(*)	-0.073	-0.147	,997(**)	,580(*)	0.165	0.569	0.321	,748(**)	-0.237	,894(**)	,774(**)	,907(**)	0.524
	Significance	.	0.038	0.253	0.019	0.821	0.649	0.000	0.048	0.608	0.053	0.309	0.005	0.457	0.000	0.003	0.000	0.080
	N	12	12	12	12	12	12	12	12	12	12	12	12	12	12	12	12	12
Hours	Coefficient of correlation	-,602(*)	1.000	-0.220	0.367	-0.229	0.101	-0.568	-0.217	0.129	0.037	-0.073	-0.434	0.516	-0.535	-0.330	-0.519	0.000
	Significance	0.038	.	0.491	0.240	0.473	0.755	0.054	0.497	0.691	0.910	0.821	0.158	0.086	0.073	0.295	0.084	1.000
	N	12	12	12	12	12	12	12	12	12	12	12	12	12	12	12	12	12
Stiffness	Coefficient of correlation	0.358	-0.220	1.000	-0.364	,608(*)	-,643(*)	0.350	,777(**)	0.112	0.007	0.392	0.331	0.126	0.092	-0.047	0.141	-0.120
	Significance	0.253	0.491	.	0.245	0.036	0.024	0.265	0.003	0.729	0.983	0.208	0.293	0.697	0.775	0.884	0.661	0.711
	N	12	12	12	12	12	12	12	12	12	12	12	12	12	12	12	12	12
Elongation	Coefficient of correlation	-,661(*)	0.367	-0.364	1.000	0.385	0.035	-,667(*)	-0.331	-,587(*)	-0.455	-0.168	-0.462	-0.220	-0.496	-,644(*)	-0.516	-0.545
	Significance	0.019	0.240	0.245	.	0.217	0.914	0.018	0.293	0.045	0.138	0.602	0.130	0.492	0.101	0.024	0.086	0.067
	N	12	12	12	12	12	12	12	12	12	12	12	12	12	12	12	12	12
Strength	Coefficient of correlation	-0.073	-0.229	,608(*)	0.385	1.000	-0.510	-0.097	0.311	-0.308	-0.462	-0.028	0.140	-0.252	-0.252	-0.444	-0.241	-0.541
	Significance	0.821	0.473	0.036	0.217	.	0.090	0.765	0.324	0.331	0.131	0.931	0.665	0.430	0.429	0.148	0.450	0.069
	N	12	12	12	12	12	12	12	12	12	12	12	12	12	12	12	12	12
Area	Coefficient of correlation	-0.147	0.101	-,643(*)	0.035	-0.510	1.000	-0.152	-0.520	0.098	-0.112	-0.280	-0.028	-0.149	-0.025	0.222	-0.083	0.174
	Significance	0.649	0.755	0.024	0.914	0.090	.	0.637	0.083	0.762	0.729	0.379	0.931	0.643	0.938	0.488	0.797	0.588
	N	12	12	12	12	12	12	12	12	12	12	12	12	12	12	12	12	12
Colour	Coefficient of correlation	,997(**)	-0.568	0.350	-,667(*)	-0.097	-0.152	1.000	,581(*)	0.203	0.575	0.336	,737(**)	-0.181	,896(**)	,783(**)	,904(**)	0.536
	Significance	0.000	0.054	0.265	0.018	0.765	0.637	.	0.047	0.528	0.050	0.286	0.006	0.573	0.000	0.003	0.000	0.073
	N	12	12	12	12	12	12	12	12	12	12	12	12	12	12	12	12	12
Texture	Coefficient of correlation	,580(*)	-0.217	,777(**)	-0.331	0.311	-0.520	,581(*)	1.000	-0.197	0.201	,808(**)	0.472	-0.053	0.502	0.098	0.544	-0.033
	Significance	0.048	0.497	0.003	0.293	0.324	0.083	0.047	.	0.539	0.531	0.001	0.121	0.870	0.096	0.761	0.067	0.919
	N	12	12	12	12	12	12	12	12	12	12	12	12	12	12	12	12	12
DM	Coefficient of correlation	0.165	0.129	0.112	-,587(*)	-0.308	0.098	0.203	-0.197	1.000	0.245	-0.350	0.016	,684(*)	-0.017	0.469	-0.042	0.516
	Significance	0.608	0.691	0.729	0.045	0.331	0.762	0.528	0.539	.	0.443	0.265	0.961	0.014	0.959	0.124	0.898	0.086
	N	12	12	12	12	12	12	12	12	12	12	12	12	12	12	12	12	12
CrI	Coefficient of correlation	0.569	0.037	0.007	-0.455	-0.462	-0.112	0.575	0.201	0.245	1.000	0.070	0.287	0.024	0.576	,662(*)	,612(*)	,679(*)
	Significance	0.053	0.910	0.983	0.138	0.131	0.729	0.050	0.531	0.443	.	0.829	0.366	0.942	0.050	0.019	0.035	0.015
	N	12	12	12	12	12	12	12	12	12	12	12	12	12	12	12	12	12
LOI	Coefficient of correlation	0.321	-0.073	0.392	-0.168	-0.028	-0.280	0.336	,808(**)	-0.350	0.070	1.000	0.096	0.074	0.395	-0.004	0.408	-0.091
	Significance	0.309	0.821	0.208	0.602	0.931	0.379	0.286	0.001	0.265	0.829	.	0.767	0.819	0.204	0.991	0.188	0.779
	N	12	12	12	12	12	12	12	12	12	12	12	12	12	12	12	12	12
Defibrillation	Coefficient of correlation	,748(**)	-0.434	0.331	-0.462	0.140	-0.028	,737(**)	0.472	0.016	0.287	0.096	1.000	-0.395	,608(*)	0.539	,626(*)	0.346
	Significance	0.005	0.158	0.293	0.130	0.665	0.931	0.006	0.121	0.961	0.366	0.767	.	0.204	0.036	0.070	0.029	0.271
	N	12	12	12	12	12	12	12	12	12	12	12	12	12	12	12	12	12
Surface	Coefficient of correlation	-0.237	0.516	0.126	-0.220	-0.252	-0.149	-0.181	-0.053	,684(*)	0.024	0.074	-0.395	1.000	-0.364	0.074	-0.379	0.286
	Significance	0.457	0.086	0.697	0.492	0.430	0.643	0.573	0.870	0.014	0.942	0.819	0.204	.	0.245	0.820	0.224	0.367
	N	12	12	12	12	12	12	12	12	12	12	12	12	12	12	12	12	12
PE	Coefficient of correlation	,894(**)	-0.535	0.092	-0.496	-0.252	-0.025	,896(**)	0.502	-0.017	0.576	0.395	,608(*)	-0.364	1.000	,630(*)	,990(**)	0.345
	Significance	0.000	0.073	0.775	0.101	0.429	0.938	0.000	0.096	0.959	0.050	0.204	0.036	0.245	.	0.028	0.000	0.272
	N	12	12	12	12	12	12	12	12	12	12	12	12	12	12	12	12	12
PGU	Coefficient of correlation	,774(**)	-0.330	-0.047	-,644(*)	-0.444	0.222	,783(**)	0.098	0.469	,662(*)	-0.004	0.539	0.074	,630(*)	1.000	,624(*)	,896(**)
	Significance	0.003	0.295	0.884	0.024	0.148	0.488	0.003	0.761	0.124	0.019	0.991	0.070	0.820	0.028	.	0.030	0.000
	N	12	12	12	12	12	12	12	12	12	12	12	12	12	12	12	12	12
PE_time	Coefficient of correlation	,907(**)	-0.519	0.141	-0.516	-0.241	-0.083	,904(**)	0.544	-0.042	,612(*)	0.408	,626(*)	-0.379	,990(**)	,624(*)	1.000	0.376
	Significance	0.000	0.084	0.661	0.086	0.450	0.797	0.000	0.067	0.898	0.035	0.188	0.029	0.224	0.000	0.030	.	0.228
	N	12	12	12	12	12	12	12	12	12	12	12	12	12	12	12	12	12
PGU_time	Coefficient of correlation	0.524	0.000	-0.120	-0.545	-0.541	0.174	0.536	-0.033	0.516	,679(*)	-0.091	0.346	0.286	0.345	,896(**)	0.376	1.000
	Significance	0.080	1.000	0.711	0.067	0.069	0.588	0.073	0.919	0.086	0.015	0.779	0.271	0.367	0.272	0.000	0.228	.
	N	12	12	12	12	12	12	12	12	12	12	12	12	12	12	12	12	12

*. The correlation is significant to the level of 0.05

**. The correlation is significant to the level of 0.01

Table 4.6: Spearman correlations

4.3 Experiments for cross-validation of properties measured by AFM

4.3.1 Visual evaluation

For the AFM study, the buffer solution, alkalization, alkalization + acetylation and Pectinex treatments were chosen as described in Chapter 3.2.2. Samples were analyzed with respect to colour and texture. The results and pictures of all samples are compiled in Figure 4.21 and Table 4.7.

The alkalized, acetylated and enzymatically treated fibres all featured a slightly lighter colour in comparison to the sample treated in buffer solution. Alkalization and acetylation made the fibres harder to the touch, while the enzymes yielded a softer fibre texture. Macroscopically speaking, alkalization and enzyme treatment both resulted in a comparable level of defibrillation superior to the fibres treated in buffer solution only. Acetylation did not have any macroscopic effect on fibre separation.

Table 4.7: Summary of subjectively determined sample properties after enzyme treatments.

Treatment	*Colour*	*Texture*
Buffer pH4.5 6 hrs	No change	Medium
Pectinex 3.5 hrs	Lighter	Soft
Alkalized	Lighter	Medium-hard
Acetylated	Lighter	Hard

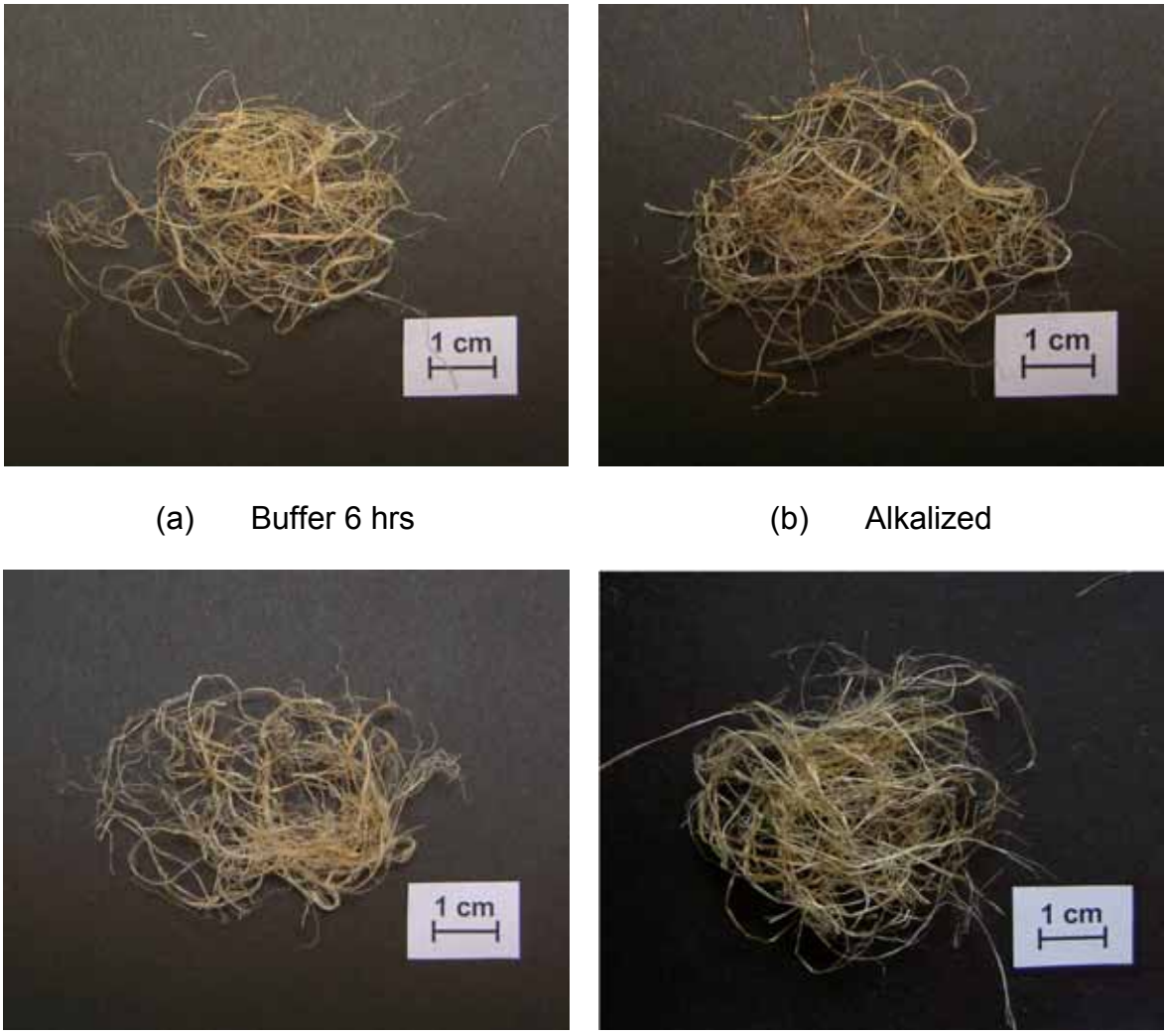

(a) Buffer 6 hrs (b) Alkalized

(c) Alkalized + acetylated (d) Pectinex 3.5 hrs

Figure 4.21: Samples after treatments.

4.3.2 FTIR analysis

The spectra recorded for the four samples of interest for the cross-validation of AFM measurements showed far more differences than those described before in Chapter 4.2.2. This was expected as the treatments were chosen to yield fibres of greatest possible dissimilarity. The baseline-corrected and area-normalized spectra are shown in Figure 4.22 and Figure 4.23 to Figure 4.27, respectively.

For the description of the FT-IR peaks the following abbreviations are used

- vw very weak
- w weak
- m medium
- s strong
- vs very strong
- sh shoulder
- → peak shifted to

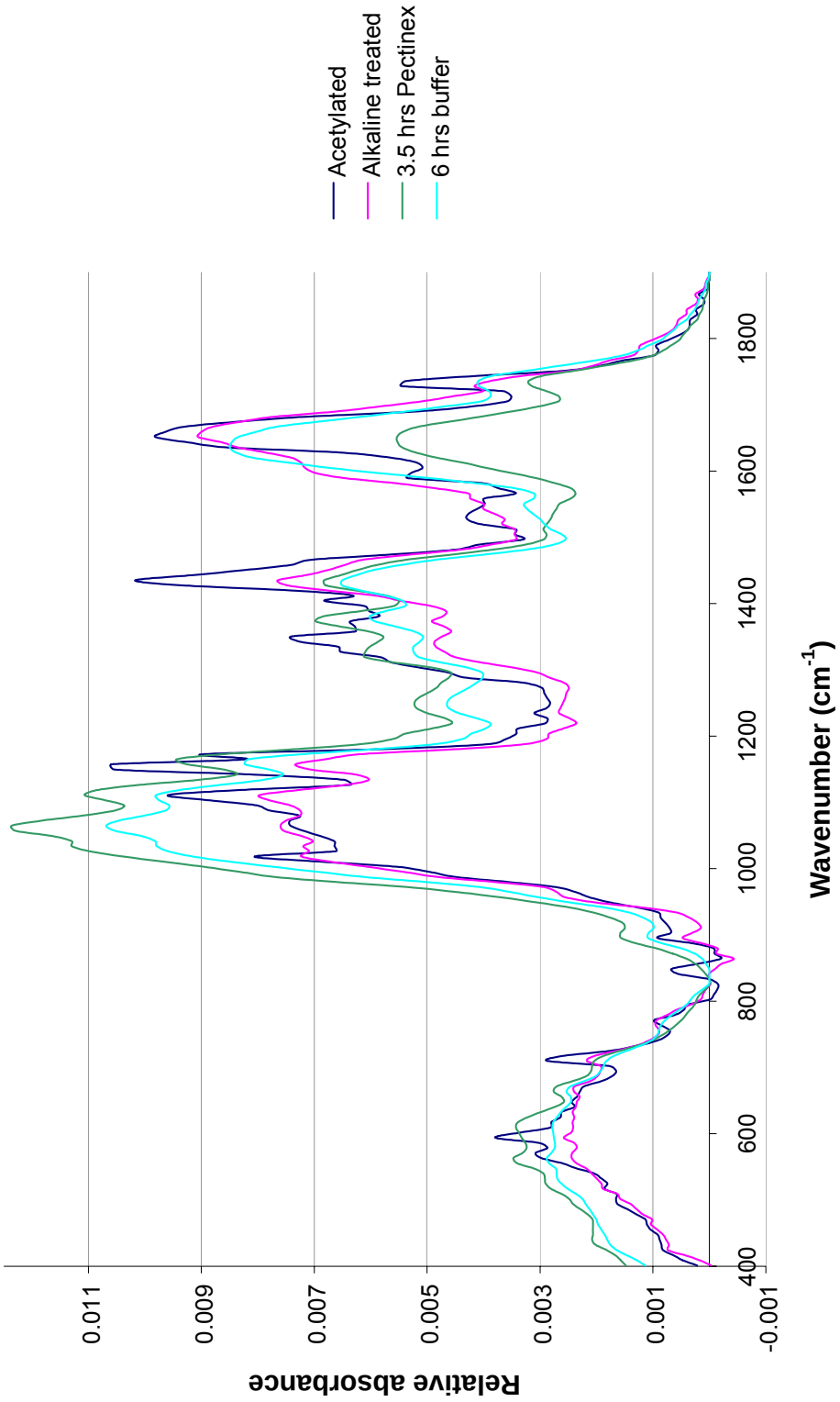

Figure 4.22: FTIR spectra for acetylated, alkaline-treated, enzyme-treated and untreated fibres.

500-950 cm^{-1}

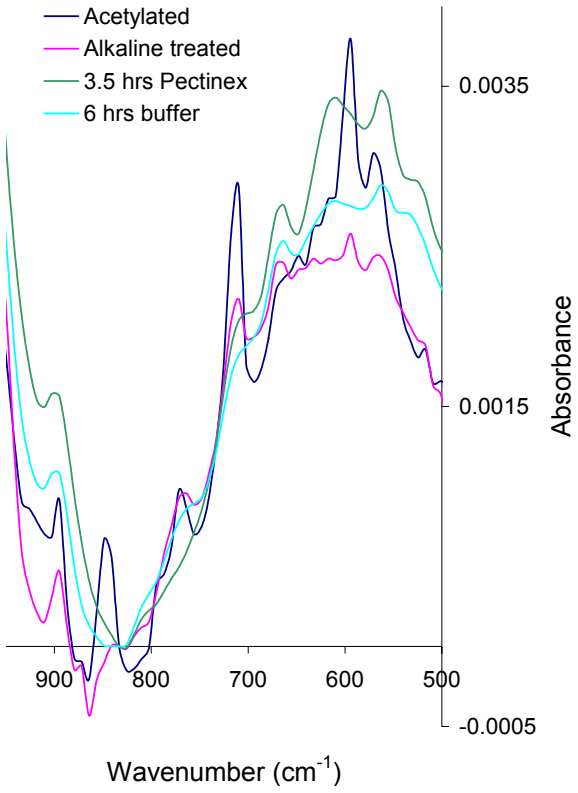

Figure 4.23: FT-IR spectrum at 500-950 cm^{-1}

The absorbance at 898 cm^{-1} shifted to lower wavenumbers and increased after alkalization as was reported by Oh *et al*. [24]. The absorbance at this wavenumber is also used to determine the lateral order index (LOI) as will be described in the Section *Crystallinity,* page 108.

Unfortunately, the lower wavenumbers below approximately 800 cm^{-1} in the near infrared region are hardly used for spectroscopic analysis. Therefore, no more explicit assignments than those presented in Table 4.8 could be found in the literature. However, the peaks at 771 and 840 cm^{-1} also appeared in spectra of acetylated hemp published by Tserki *et al*.[53].

Table 4.8: Peaks of the spectral region 500 – 950 cm^{-1}

cm^{-1}	*Buffer*	*Pectinex*	*Alkaline*	*Acetylated*	*Assignment*
516				vw	
563	w	m	w	w → 570	
594			w	s	
663	w	w	w	vw → 648	670 C-OH out of plane bending mode
709	sh	sh	m	s	715 rocking vibration CH_2 in cellulose I_β
771	sh		w	m	In spectra of acetylated hemp by Tserki [53]
840			w	s → 848	858 C-H out of plane in position 2, 5, 6 of G units (MWL)
897	w → 898	w → 898	m→ 894	w→ 894	895-892 Anomere C-groups, C_1-H deformation, ring valence vibration

950-1200 cm^{-1}

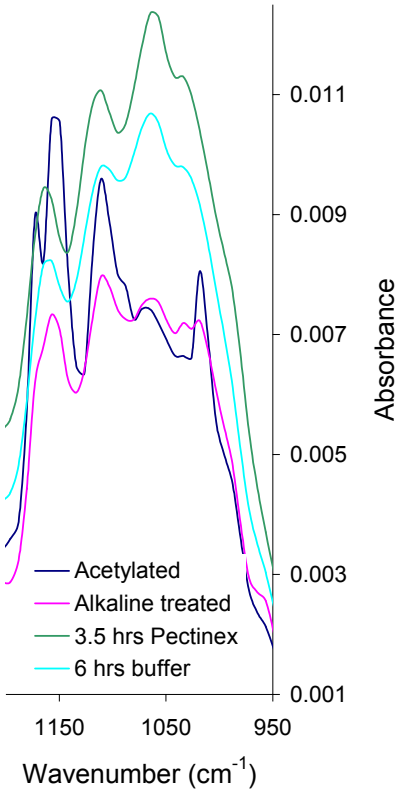

Figure 4.24: FT-IT spectrum at 950-1200 cm^{-1}.

In the spectral window shown in Figure 4.24, overlapping peaks from all major components can be expected. However, due to the far larger cellulose content, the latter will make the main contribution. The treatments applied to the fibres show clear tendencies as to spectral changes in this region. Alkalization results in decreased absorption in general. Enzyme and untreated fibres show strong peaks at 1064 cm^{-1} and acetylation increases absorbance at 1018, 1109, and around 1160 cm^{-1} as has also been presented by Tserki *et al*. [53]. A slightly stronger formation of local extrema can be observed after enzyme treatment in comparison to the very similar spectrum of the buffer treated sample.

According to Windeisen *et al*. [111], the described sharpening of peaks should be explained by progressing depolymerisation of the polysaccharides, which enables “easier” stimulation of absorption bands. Research on the impact of cellulase on cellulose structure was also carried out by Cao and Tan [112, 113]; they found evidence demonstrating that cellulase simultaneously decreases the degree of polymerization and increases the crystallinity index as amorphous cellulose is more readily hydrolyzed than crystalline cellulose I. As will be shown below, evidence for the latter conclusion could likewise be found in the present work. A decrease in the degree of polymerization has also been reported by Gassan and Bledzki, [22].

Table 4.9: Peaks of the spectral region 950 -1200 cm^{-1}

cm^{-1}	*Buffer*	*Pectinex*	*Alkaline*	*Acetylated*	*Assignment*
1018			w	s	1015-1060 C-O valence vibration, mainly from C3-O3H
1064	s	s	m	w →1072	
1109	w	m	s	s	1107-1110 Ring asymmetric valence vibration
1157-1172	s 1164	s 1164	s 1157 sh 1172	s 1157 m 1172	1125-1162 C-O-C asymmetric valence vibration

1300-1500 cm^{-1}

The band at 1426 cm^{-1} is assigned to CH_2 bending vibration in crystallised cellulose and amorphous cellulose mixture. A shift to 1430 cm^{-1} is characteristic of crystallised cellulose I (Liang and Marchessault, [114]) and thus this peak is used to calculate the LOI.

A second indicator for structural changes in cellulose is reported by Colom, [115]. The spectroscopic evolution of the doublet at 1335-1316 cm^{-1} assigned to the cellulosic component of wood and only appearing in celluloses with a high crystallised cellulose I content, [46], indicates an increase in crystallinity of hemp fibre cellulose.

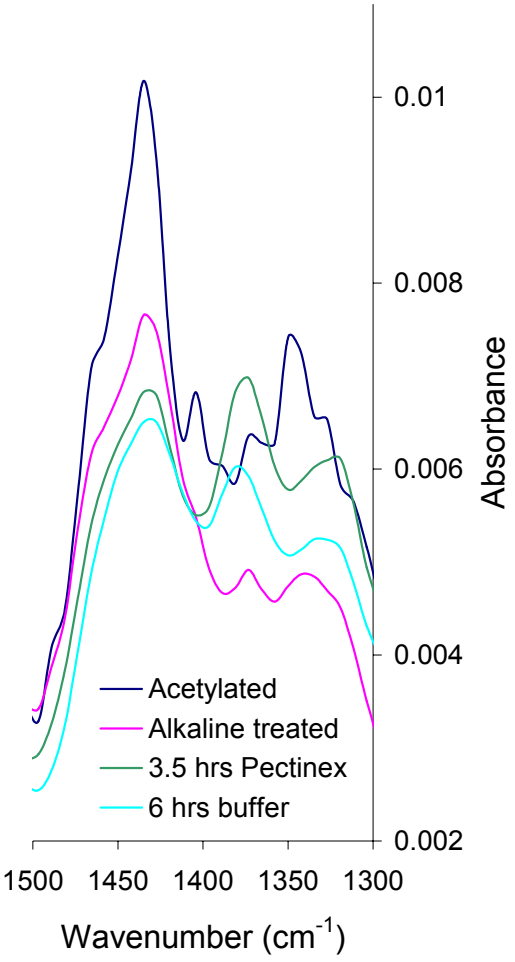

Figure 4.25: FT-IR spectrum at 1300-1500 cm^{-1}.

Previous studies by Colom *et al*. have shown that the band at 1335 cm^{-1} is composed of a broad, poorly defined main band with an accompanying shoulder. When the crystallised cellulose I and/or II content is increased, this band is gradually converted into a perfectly defined doublet. From this doublet the ratio 1335/1316 can be used to monitor the conversion process. The decrease observed for this ratio can be interpreted as an increase in the crystallised cellulose I content. No real doublet formation can be observed in the presented spectrum in Figure 4.25. As a general observation it can however be noted that in comparison to buffer treated fibre, the enzyme treatment yields a higher absorption towards 1319 cm^{-1} and alkaline and acetylation treatment result in an increased absorption towards 1335-1350 cm^{-1}. It can be concluded from this observation that Pectinex slightly increases the cellulose I content. Alkaline treatment on the other hand does cause a shift towards 1335 cm^{-1} possibly indicating beginning conversion of cellulose I to cellulose II. Acetylation amplifies the latter peak and induces a further shift to 1350 cm^{-1} that has also been measured by Tserki *et al*. [53]. Additionally, a general decrease of absorbance was found for the bands at 1375, 1335 and 1316 cm^{-1} after mercerization in accordance with results presented by Oh [24]. An increase in absorption for a peak at 1369 cm^{-1} has been reported to indicate successful acetylation. No increased peak could be found at 1369 cm^{-1}, however, both neighbouring peaks at 1350 and 1373 cm^{-1} show a higher absorption in comparison to the basic, alkaline treated fibres.

A peak at 1404 cm^{-1} was recorded for the acetylated fibres only, but no assignment was found in the literature.

Table 4.10: Peaks of the spectral region 1300-1500 cm^{-1}

cm^{-1}	*Buffer*	*Pectinex*	*Alkaline*	*Acetylated*	*Assignment*
1319-1350	m 1326	m 1319	m 1342	sh 1311 w 1326	1315-1317 CH_2 rocking vibration, C, Holo 1335-1365 OH plane deformation vibration
1373	s → 1380	s	m	m	1373-1375 CH deformation vibration
1404				m	
1431	s	s	s 1435	vs 1435	1435 HOC bending

1550-1750 cm^{-1}

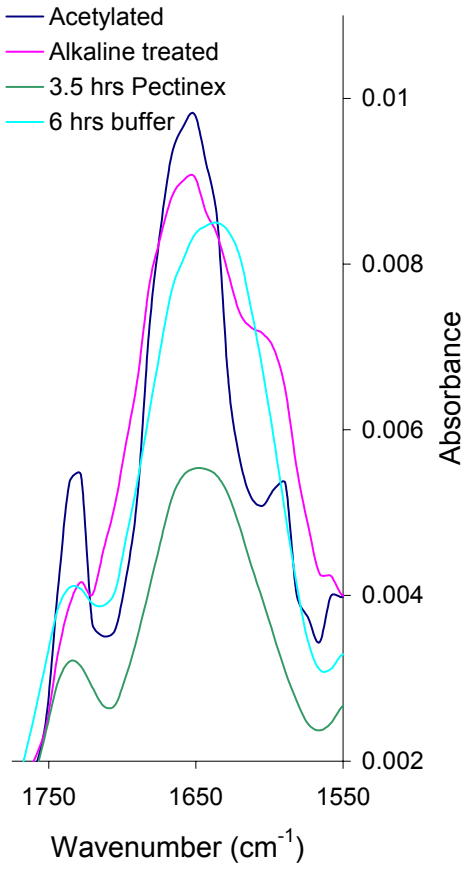

Figure 4.26: FT-IR spectrum at 1550-1750 cm^{-1}.

Both acetylated and alkalized fibres show the most prominent peaks at 1598 cm^{-1}, shifted towards higher wavenumbers at the broad peak at 1635-1651 cm^{-1} and at 1728 cm^{-1} in acetylated fibre. All three peaks are assigned to C=O vibrations. Especially the latter, strong absorption in acetylated fibres is associated with C=O in acetyl and COOH-groups. Naturally, the same peak was decreased after alkalization only due to the high pH that leads to ionization of the carboxyl group.

Table 4.11: Peaks of the spectral region 1550-1750 cm^{-1}.

cm^{-1}	*Buffer*	*Pectinex*	*Alkaline*	*Acetylated*	*Assignment*
1558			w	W	NH bending [62]
1598			sh	W	1593-1605 Aromatic skeletal vibration plus C=O stretch; S>G; G condensed > G esterified in MWL
1635-1651	s 1635	s 1647	s 1651	s 1651	1635 adsorbed water 1655-1675 C=O stretch
1735	w	m	vw 1728	s 1728	1725-1730 C=O valence vibration of acetyl- or COOH-groups

2500-4000 cm^{-1}

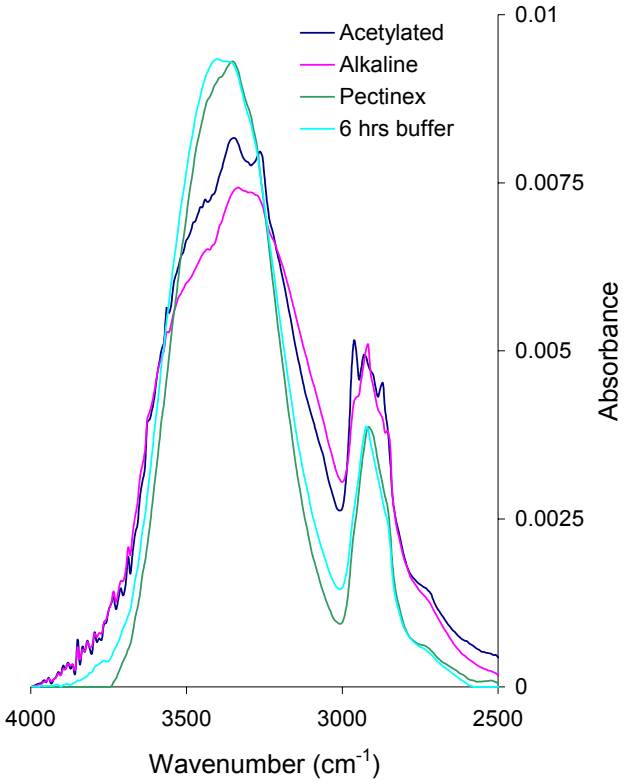

The lowering of the intensities of the OH stretching band at 3337 cm^{-1} is a result of alkalization [53]. Formation of additional peaks around the absorbance at 2900 cm^{-1} can also be seen in spectra recorded by Tserki *et al*. [53] of acetylated hemp.

Figure 4.27: FT-IR spectrum at 2500-4000 cm^{-1}.

Table 4.12: Peaks of the spectral region 2500-4000 cm^{-1}

cm^{-1}	*Buffer*	*Pectinex*	*Alkaline*	*Acetylated*	*Assignment*
2869				w	CH_2 valence vibrations Hydrogen bonded OH-groups
2923	s	s	s	s	
2962			sh	w	
3363-3409	s 3363-3409	s 3363	s 3363-3271 sh 3409	w 3271 s 3363 sh 3409	

Crystallinity

The CrI and LOI for the four samples were calculated as explained above in Chapter 4.2.2 and the results are shown in Figure 4.28.

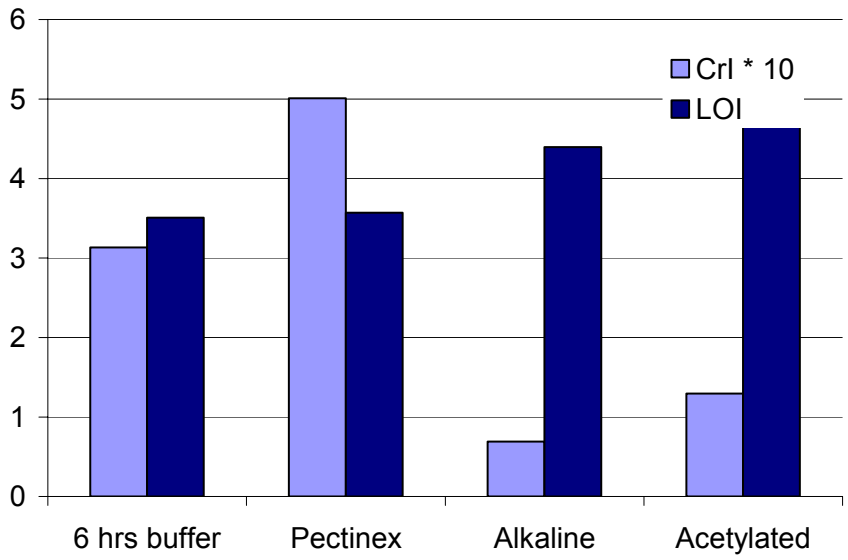

Figure 4.28: Crystallinity index CrI = a_{1372} / a_{2900} and lateral order index LOI = a_{1429}/a_{893} after various fibre treatments.

According to the CrI, alkaline-treated fibre exhibits a substantial drop in crystallinity. This would indicate removal of the greater part of the crystalline cellulose fraction. However, this is probably not likely since this would lead to severe degradation of the fibre and the value of the CrI should not drop below approximately 0.2 [106]. It is therefore more likely, that the peaks used for this index are not suitable for such differing treatments and indicate qualitative

changes rather than giving quantitative data. This comparison is not commonly applied in the literature as the LOI is more comparable to the X-ray crystallinity index. This work shows that the peaks traditionally used to calculate the CrI might be invalidated by neighbouring peaks from other components. Nelson *et al*. mainly tested pure cellulose mixtures to establish this ratio [106]. Similarly, spectra published by Mwaikambo *et al*. [45] show an increased absorbance around 2900 cm^{-1} and a decreased peak around 1372 cm^{-1} which would equally result in a decreased CrI. Nevertheless, the paper does state an increased x-ray crystallinity index, as has been found in the scope of this project (see below), which correlates well with the LOI [35].

The results of the calculation of the LOI are also visualized in Figure 4.28. The variation of this index is not as large as that described for the CrI. Pectinex treatment changes the LOI only as much as 0.07. Alkaline treatment on the other hand causes an increase of 25%. This observation is in accordance with results reported in the literature, where no significant change or an increase in LOI are published for similar treatment conditions [22, 44, 45]. Conversion of cellulose I to cellulose II takes place at concentrations of ~10 wt.% NaOH and goes to completion at concentrations of 15-20 wt.% NaOH [23, 47]. Therefore, it can be assumed, that the predominant lattice structure found in the presented samples is cellulose I since the LOI would decrease with the transformation to cellulose II. Cellulose II is spectroscopically similar to amorphous cellulose and cannot be distinguished by the LOI [106, 107]. Acetylation yields a further increase in lateral order by 9%.

4.3.3 Tensile testing

General observations for the tensile tests, such as diameter dependency, have already been described in Chapter 4.2.3 and are equally true for the tests described here. Averaged values of the mechanical properties including deviations of the four samples of interest are illustrated in the plots in Figure 4.29. Regarding the stiffness of the fibres, it is obvious that alkaline treatment reduces this property from 105 GPa (buffer treated) to less than 50% of the initial value (50 GPa). Acetylation and Pectinex treatment cause minor improvements of Young's modulus in comparison to alkaline and buffer treated samples respectively. The

modulus increase after enzyme treatment is 4.5 GPa (E = 109.5 GPa) and after acetylation is 1 GPa (E = 51 GPa). However, the deviations of all samples are far too high compared to these improvements and therefore they should not be overrated.

The influence of each treatment on fibre strength is reversed. Fibre strength is improved to 325 MPa by alkalization from 294 MPa after the buffer treatment. Both enzymes and acetylation weaken the fibre, yielding tensile strengths of 207 and 271 MPa, respectively.

As is usually observed, alkalization increases elongation at break dramatically. Buffer treated samples exhibit an elongation of 2.6% at break, which is raised to 6.4% after alkaline treatment. Again, Pectinex and acetylation induce the same changes. The elongation is reduced to 1.9% by the enzymes and 6.0% by acetylation.

These results show an overall good accordance with the literature. A graphical comparison between literature values for similar treatment conditions and the results obtained in the scope of this project is given in Figure 4.30. All values are normalized to the values of the respective control samples, usually untreated or water treated samples.

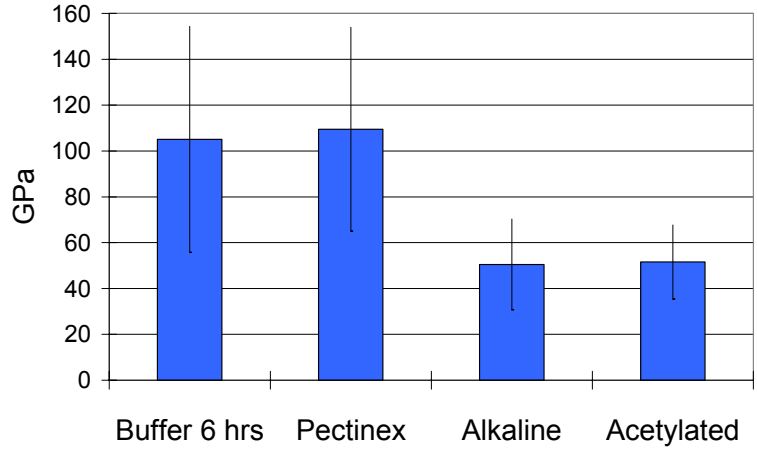

(a) Young's modulus

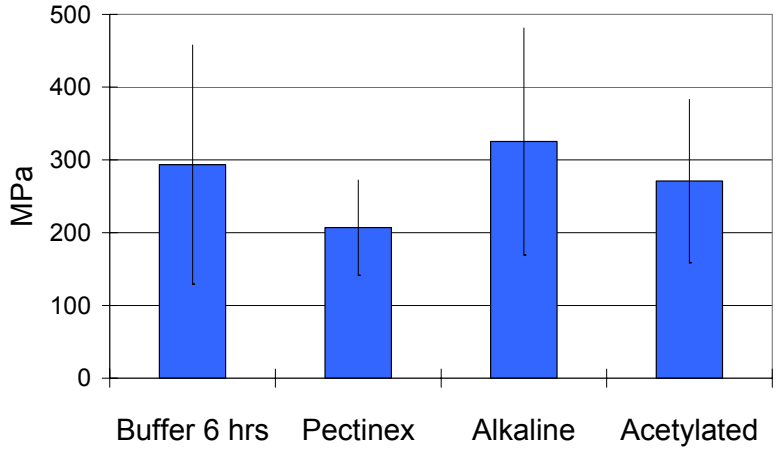

(b) Tensile strength

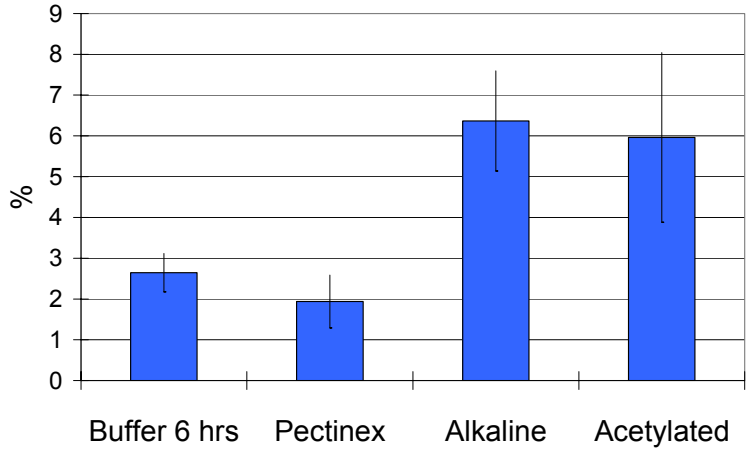

(c) Elongation at break

Figure 4.29: Results from single hemp fibre tensile tests.

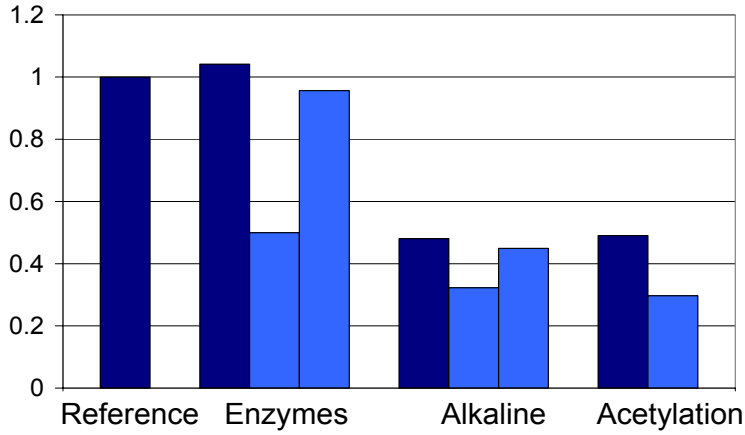

(a) Young's modulus

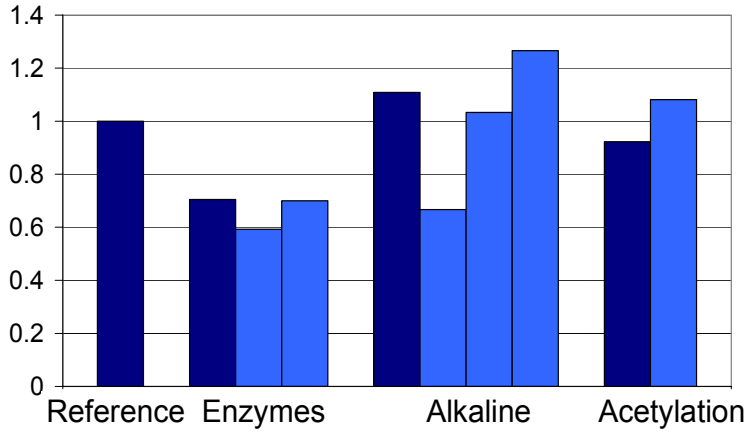

(b) Tensile strength

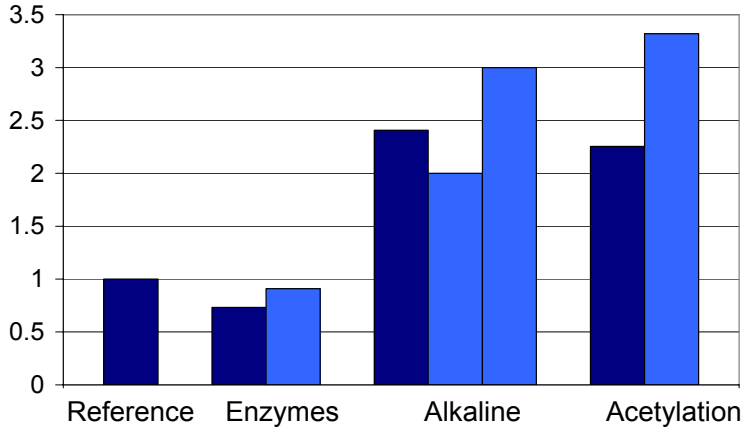

(c) Elongation at break

Figure 4.30: Results from single hemp fibre tensile tests (dark blue) in comparison to results from references [35, 47, 59, 108, 116] (light blue).

Alkalization results in greater extensibility and lower modulus. Rong *et al*. [59] explained this phenomenon by structural variation in the ultimate cell, specifically swelling and partial removal of hemicellulose and lignin. Apparently, the removal of these cementing materials facilitates an easier rearrangement and stretching of the microfibrils [22]. With uncoiling of the fibrils being one of the predominant failure mechanisms [59], this structural change is bound to greatly influence fibre properties.

Both acetylation and enzyme treatment do not significantly alter the fibres' stiffness. Tensile strength and elongation at break are decreased in comparison to buffer and alkaline treated fibre after the respective treatments. Although Hill *et al*. [52] observed an improvement in tensile strength after acetylation of coir and oil palm fibre at comparable treatment conditions, they also reported beginning damaging of the fibre structure, which led to weakening of the examined fibre at higher temperatures in their study. The investigated fibre samples had not been pre-retted and were treated in large bundles. It does seem possible therefore that the fibres investigated here already suffered some damage that lead to the decrease in tensile strength. At constant tensile modulus this evidently results in a decreased elongation at break as can be seen in Figure 4.29. Similar effects are plausible for the decrease observed in strength and extensibility after enzymatic treatment.

4.3.4 Flexural properties of hemp-epoxy composites

The 3-point bend (3PB) tests yielded both data on the mechanical properties of the prepared composites and an insight into the interfacial properties obtained by the different treatments. A typical 3PB specimen before and after testing is shown in Figure 4.30.

Figure 4.31: Failure of a hemp-epoxy composite in 3-point bending. From left to right: as received specimen, bottom side of fractured specimen, top side of fractured specimen, separated specimen halves.

Due to the preparation method described in Chapter 3.3.6 a variation in fibre weight fraction was possible. For this reason, all samples were weighed and measured after preparation to obtain an approximation of the actual fibre content. The average flexural stiffness, strength and strain in the outer fibre at break are shown in Figure 4.32. The values of all properties are also given with the respective deviations in Table 4.13.

It is obvious from Figure 4.32 that reinforcement with hemp generally increases the stiffness of epoxy resin specimens. The greatest improvement was obtained after reinforcement with buffer (38%) and alkali treated (31%) hemp followed by an increase by 25 and 13% after treatment of the fibres by Pectinex and acetylation.

Figure 4.32: Flexural modulus, flexural strength and strain at failure of hemp-epoxy composites.

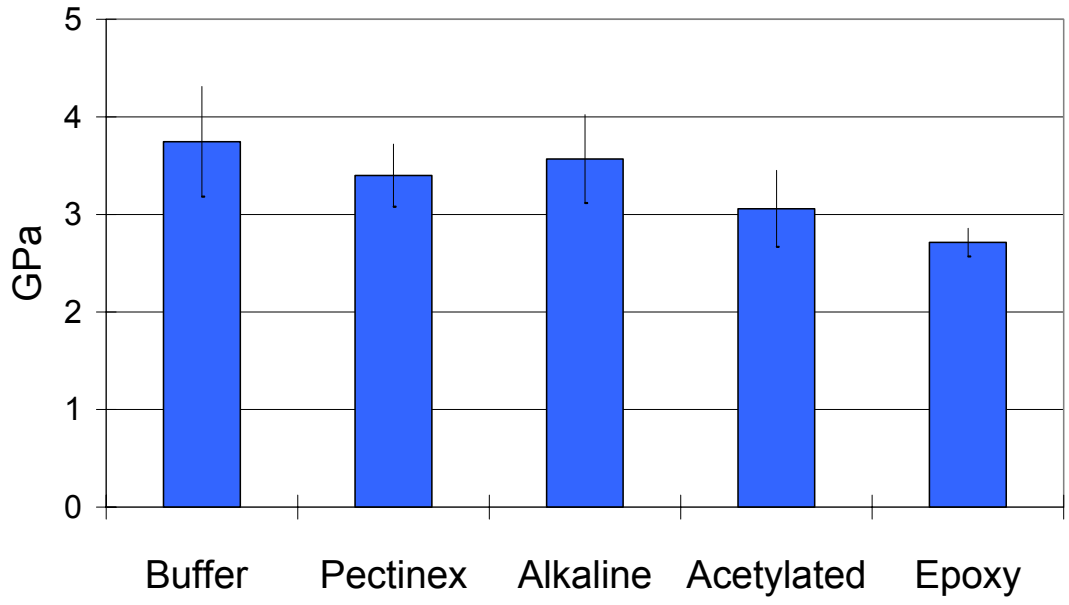

(a) Modulus of elasticity in bending

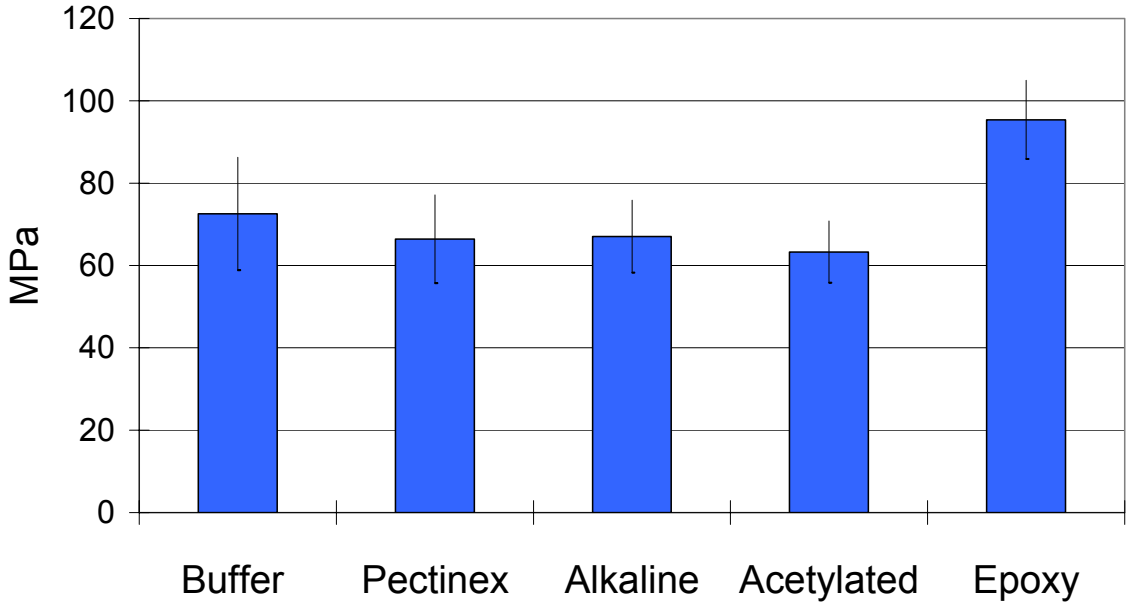

(b) Flexural strength

Figure 4.32: Flexural modulus, flexural strength and strain at failure of hemp-epoxy composites.

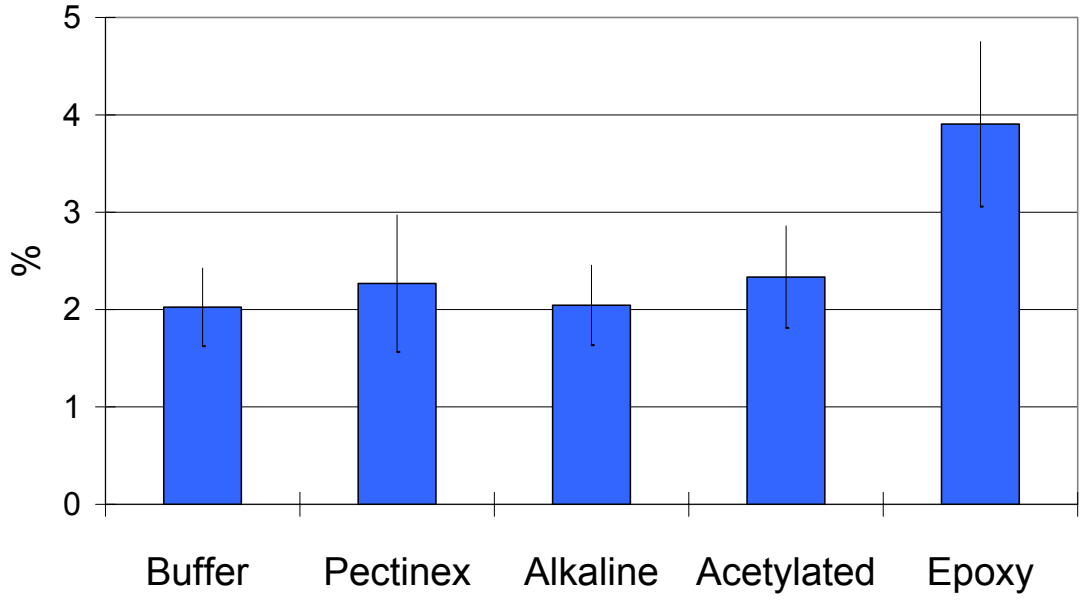

(c) Strain in outer fibre at failure

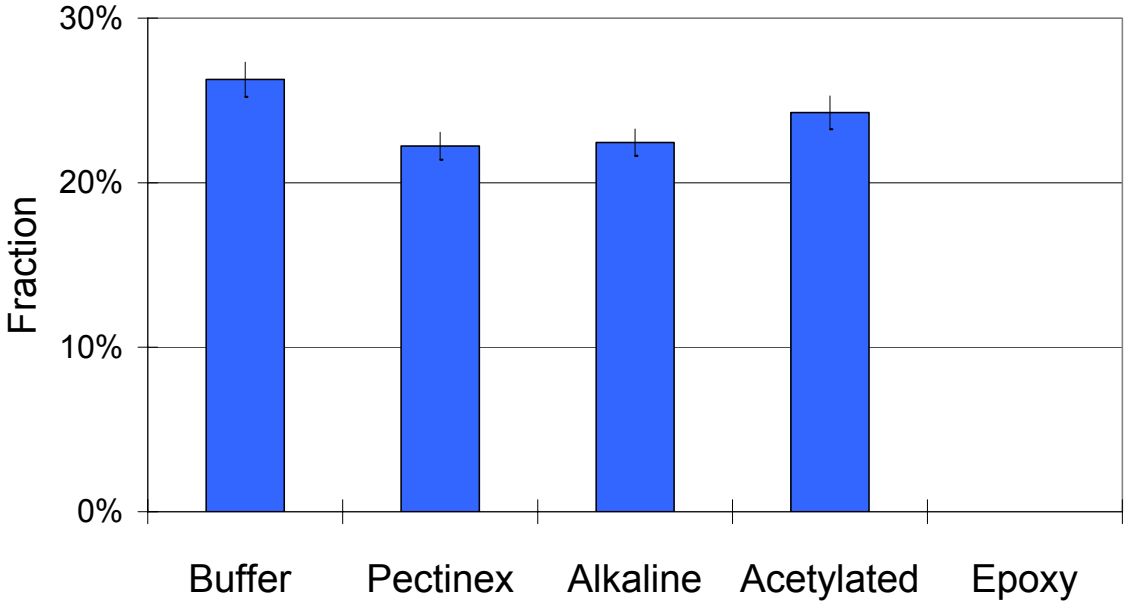

(d) Fibre weight fraction

Table 4.13: Mechanical properties of hemp-epoxy composites

	Buffer	*Pectinex*	*Alkaline*	*Acetylated*	*Epoxy*
Elastic modulus (GPa)	3.57 (0.57)	3.40 (0.32)	3.57 (0.45)	3.06 (0.39)	2.71 (0.15)
Flexural strength (MPa)	72.56 (13.71)	66.44 (10.71)	67.07 (8.81)	63.31 (7.51)	95.42 (9.57)
Strain at failure (%)	2.02 (0.40)	2.27 (0.70)	2.05 (0.41)	2.33 (0.53)	3.90 (0.85)
Fibre weight fraction	0.26 (0.01)	0.22 (0.01)	0.22 (0.01)	0.24 (0.01)	- / -

Flexural strength on the other hand was reduced by fibre reinforcement. All measured composite strengths were reduced by approximately 30%, with buffer treated hemp yielding the strongest composites and acetylated hemp the weakest.

The bending strains of the composites were reduced by nearly 50% compared with neat epoxy (3.9%). Buffer and alkaline treated fibres led to a strain at failure of 2% and acetylation and Pectinex resulted in the maximum composite strain of 2.3%.

Assuming equal stress transfer between matrix and fibre (*i.e.* equal fibre geometry and interfacial bonding), the mechanical properties of the composites should be proportional to those obtained for the fibre bundles. A comparison of the two results does however falsify this assumption.

In the literature, many different mathematical models can be found to calculate theoretical composite properties. One of the most widely used theories to model random in-plane fibre reinforced composite stiffness was developed by Cox and Krenchel. Starting with the 'rule of mixtures', Cox [117] added a factor to account for the limited efficiency of stress transfer from the matrix to the fibres due to finite fibre length, η_L. Krenchel [118] added a factor to account for fibre orientation, η_0. The Cox–Krenchel theory can be written as given in Equation (4.4):

$$E_c = \eta_0 \eta_L V_f E_f + (1 - V_f) E_m \qquad (4.4)$$

where E_f, E_m and V_f are the fibre and matrix stiffness and the fibre volume fraction respectively. From the 'shear lag' theory developed by Cox an expression for η_L is found:

$$\eta_L = \left(1 - \frac{\tanh(\beta L/2)}{\beta L/2}\right) \qquad (4.5)$$

where:

$$\beta = \frac{2}{d}\sqrt{\frac{2G_m}{E_f \ln(\sqrt{\pi / X_i V_f})}} \qquad (4.6)$$

and where d, L and G_m are the fibre diameter, fibre length and shear modulus of the matrix respectively. X_i depends on the geometrical packing arrangement of the fibres and X_i = 4 can be used for square packing [119]. For the random in-plane orientation of the fibres in the specimens used here, it has been shown that η_0=0.375 [118, 119]. As mechanical input parameters, the elastic moduli were used as reported in Chapter 4.3.3, L = 5 mm, E_m = 2.71 GPa from the 3-point bend tests carried out, and $G_m = E_m/2(1+\nu)$ = 1.02 GPa accordingly. The diameter was calculated from the averaged values measured on single fibres and bundles during the tensile tests. It should be noted, however, that these values are not totally representative as they represent a small fraction of samples and only those suitable for tensile testing. Consequently, an average of 0.084 mm was used for all calculations as a reliable value for each treatment could not be established. No quantitative comparison between fibres with respect to the diameter influence is possible. Moreover, the fibre diameter does not have a significant effect in the Cox-Krenchel model [120]. Having determined the diameter and length for the calculations it was verified that the Cox-Krenchel model is applicable given the resulting aspect ratio of 119 [119].

Table 4.14: Calculated composite modulus

	E (GPa)
Buffer	10.9
Pectinex	9.9
Alkaline	5.9
Acetylation	6.3

The modulus values calculated by the Cox-Krenchel model are shown in Table 4.14. All moduli are significantly above the measured values of 3.1 to 3.6 GPa. They are however in the same order of magnitude and reductions can occur due to numerous reasons that will be discussed further after a comparison of all mechanical composite data.

Tensile strength of composites can also be predicted with well-known models. Although the flexural strength was investigated here, the tensile strength will be

calculated for reasons of comparison as the actual failure during bending tests occurs in the specimen part under tension. As the interfacial strength is the only unknown variable in the equation used to calculate tensile strength, the respective values will be calculated with the measured strength as an input value and the resulting interfacial strengths rather than the tensile strengths will be the values of interest to be compared against each other as relative values. The commonly employed model to determine polymer composite strength is the Kelly-Tyson model [121]:

$$\sigma_{uc} = \sum_i \left[\frac{\tau L_i V_i}{D} \right] + \sum_j \left[\sigma_{fj} V_j \left(1 - \frac{L_c}{2L_j} \right) \right] + (1 - V_f)\sigma_{um} \qquad (4.7)$$

where τ is the interfacial strength, $V_{i,j}$ the volume fraction of fibres of length $L_{j,\,i}$, σ_{fj} is the fibre strength, σ_{um} is the matrix strength at the fibre failure strain equal to $E_m \sigma_f / E_f$ and L_c is a critical fibre length defined by $L_c = \sigma_f D / 2\tau$. The first two summation terms in Equation (4.7) arise from the contributions of fibres of subcritical and supercritical length. As the fibre lengths have not been measured separately and no quantitative data is aimed for, the intended length of 5 mm will be assumed for all fibres and consequently summation will be carried out over one i, j only. The fibre diameter, fibre strength and stiffness, fibre content and matrix strength and stiffness will again be calculated from the results presented in this and the preceding chapter. A ratio of 1.6 between flexural and tensile strength has been reported for epoxy elsewhere [122] and similarly a ratio near 1.5 for fibre composites [123-125]. These factors were used for the calculation of epoxy and composite tensile strength from the 3-point bend results presented above. In order to account for the randomly oriented fibres in the examined composites, Thomas *et al*. [121] proposed a factor of 0.2 to modify the fibre contribution in Equation (4.7). As they obtained good correlation with their data and this procedure is similar to that followed for the calculation of composite stiffness, the same factor will be used here. Introducing the described assumptions, the resulting equation for the calculation of the interfacial strengths is:

$$\sigma_{uc} = \left[\frac{\tau L V_f}{D} \right] + 0.2 \left[\sigma_f V_f \left(1 - \frac{\sigma_f D}{4L\tau} \right) \right] + (1 - V_f)\sigma_{um} \qquad (4.8)$$

$$\Leftrightarrow \left[\frac{\tau L V_f}{D}\right] - 0.2\frac{V_f {\sigma_f}^2 D}{4L\tau} + 0.2\sigma_f V_f + (1-V_f)\sigma_{um} - \sigma_{uc} = 0 \qquad (4.9)$$

$$\Leftrightarrow \frac{LV_f}{D}\tau^2 + \left(0.2\sigma_f V_f + (1-V_f)\sigma_{um} - \sigma_{uc}\right)\tau - 0.2\frac{V_f {\sigma_f}^2 D}{4L} = 0 \qquad (4.10)$$

$$\Leftrightarrow \tau^2 + \frac{D}{LV_f}\left(0.2\sigma_f V_f + (1-V_f)\sigma_{um} - \sigma_{uc}\right)\tau - 0.2\frac{{\sigma_f}^2 D^2}{4L^2} = 0 \qquad (4.11)$$

$$\text{with } \frac{D}{LV_f}\left(0.2\sigma_f V_f + (1-V_f)\sigma_{um} - \sigma_{uc}\right) = p, \quad -0.2\frac{{\sigma_f}^2 D^2}{4L^2} = q$$

$$\Rightarrow \tau_{1,2} = -\frac{p}{2} \pm \sqrt{\left(\frac{p}{2}\right)^2 - q} \qquad (4.12)$$

with only τ_1 yielding physically sensible positive values for the interfacial strength. The relative values (normalized to $\tau_{buffer} = 1$) calculated for the interfacial strengths are presented in Table 4.15. The absolute values of 0.5-0.8 MPa are lower than the values of 3-9 MPa reported elsewhere [121, 126]. However, the cited values were measured for aramid and glass fibre composites which are known to exhibit superior interfacial adhesion in comparison to natural fibres. The calculated interfacial strengths are therefore of plausible magnitudes. In addition, this comparison is an explanation for the difference between calculated values of the composite stiffness and the actually obtained results. With interfacial bonding reduced to a fraction of the values obtained for synthetic fibres it is clear that the difference between above-calculated and actual modulus values is equally large as the calculation based on the assumption of perfect bonding.

Table 4.15: Absolute and relative interfacial strengths.

	τ_{abs} (MPa)	τ_{rel}
Buffer	0.80	1
Pectinex	0.46	0.57
Alkaline	0.75	0.94
Acetylation	0.60	0.75

Examining the data presented in Figure 4.32, it is clear that addition of fibre severely reduces the strain to failure of the material. This trend is also found in results published in the literature, and the explanation of the phenomenon generally given is that stress concentrations at the fibre ends lead to matrix cracking, which ultimately leads to failure when the surrounding matrix and fibres can no longer support the increased load caused by the local failure [121, 127]. Thomason *et al*. [121] postulated from their data that the observed strain is either

dominated by the matrix or by the fibre with increasing fibre content. The strain of failure found here corresponds well with the maximum strain found for untreated and enzyme treated fibres. The alkali treated and acetylated fibres did exhibit a greater elasticity. However, it has been argued earlier, that the observed increase in elongation at break is most likely due to an easier rearrangement of the microfibrils under tensile stress. If incorporated into a composite the fibrils are bound to the matrix and if the interfacial strength is high enough it might obstruct this mechanism, resulting in similar elasticity values as those observed for the other fibres. The pictures of fractured specimens shown in Figure 4.33 support the assumption that the interfacial strength is high enough to prevent fibril stretch.

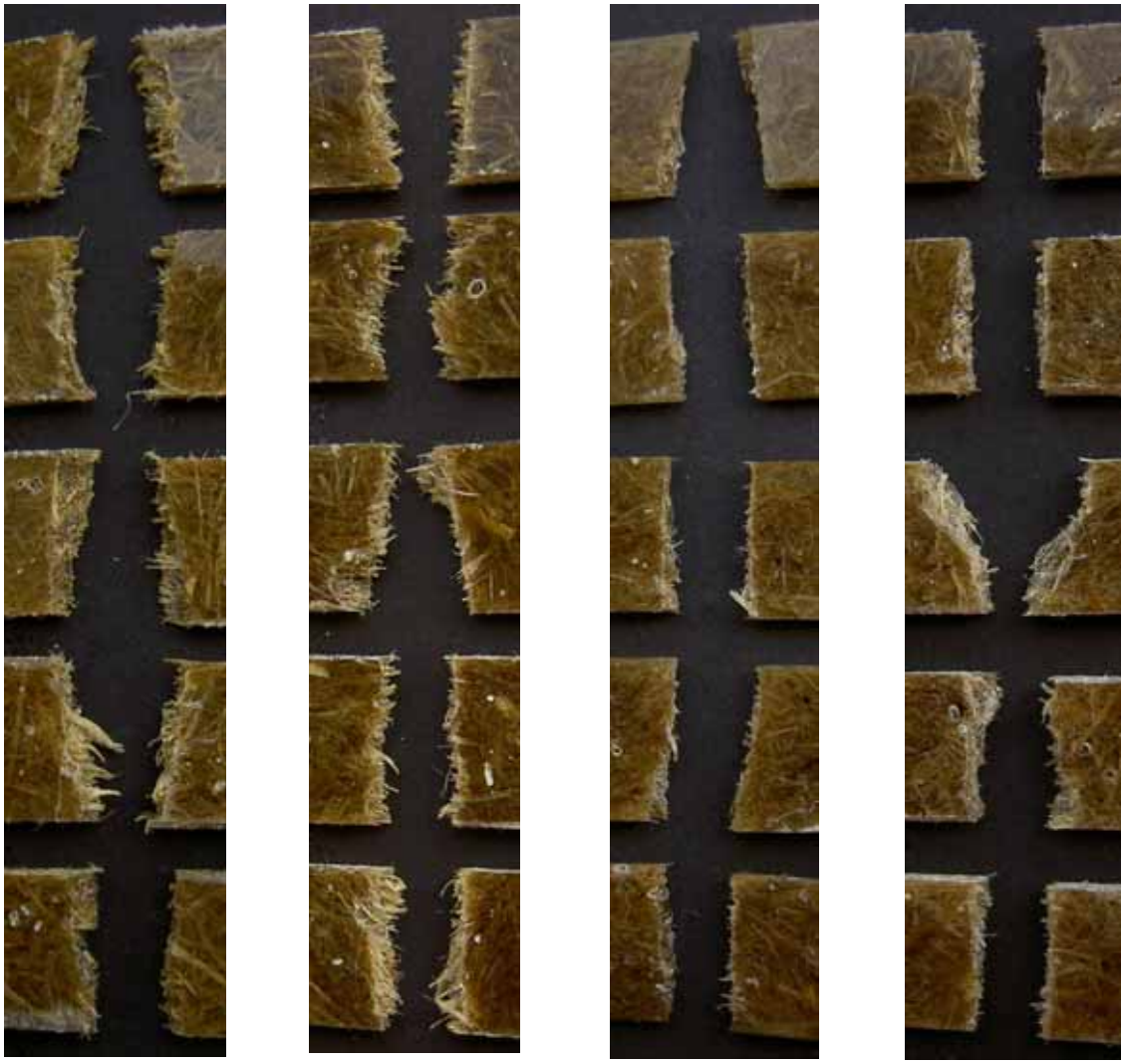

(a) Buffer (b) Pectinex (c) Alkaline (d) Acetylated

Figure 4.33: Fracture edges after 3-Point-Bending tests.

The pull-out lengths of the fibres shown in Figure 4.33 exhibit an excellent correlation with the interfacial strengths calculated above. Both buffer and alkali treated fibres are hardly being pulled out of the matrix. Some thicker bundles can be seen in case of the buffer treated fibres but these specific fibres possess far lower surface area in comparison to cross-sectional area and are therefore more likely to be pulled out of the matrix as opposed to fracturing while still embedded. Acetylated fibres show a slightly greater tendency to be pulled out of the matrix. Taking into account the reduced fibre strength in comparison to alkali treated fibres this result also correlates well with the calculated interfacial strength. The fibres treated with Pectinex show a significantly larger tendency to fibre pull-out. Again, at half the interfacial strength compared to buffer treated fibres this is a plausible consequence.

In case of the buffer-treated hemp, it could be assumed that bonding occurs between the less polar covering layer of the fibres and epoxy matrix. As long as the interfacial strength is larger than the transferred stress, the resulting composites will exhibit fibre or matrix fracture rather than fibre pull-out. Support for these conclusions will be possible by additionally considering scanning electron micrographs of the fracture surfaces (Chapter 4.3.6) and dynamic mechanical data (Chapter 4.3.5).

The resulting composite strengths obtained for the composites cannot be explained by the calculated interfacial strength values and fibre strength. Especially Pectinex-treated fibre that exhibits both low adhesion and low tensile strength should not result in composites of comparable flexural strength considering these factors only. Thus, two other factors should be noted. Firstly, the defibrillation (and thus interfacial area) which will influence the final composite strength was not investigated quantitatively. Analysis of the scanning electron micrographs however did point to a greatly improved defibrillation of the bundles (Chapter 4.3.6) as has been noted before after a macroscopic evaluation of defibrillation (Chapter 4.3.1). Secondly, the stiffness of the fibres might have a supporting role in the compressed part of the bending specimens. If the matrix withstands the compressive force well enough to prevent fibre kinking then the stiff enzyme treated fibres might yield a better support of the composite in the

compressed part compared to the less stiff alkalized and acetylated fibres. Judging by the superior strength of the non-reinforced epoxy the matrix strength is likely to be sufficient for this purpose. Unfortunately, this factor cannot be analyzed any further due to the lack of composite compression data.

4.3.5 Dynamic Mechanical Analysis

A typical plot of the recorded dynamic mechanical data as illustrated by the machine's software is shown in Figure 4.34. The measured properties depend on the frequency used for an experiment. As in static tensile tests, the modulus increases with increased strain rate. Accordingly, at higher frequencies both storage and loss modulus increase. However, the loss modulus shows a sharper increase and therefore, the loss factor tan δ also exhibits a rise with frequency.

Maximum energy dissipation occurs at the temperature T_t where E'' and tan δ are at a maximum, indicating a transition of the system [55, 56, 128, 129]. The epoxy's T_t of approximately 82°C is influenced by the fibre content, coupling agent, humidity, processing parameters, etc [129]. An increase in T_t values can be related to the reduced mobility of macromolecules by the flax fibres [129].

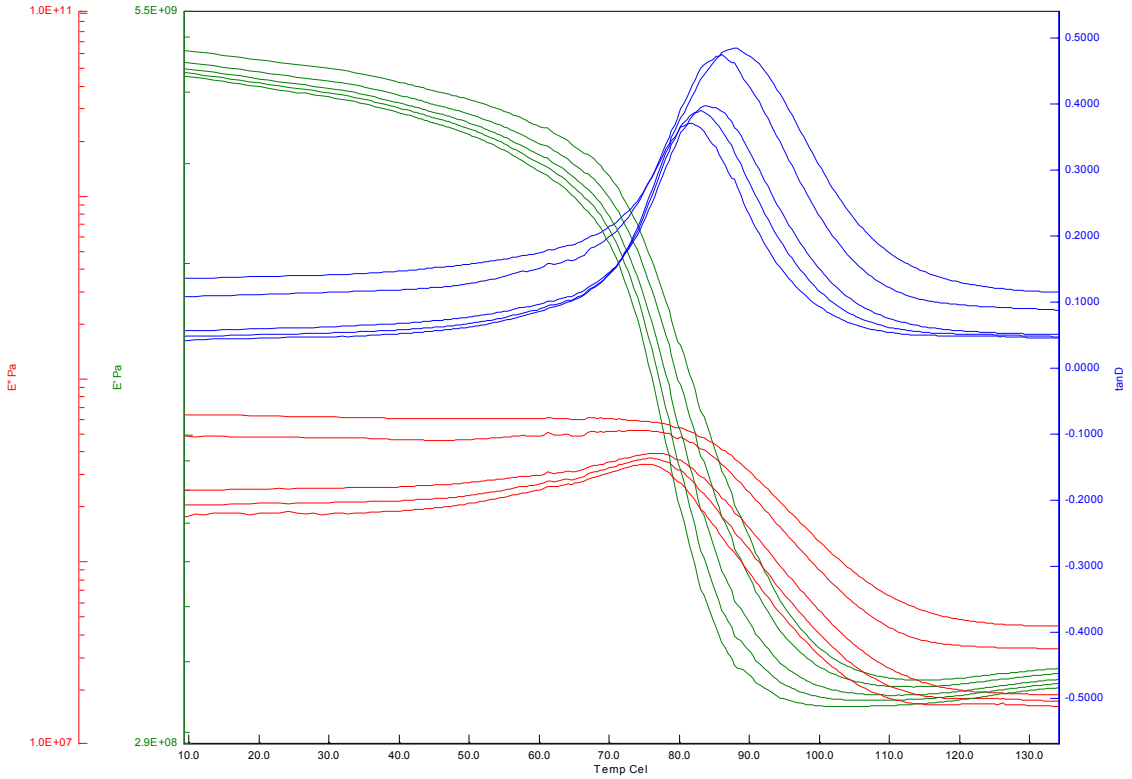

Figure 4.34: Typical plot of results from DMA. Storage modulus (E', green), loss modulus (E'', red), and tanδ (blue) as a function of temperature and frequency (10, 5, 2, 1 and 0.5 Hz).

Figure 4.35 gives an overview of the maximum loss factors and the temperatures at which they occur. It is obvious that pure epoxy exhibits significantly higher damping and that it goes through the glass transition at a lower temperature than the hemp-epoxy composites. The hemp reinforcement is responsible for a reduction in damping and an increase in T_t [129]. All reinforced samples exhibited a higher T_t and lower damping than the neat epoxy. The significant drop in damping is mainly caused by the reduction of the polymeric fraction [129]. The relatively higher damping found for the alkaline-treated and acetylated fibre composites are probably due to the reduced stiffness and increased extensibility of the reinforcing fibres in comparison to those treated with buffer solution and Pectinex (see Chapter 4.3.3). The slightly higher damping of the samples with buffer treated fibres in comparison to those treated with Pectinex might be a result of the increased amount of accompanying substances on the fibre surface. However, this cannot be said with certainty as the influence of local

fibre content might cause such variation and cannot be estimated on the basis of the obtained data. The samples reinforced with fibres that were either Pectinex-treated or acetylated exhibit a smaller increase in T_t. Inferior bonding and therefore easier release of the polymer matrix molecules from the fibres may explain this observation, which is also supported by the interfacial strength results in the previous chapter. Both Pectinex-treated or acetylated fibres also exhibited lower strength in tensile and bending tests. Therefore, a weakening of the interface due to local fracture of the reinforcing fibres cannot be ruled out as an explanation either.

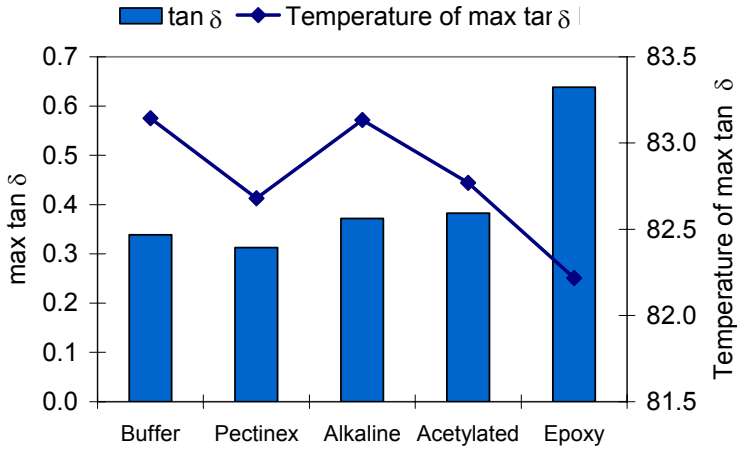

	T_t (°C)	Tan δ
Buffer	83.14	0.34
Pectinex	82.68	0.31
Alkaline	83.13	0.37
Acetylated	82.77	0.38
Epoxy	82.22	0.64

Figure 4.35: Maximum damping and corresponding temperatures.

The complete damping and storage modulus curves for all tested samples are shown in Figure 4.36. A good consistency between the two measurements taken for each composite type can be seen in the coloured graph. Apart from the damping characteristics described above, differences in the elastic behaviour (storage modulus) were also noted. The steep loss in E' is due to the matrix transition at T_t and therefore related to the temperatures stated in the previous paragraph. The initial values and development of the storage modulus is therefore of greater interest. A comparison of the values measured at 30°C is shown in Figure 4.37.

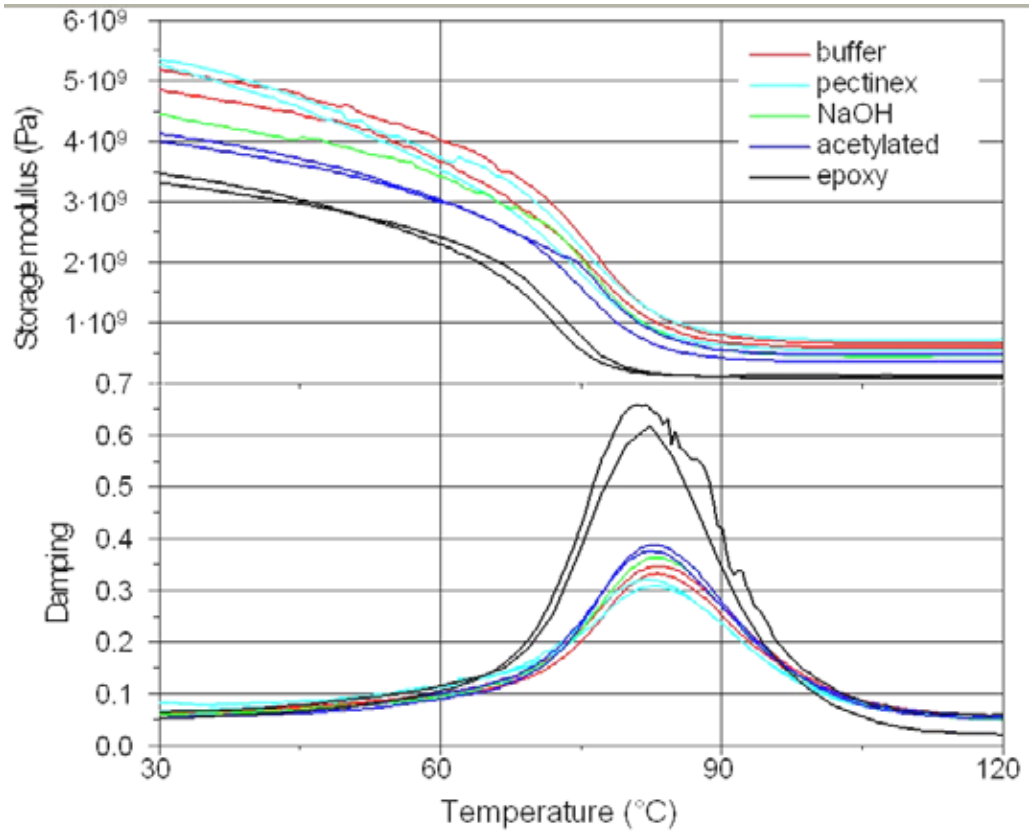

Figure 4.36: Storage modulus and damping (tanδ) measured at 1 Hz as a function of temperature (30-120°C).

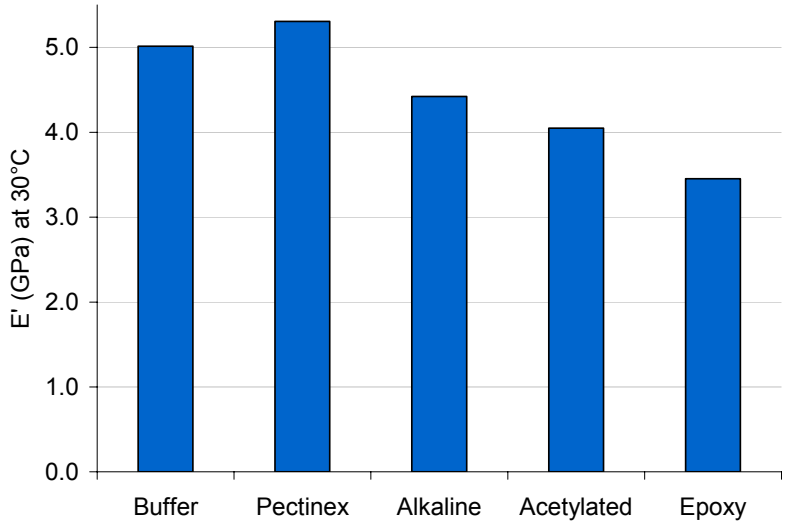

Figure 4.37: Storage modulus at 30°C from DMA

The general trend observed for the storage modulus correlates with the static modulus found in composite bending tests. The specimens reinforced with Pectinex treated fibres represent an anomaly in this trend as they only exhibited a

flexural stiffness on the level of composites reinforced with acetylated fibres. Consulting the data obtained from single fibre tensile tests, this observation can be explained by the superior fibre stiffness found in these tests. It can be concluded that for the resistance to dynamic load the stiffness of the reinforcement becomes more important than under static load.

Another characteristic worth noting in Figure 4.36 is the slope of the storage modulus curves. Especially the stiffest sample with Pectinex treated fibre reinforcement exhibits a higher gradient in the first phase of the test up to approximately 70°C. No certain explanation can be given at this point, although this appears to correlate well with the hypothesis that the Pectinex-treated fibres not only exhibit inferior fibre-matrix adhesion, but they also combine a high stiffness with low extensibility. It is therefore plausible that such a combination not only fails earlier but also continuously under dynamic load, resulting in a loss in storage modulus not only due to rising temperature but also to progressing disruption of fibre and matrix material at the interface. Such behaviour has been reported in the literature as a result of cyclic fatigue test on composites reinforced with discontinuous fibres [130]. Unfortunately, a deeper analysis of the interface in combination with SEM would be necessary to falsify or back up this explanation.

4.3.6 SEM

Scanning electron micrographs have been taken of the fracture surfaces of both single fibres and composite specimens. The micrographs of the fibres after the tensile tests are compiled in Figure 4.38. The most important features observable under the SEM are the degree of defibrillation and the surface structure of specimens. The former aspect did not yield completely new results as the observations carried out under SEM are in accordance with the macroscopic defibrillation reported in Chapter 4.3.1. The buffer-treated sample shows single fibres released from the main bundle probably due to the stress during tensile testing. The main bundle has not been split up by treatment in the buffer solution. The specimen shown in Figure 4.38 (b) shows the highest defibrillation. Apart from the break up of the bundle into several fibres and smaller bundles, the fibrils can be identified within the bundle and at the fractured end of the fibre. This indicates a

removal of the cementing materials which cover the fibrils as is the case for the buffer treated fibre in Figure 4.38 (a).

Alkalization (Figure 4.38 (c)) leads to a medium defibrillation. The bundle has split up into smaller agglomerates but single fibres cannot be identified on the surface. This difference between Pectinex and alkali treatment is due to the different mechanisms of action. Alkaline solution is used to dissolve lignins from the lignocellulosic complexes linked to the fibrils while Pectinex degrades pectins and hemicelluloses at the surface of the fibre. Both methods can lead to separation of the fibres but the enzymes are bound to yield a cleaner surface morphology. Similar micrographs have been published by Ouajai and Shanks [47] after treatment of hemp fibres.

Acetylation leads to a slight improvement in defibrillation, especially visible at the ends of the fibre (see Figure 4.38 (d)). Additionally, the fibre shown on the left at a magnification of 1000 x possesses an amorphous surface layer which looks different from that observed on the buffer-treated fibres. The covering material seems to have been macerated by the chemical treatment and in some areas a pronounced orientation of the structure is visible, possibly indicating uncovering of the fibrils on the surface of the bundle. The latter observation is backed up by the fracture morphology described below where a significant amount of fibrils are torn off the bundles during composite fracture.

Figure 4.38: Scanning electron micrographs of the treated fibres, magnifications x100 (left) and x1000 (right)

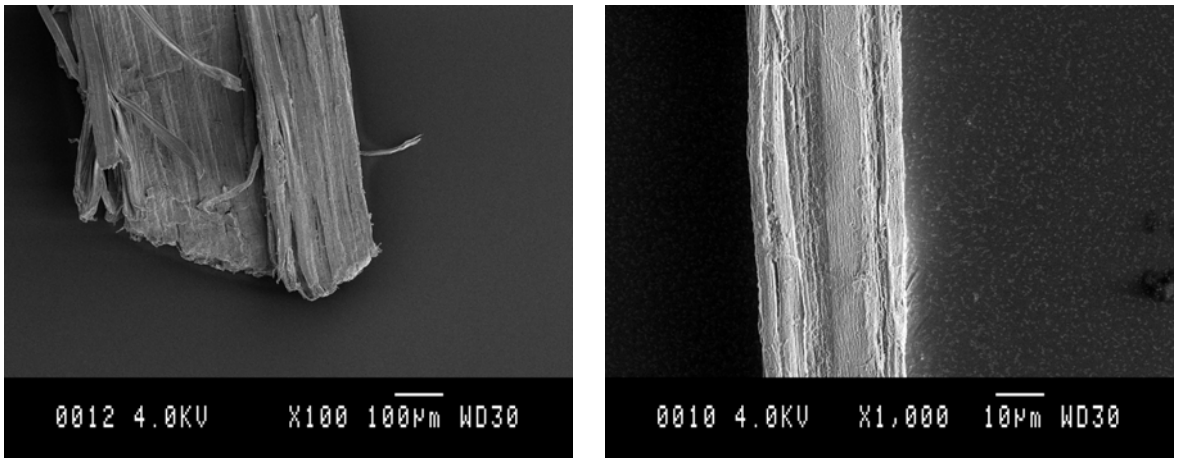

(a) Buffer

Figure 4.38: Scanning electron micrographs of the treated fibres, magnifications x100 (left) and x1000 (right)

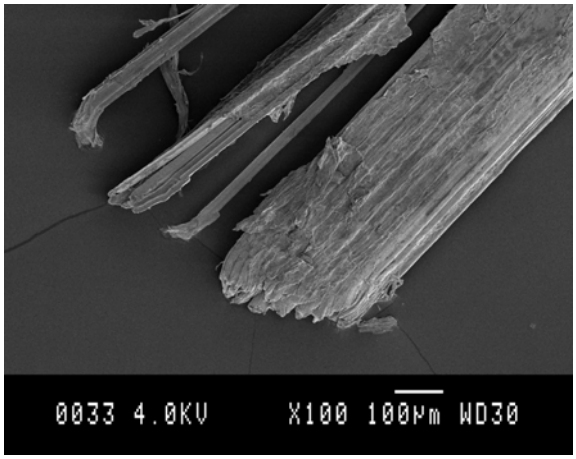

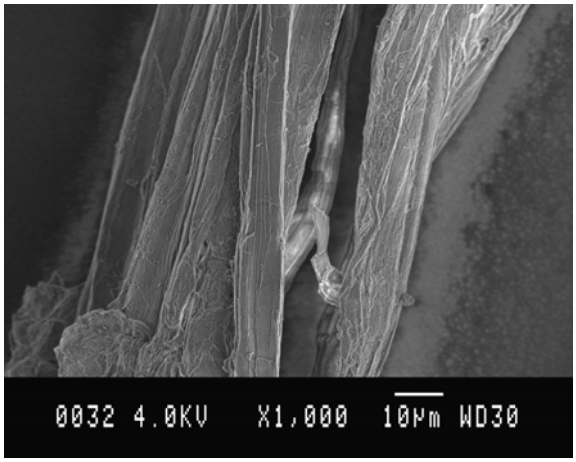

(b) Pectinex

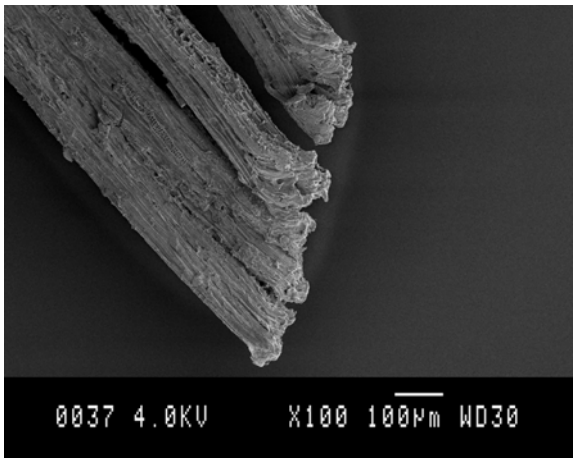

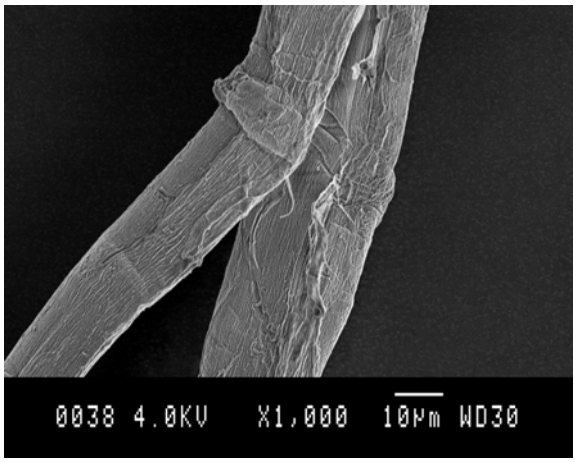

(c) Alkalized

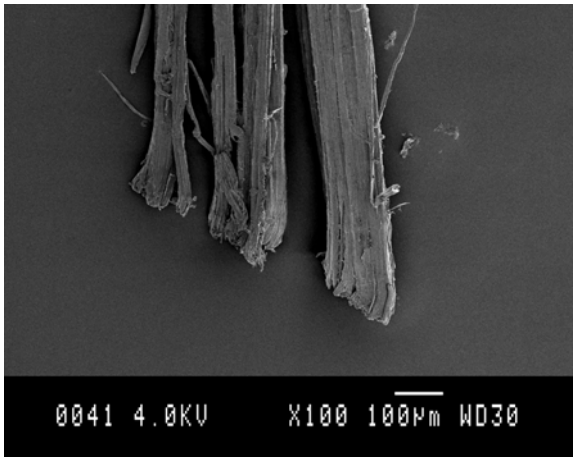

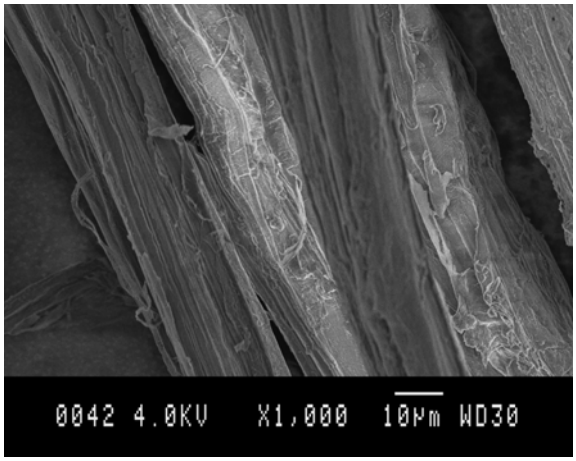

(d) Acetylated

The micrographs taken of the fracture surfaces of the 3PB specimens are shown in Figure 4.39. The punctured, amorphous layers covering most specimen surfaces should not be confused with the composite structure itself. These carbon strips were used both to fix the specimens in an upright position and to improve electric conductivity.

Figure 4.39: SEM micrographs of the fracture surfaces after 3PB tests.

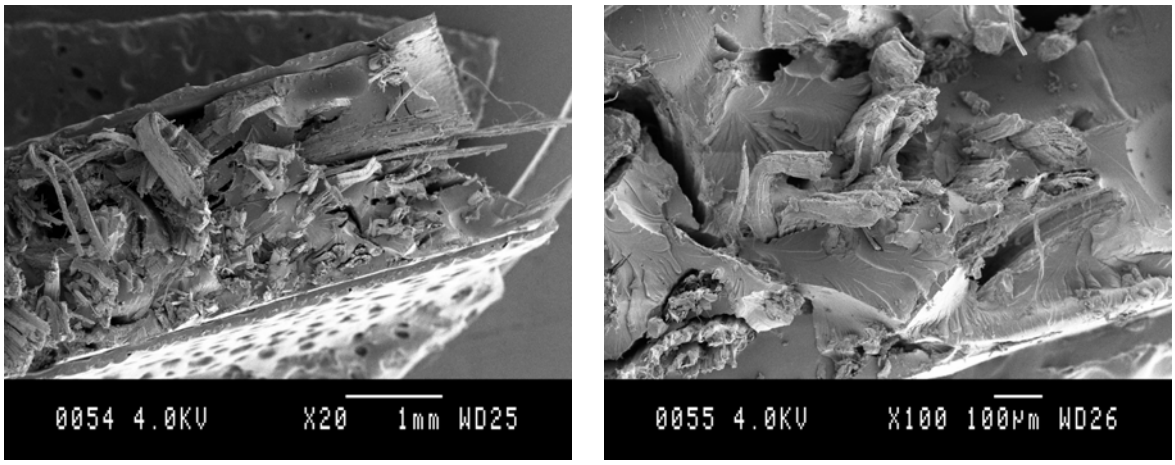

(a) Buffer

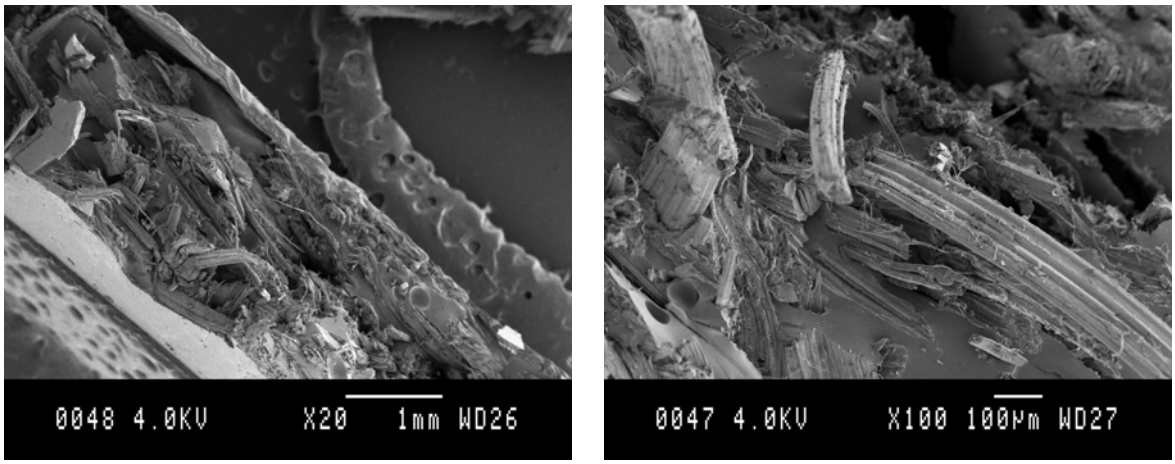

(b) Pectinex

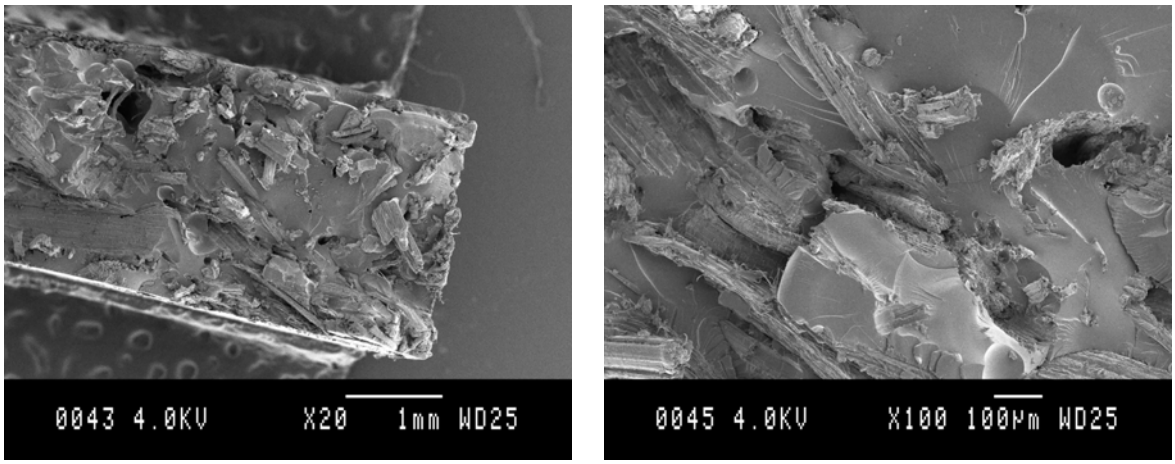

(c) Alkalization

Figure 4.39: SEM micrographs of the fracture surfaces after 3PB tests.

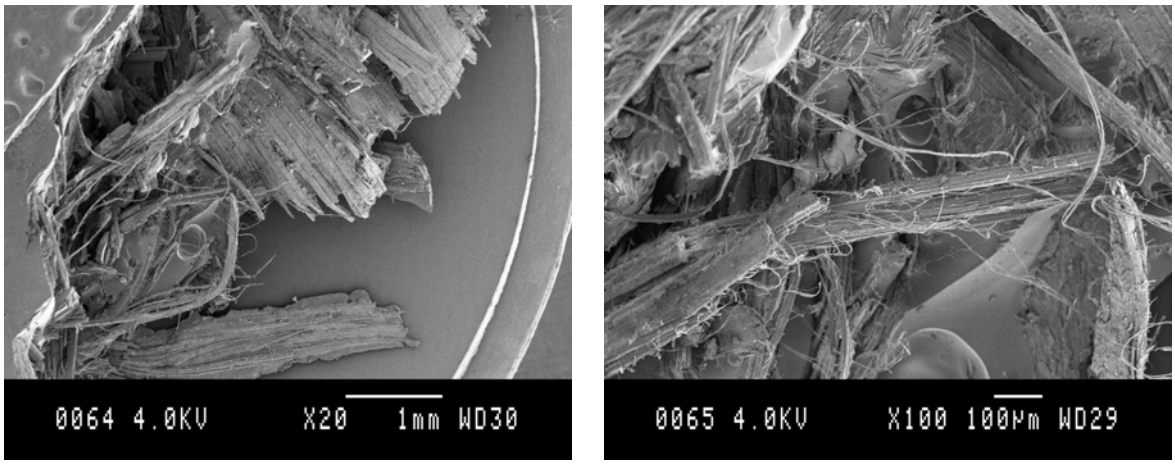

(d) Acetylation

The first micrographs shown in Figure 4.39 (a) illustrate the fracture morphology of epoxy reinforced with buffer treated fibres. As has been argued before, a fairly good matrix adhesion can be suspected from these micrographs. Only thicker fibre bundles have been pulled out of the matrix and matrix failure can be observed in several places indicating stress transfer from the fibre to the more ductile polymer matrix. No microfibrils were torn from the bundles during failure, however the covering layer observed in the micrographs of single fibres above seems to serve as bonding interface. As the layer is thought to partly consist of waxy substances after buffer treatment only, the resulting hydrophobic character of the surface would provide similar polarity as the matrix. A more detailed view of a fibre pulled out of a composite specimen is given in Figure 4.40. The formation and partly release of flakes on the surface of the fibre supports the described mechanism.

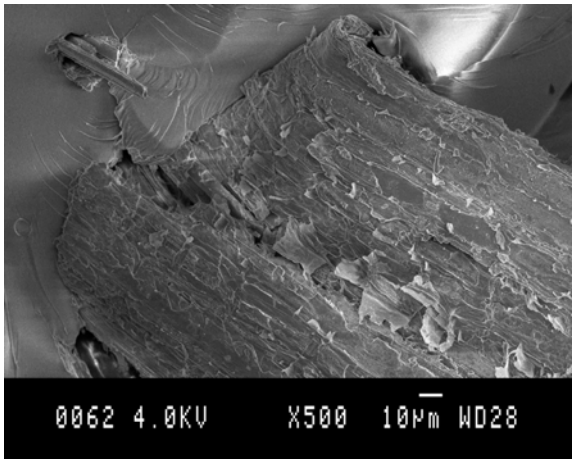

Figure 4.40: Surface flakes on buffer treated fibre after pull-out.

The hemp-epoxy composites also exhibit similar fibre morphologies as observed for the isolated fibres. However, a

considerable amount of microfibrils were released from the bundles during failure of the composite specimens (left micrograph in Figure 4.41). As even bigger samples were pulled out of the matrix (right micrograph in Figure 4.41) this release of microfibrils is due to a decreased bundle coherence, rather than high interfacial strength, as has already been concluded in previous chapters.

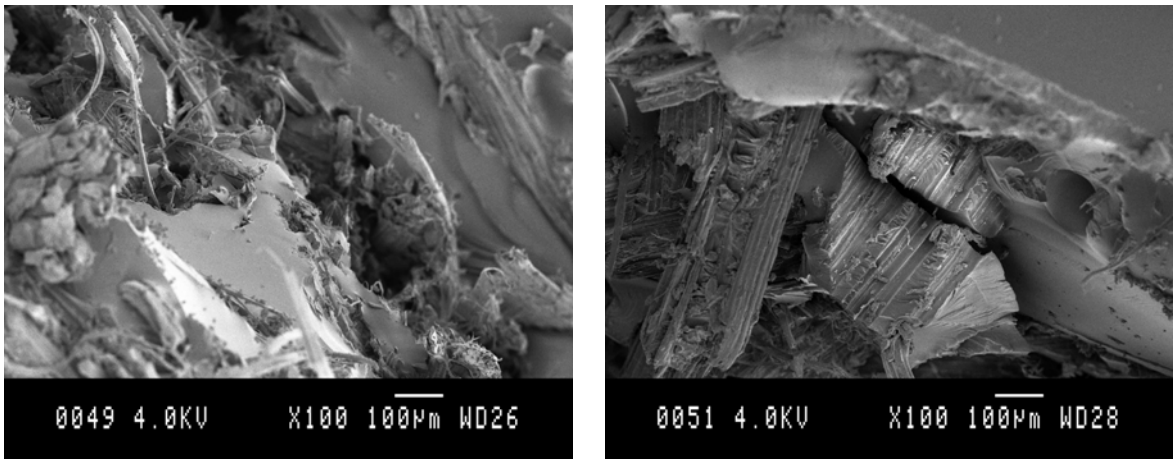

Figure 4.41: Pectinex-treated fibres after sample fracture. Left: Released fibrils on fracture surface. Right: Pull-out cavity visible after pull-out of thick fibre bundle.

Alkali treatment yielded both an improved defibrillation and sufficient fibre-matrix bonding. As has been reported above, no long fibres were pulled out of the epoxy matrix during 3PB tests. The SEM supports this observation by a superior fracture surface morphology in terms of fibre pull-out as shown in Figure 4.39 (c). Subsequent acetylation of hemp changes the fracture morphology significantly (Figure 4.39 (d)). In addition to a greater amount of thinner fibres being pulled out of the matrix, the most noticeable change is the prominent amount of released microfibrils. Together these observations indicate a fibre matrix adhesion that is lower than that of alkali treated fibres towards epoxy combined with a significantly reduced fibre adherence similar but more pronounced than that observed after Pectinex treatment.

Concluding, the observations made by SEM are in good accordance with the properties and conclusions derived from the previously described methods of analysis.

4.3.7 Atomic Force Microscopy

Pietak *et al*. [73] have shown that a correlation exists between F_{adh} measured by AFM and the wettability (or surface energy) of hemp fibre. The present work seeks to determine if a correlation exists between the AFM measurements on hemp fibre and the resulting composite properties.

The force curves measured by AFM were recorded in order to determine the respective adhesion forces (F_{adh}) of the samples and the epoxy used as matrix material. In a first calibration step the spring constant was determined to be 0.17 nN/nm. The adhesion forces were then calculated by multiplication with the spring constant and sensitivity (0.050898356 nm/V) to obtain the F_{adh} given in Table 4.16.

Table 4.16: Adhesion forces measured by AFM.

Sample	F_{adh} (nN)	StdDev (nN)
Buffer	9	1
Pectinex	16	1
Alkaline treated	29	1
Acetylated	22	6
Epoxy	15	2

Untreated fibres were indicated to have the lowest F_{adh} and thus were the most hydrophobic of the fibres. Application of Pectinex increases F_{adh} and thereby polarity to 16 nN. Treatment in alkaline solution increases the measured F_{adh} further still to a maximum value of 29 nN. F_{adh} is lowered by acetylation to 22 nN. The epoxy matrix used for all composites gave an F_{adh} of 15 nN. These results are in good accordance with those obtained in a previous project on hemp fibre treatments [131]. However, the larger standard deviation for the measurements on acetylated fibres indicate some irregularity on the fibre. In an earlier project [131] lower values were obtained under the same treatment and measurement conditions so that a deviation to lower values rather than higher is probable over the whole batch.

Interfacial strength is expected to increase as the polarities of the two materials approach the same value [59]. A common problem mentioned earlier is the unsatisfactory fibre-matrix adhesion of natural fibres due to their conflicting polarity towards non-polar polymeric matrices [59]. In this work, the interfacial strength was not measured directly by fibre pull-out, fragmentation tests or similar methods. However, interfacial properties have been assessed indirectly by testing of hemp-epoxy composites and characterisation with SEM. The results so far indicate that the buffer- and alkaline-treated fibres exhibit the best adhesion to the epoxy matrix. The adhesion force of fibre treated in the buffer solution was 9 nN which is close to that of epoxy and likely due to the hydrophobic waxes still found on the surface after this treatment. SEM and AFM both confirmed that this layer is not removed by treatment in aqueous buffer solution. The surface topography as recorded by AFM is shown in Figure 4.42 (a) and illustrates the smooth layer covering the microfibrils. Contrarily, alkaline treated fibres exhibited the highest adhesion force of 29 nN towards the AFM tip. Strong alkalization naturally introduces polarity by ionizing functional groups, thus the increased adhesion force relative to the other samples is expected. As the fibres still exhibit a good interfacial strength according to the results presented earlier, the bonding mechanism has to be related to these reactive groups rather than matching polarities, *e.g.* by intensive hydrogen bonding between fibre surface and epoxy matrix. In comparison to alkalized fibres, acetylated fibres possess lower polarity. As a result of acetylation, acetyl groups rather than hydroxyl groups populate the fibre surface leading to the measured decreased polarity. Rong *et al*. [59] found the same trend after mercerization and acetylation of sisal fibre and examination of the resulting surface energies. Pietak *et al*. [73] showed the close relationship between surface energy measurements and AFM adhesion forces, thus a direct comparison of Rong *et al*.'s results with the presented AFM data is possible.

The surface topographies obtained by AFM also help interpret the SEM fracture micrographs after 3PB tests. It can be seen in Figure 4.42 (b) and (c) that the microfibrils are visible from the outside. This is a prerequisite of the microfibril tear-off observed for acetylated and Pectinex treated fibres and could be verified by these micrographs.

Concluding, the results obtained from AFM measurements are in good accordance with what would be expected and measurements reported in the literature. Unfortunately, conclusive correlations between polarity and interfacial strength could not be identified. Further work is required to elucidate the potential usefulness of adhesion forces as measured by AFM for prediction of fibre-matrix bonding behaviour. A survey of the respective data plots against F_{adh} will be shown below in Table 4.17 (a).

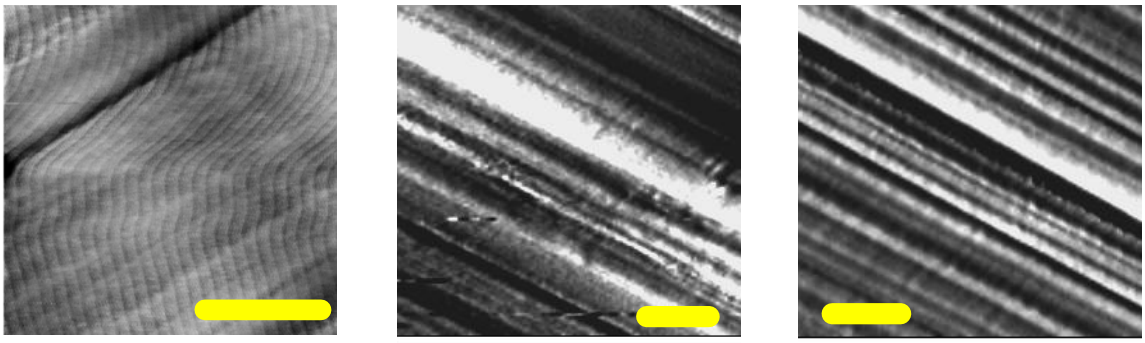

(a) Buffer treated (b) Pectinex (c) Alkalized

Figure 4.42: Surface topography of treated fibres (all scale bars show 100 nm).

4.3.8 Correlation Analysis

For the correlation analysis in SPSS the data obtained in the preceding sections of Chapter 4.3 was used. The following qualitative evaluations of fibre or composite properties have been described before and were entered as ordinal variables:

- Tendency of microfibrils to be torn off after composite fracture (Micro_tear)
- Level of defibrillation (Defibrillation)
- Tendency of fibres to be pulled out of matrix in composite tests (Pullout)
- Colour of treated fibres (Colour)
- Texture of treated fibres (Texture)

Obviously, with only four complete datasets, the calculations are not as meaningful as the analysis presented in Chapter 4.2.5. Linear correlation between two variables is unreasonably increased when two values are the same in one or

both of the variables. Therefore, only the correlations involving the AFM measurements relevant for this chapter are presented in Table 4.17. A second analysis was carried out including the data for epoxy but the small amount of data available for epoxy did not yield any new information mainly due to the large difference in properties compared to the reinforced composites. The respective matrices and calculated correlations have therefore been omitted.

The plots and figures in Table 4.17 support the conclusion drawn in the previous chapter that there is no identifiable correlation between AFM adhesion forces and other fibre characteristics. The largest correlations, although hardly significant, relate AFM forces with fibre modulus and elongation at break and both FTIR crystallinity indices. These properties are all related to the inner structure of the fibre. Consequently, a real correlation between these properties and surface measurements by AFM cannot be accepted on the basis of the presented data. A much larger dataset is required in future studies to give more meaningful results.

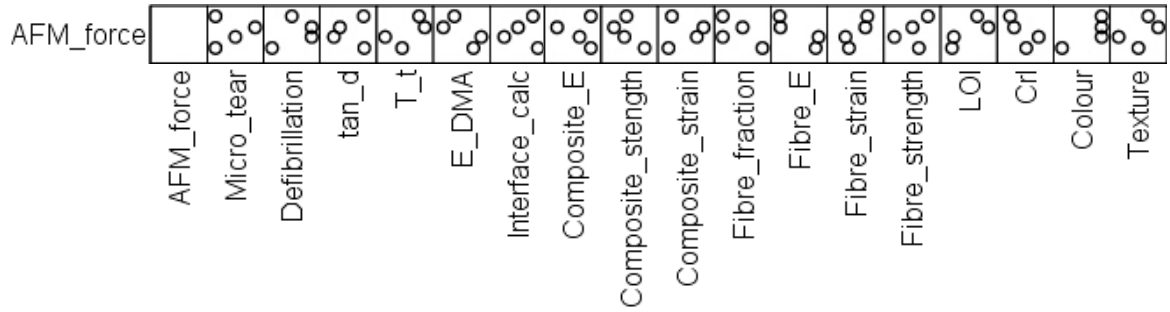

(a)

		AFM_force	Micro_tear	Defibrillation	tan_d	T_t	E_DMA	Interface_calc	Composite_E	Composite_stength
AFM_force	Correlation	1	0,123	0,408	0,028	0,631	-0,684	-0,020	-0,166	-0,654
	Significance		0,877	0,592	0,972	0,369	0,316	0,980	0,834	0,346
	N	4	4	4	4	4	4	4	4	4

		Composite_strain	Fibre_fraction	Fibre_E	Fibre_strain	Fibre_strength	LOI	CrI	Colour	Texture
AFM_force	Correlation	0,121	-0,694	-0,865	0,853	0,398	0,779	-0,713	0,782	0,504
	Significance	0,879	0,306	0,135	0,147	0,602	0,221	0,287	0,218	0,496
	N	4	4	4	4	4	4	4	4	4

(b)

Table 4.17: (a) Plots of measured AFM forces against the other variables and (b) calculated correlations.

5 Conclusions

5.1 Enzyme treatments

The first part of this study was concerned with the characterization of the impact of seven different enzyme solutions on pre-retted hemp fibre. The analysis with regard to qualitative properties, such as defibrillation and morphology, and quantitative, mechanical values aimed at identifying the most suitable enzyme solution for future projects concerned with the ecological treatment of hemp fibres. Pectinex® Ultra SP-L emerged as the superior formulation. Its retting efficiency in terms of treatment duration is at least ten times as high as all other tested enzymes. In only 3.5 hours a distinct improvement in defibrillation could be achieved accompanied by top values for crystallinity, stiffness and strength of the fibres in comparison to the other treatments applied for 24 hours.

An additional benefit for future evaluations of enzyme treatments on hemp fibres can be derived from the correlation analysis that was part of the analysis. Valuable correlations between mainly specific enzyme activities and resulting fibre properties were revealed that contribute towards the understanding of the enzymes' action and can be used as a basis for purposeful process improvements.

5.2 AFM analysis

The main objective of this part of the project was to assess potential correlations between fibre or composite properties and easily determinable AFM adhesion forces. For this purpose, four samples of hemp were analyzed which were expected to exhibit a maximum degree of dissimilarity while all suitable for composite reinforcement. In order to obtain a broad basis upon which correlations can be identified, the fibre analysis included the examination of the molecular structure by FTIR, the fibres' outer and fracture morphology and their tensile properties. Composites were prepared from epoxy and all fibre batches and characterized mechanically and morphologically by 3-point bend tests, dynamic mechanical analysis and scanning electron microscopy of the composite fracture surfaces.

Unfortunately, no clear correlations could be found between AFM data and the other properties under investigation. As this correlation analysis was only a part of the project, these result should not be taken as final and although none of the other methods can be omitted by AFM the obtained data is still vital for the clarification of the transitions taking place during fibre treatments. In order to gain a better basis for further analyses future projects could focus on single relevant aspects such as the wettability of hemp by the respective matrix materials instead of the formerly investigated water wettability and corresponding AFM measurements. The samples used for this project were selected with regard to a maximum dissimilarity in order to estimate the margins of all investigated values. Consequently, the samples were influenced by multiple factors that could not be separated in order to identify individual effects. A subsequent project supporting further applicability of the AFM technique should therefore focus on fibres and composites of smaller and better controllable differences and include an exploration of all data that can possibly be obtained by AFM.

Although no time-intensive analytical methods could be substituted by AFM as an outcome of this project, the extensive analysis of the produced fibre and composite samples nevertheless yielded valuable results. For example, the treatment in Pectinex proved a non-polluting method to achieve bundle defibrillation and thus increase the aspect ratio and bonding surface of the fibres. As a result of the composite analysis the enzyme treated fibres disqualified as suitable reinforcement fibres due to a lack of fibre-matrix-bonding. Alkalization on the other hand led to far superior bonding by a substantial change in the fibre surface structure as demonstrated by composite analysis and AFM. The presented data therefore implies a combination of Pectinex application with a subsequent mild alkaline treatment of the defibrillated fibres as a promising and ecologically friendly process in order to produce attractive fibres for composite reinforcement.

Concluding, the strengths and weaknesses of each treatment were established and therefore a more direct approach at optimizing future treatments can be taken.

6 References

[1] nova-Institut für Ökologie und Innovation, Nachwachsende Rohstoffe - Industrial Crops, 2003

[2] Centre of Lightweight Structures TU Delft, Recent projects - Natural fibre composites from upholstery to structural components, 2005

[3] Koch, P.-A., *Flachs sowie andere Bast- und Hartfasern.* Faserstofftabellen nach P.-A. Koch, 1994.

[4] Krässig, H., J. Schurz, R.G. Steadman, K. Schliefer, and W. Albrecht, *Cellulose*, in *Ulmann's Encyclopedia of Industrial Chemistry*. 2002, Wiley-VCH Verlag.

[5] Bledzki, A.K. and J. Gassan, *Composites reinforced with cellulose based fibres.* Progress in Polymer Science, 1999. **24**(2): p. 221-274.

[6] Garcia-Jaldon, C., D. Dupeyre, and M.R. Vignon, *Fibres from semi-retted hemp bundles by steam explosion treatment.* Biomass and Bioenergy, 1998. **14**(3): p. 251-260.

[7] Haudek, H.W. and E. Viti, *Textilfasern*. 1980, Verlag Johann L. Bondi & Sohn, Wien-Perchtelsdorf.

[8] Esau, K., *Pflanzenanatomie*. 1969, Gustav Fischer Verlag, Stuttgart.

[9] Gassan, J., *Naturfaserverstärkte Kunststoffe - Korrelation zwischen Struktur und Eigenschaften der Fasern und der Composites*, Dissertation, Universität-GH Kassel, p., 1997

[10] Gassan, J., A. Chate, and A.K. Bledzki, *Calculation of elastic properties of natural fibers.* Journal of Materials Science, 2001. **36**(15): p. 3715-3720.

[11] Salmén, L. and A. De Ruvo, *A model for the prediction of fibre elasticity.* Wood and Fiber Science, 1985. **17**(3): p. 336.

[12] Page, D.H., F. El-Hosseiny, K. Winkler, and A.P.S. Lancaster, *Elastic modulus of single wood pulp fibers.* Tappi, 1977. **60**(4): p. 114-117.

[13] Treiber, E., ed. *Die Chemie der Pflanzenzellwand*. 1957, Springer Verlag, Berlin-Göttingen-Heidelberg.

[14] Adler, E., *Lignin chemistry-past, present and future.* Wood Science and Technology, 1977. **11**: p. 169-218.

[15] Willats, W.G.T., L. McCartney, W. Mackie, and J.P. Knox, *Pectin: cell biology and prospects for functional analysis.* Plant Molecular Biology, 2001. **47**: p. 9-27.

[16] Thibault, J.F., C.M.G.C. Renard, M.A.V. Axelos, P. Roger, and M.J. Crepeau, *Studies of the length of homogalacturonic regions in pectins by acid-hydrolysis.* Carbohydrate Research, 1993. **238**: p. 271-286.

[17] Zhan, D., P. Janssen, and A.J. Mort, *Scarcity or complete lack of single rhamnose residues interspersed within the homogalacturonan regions of citrus pectin.* Carbohydrate Research, 1998. **308**: p. 373-380.

[18] Albersheim, P., A.G. Darvill, M.A. O'Neill, H.A. Schols, and A.G.J. Voragen, *An hypothesis: the same six polysaccharides are components of the primary cell walls of all higher plants*, in *Pectins and Pectinases*, J. Visser and A.G.J. Voragen, Editors. 1996, Elsevier Science: Amsterdam. p. 47-55.

[19] O'Neill, M.A., P. Albersheim, A.I.P.M.D.E.M. Darvill, v. in Plant Biochemistry, Academic Press, London,, and p. 415–441., *The pectic polysaccharides of primary cell walls*, in *Methods in lant Biochemistry*, P.M. Dey, Editor. 1990, Academic Press: London. p. 415-441.

[20] Schols, H.A. and A.G.J. Voragen, *Complex pectins: structure elucidation using enzymes*, in *Pectins and Pectinases*, J. Visser and A.G.J. Voragen, Editors. 1996, Elsevier Science: Amsterdam. p. 3-19.

[21] Vidal, S., T. Doco, P. Williams, P. Pellerin, W.S. York, M.A. O'Neill, and e. al., *Structural characterization of the pectic polysaccharide rhamnogalacturonan II: evidence for the backbone location of the aceric acid-containing oligoglycosyl side chain.* Carbohydrate Research, 2000. **326**: p. 277-294.

[22] Gassan, J. and A.K. Bledzki, *Alkali Treatment of Jute Fibers: Relationship Between Structure and Mechanical Properties.* Journal of Applied Polymer Science, 1999. **71**: p. 623-629.

[23] Jahn, A., M.W. Schroder, M. Futing, K. Schenzel, and W. Diepenbrock, *Characterization of alkali treated flax fibres by means of FT Raman spectroscopy and environmental scanning electron microscopy.* Spectrochimica Acta Part A: Molecular and Biomolecular Spectroscopy, 2002. **58**(10): p. 2271-2279.

[24] Oh, S.Y., D.I. Yoo, Y. Shin, and G. Seo, *FTIR analysis of cellulose treated with sodium hydroxide and carbon dioxide.* Carbohydrate Research, 2005. **340**(3): p. 417-428.

[25] Ramos, L.P., *The chemistry involved in the steam treatment of lignocellulosic materials.* Quim. Nova, 2003. **26**(6): p. 863-871.

[26] Vignon, M.R., D. Dupeyre, and C. Garcia-Jaldon, *Morphological characterization of steam-exploded hemp fibers and their utilization in polypropylene-based composites.* Bioresource Technology, 1996. **58**(2): p. 203-215.

[27] Lipp-Symonowicz, B., B. Tanska, and A. Sapieja, *Ecological Aspect of Preliminary Treatments of Flax Fibre.* Fibres & Textiles in Eastern Europe, 2004. **12**(2 (46)): p. 63-66.

[28] Novozymes A/S, *Enzymes in the textile industry - easier, cleaner, greener*. 2003.

[29] Olsen, H.S., *Enzymes at work*. 2004, Novozymes A/S.

[30] Jayani, R.S., S. Saxena, and R. Gupta, *Microbial pectinolytic enzymes: A review.* Process Biochemistry, 2005. **40**: p. 2931–2944.

[31] www.biologymad.com, Enzymes, 2004

[32] Akin, D.E., J.A. Foulk, R.B. Dodd, and I. McAlister, David D., *Enzyme-retting of flax and characterization of processed fibers.* Journal of Biotechnology, 2001. **89**(2-3): p. 193-203.

[33] Evans, J.D., D.E. Akin, and J.A. Foulk, *Flax-retting by polygalacturonase-containing enzyme mixtures and effects on fiber properties.* Journal of Biotechnology, 2002. **97**(3): p. 223-231.

[34] Henriksson, G., D.E. Akin, D. Slomczynski, and K.-E.L. Eriksson, *Production of highly efficient enzymes for flax retting by Rhizomucor pusillus.* Journal of Biotechnology, 1999. **68**(2-3): p. 115-123.

[35] Shanks, R.A. and S. Ouajai, *Morphology and Structure of Hemp Fibre after Bioscouring.* Macromolecular Bioscience, 2005. **5**: p. 124–134.

[36] Buschle-Diller, G., C. Fanter, and F. Loth, *Structural changes in hemp fibres as a result of enzymatic hydrolysis with mixed enzyme systems.* Textile Research Journal, 1999. **69**(4): p. 244-251.

[37] Zhang, J., G. Henriksson, and G. Johannson, *Polygalacturonase is the key component in enzymatic retting of flax.* Journal of Biotechnology, 2000. **81**: p. 85-89.

[38] Erblöh Geisenheim Getränketechnologie GmbH & Co. KG, *Pectin hydrolysis with Trenolin® Mash DF and Trenolin® Thermo DF*. 2004. p. 1-5.

[39] Sakai, T., T. Sakamoto, J. Hallaert, and E.J. Vandamme, *Pectin, pectinase and protopectinase: production, properties and applications.* Advanced Applied Microbiology, 1993. **39**(231-294).

[40] Codner, R.C., *Pectinolytic and cellulolytic enzymes in the microbial modification of plant tissues.* Journal of Applied Bacteriology, 2001. **84**: p. 147-160.

[41] Whitaker, J.R., *Pectic substances, pectic enzymes and haze formation in fruit juices.* Enzyme and Microbial Technology, 1984. **6**: p. 341-37.

[42] Cosgrove, D.J., *Assembly and enlargement of the primary cell wall in plants.* Annu Rev Cell Dev Biol, 1997. **13**: p. 171-201.

[43] Voragen, F., H. Schols, and R. Visser, eds. *Advances in Pectin and Pectinase Research*. 2003, Kluwer Academic Publishers.

[44] Ouajai, S. and R.A. Shanks, *Composition, structure and thermal degradation of hemp cellulose after chemical treatments.* Polymer Degradation and Stability, 2005. **89**(2): p. 327-335.

[45] Mwaikambo, L.J. and M.P. Ansell, *Chemical Modification of Hemp, Sisal, Jute, and Kapok Fibers by Alkalization.* Journal of Applied Polymer Science, 2002. **84**: p. 2222-2234.

[46] Colom, X. and F. Carrillo, *Crystallinity changes in lyocell and viscose-type fibres by caustic treatment.* European Polymer Journal, 2002. **38**(11): p. 2225-2230.

[47] Ouajai, S., A. Hodzic, and R.A. Shanks, *Morphological and Grafting Modification of Natural Cellulose Fibers.* Journal of Applied Polymer Science, 2004. **94**: p. 2456–2465.

[48] Gassan, J. and A.K. Bledzki, *Possibilities for improving the mechanical properties of jute/epoxy composites by alkali treatment of fibres.* Composites Science and Technology, 1999. **59**(9): p. 1303-1309.

[49] Van de Weyenberg, I., J. Ivens, A. De Coster, B. Kino, E. Baetens, and I. Verpoest, *Influence of processing and chemical treatment of flax fibres on their composites.* Composites Science and Technology, 2003. **63**(9): p. 1241-1246.

[50] Aziz, S.H. and M.P. Ansell, *The effect of alkalization and fibre alignment on the mechanical and thermal properties of kenaf and hemp bast fibre composites: Part 1 – polyester resin matrix.* Composites Science and Technology, 2004. **64**: p. 1219-1230.

[51] Korte, S. and M.P. Staiger, *Effect of Processing Route on the Composition and Properties of Hemp Fibre.* To be published, 2006.

[52] Hill, C.A.S., H.P.S.A. Khalil, and M.D. Hale, *A study of the potential of acetylation to improve the properties of plant fibres.* Industrial Crops and Products, 1998. **8**(1): p. 53-63.

[53] Tserki, V., N.E. Zafeiropoulos, F. Simon, and C. Panayiotou, *A study of the effect of acetylation and propionylation surface treatments on natural fibres.* Composites Part A: Applied Science and Manufacturing, 2005. **36**(8): p. 1110-1118.

[54] Koenig, J.L., *Spectroscopy of polymers*. 2nd ed. 1999, New York, Elsevier.

[55] Li, L., *Dynamic Mechanical Analysis (DMA) Basics and Beyond.* Perkin Elmer Thermal Analysis, 2000.

[56] Menard, K.P., *Dynamic Mechanical Analysis Basics: Part 1 How It Works.* Perkin Elmer Thermal Analysis Application Note.

[57] Owen, R., *Tech12/04 - A practical guide to AFM force spectroscopy and data analysis*. 2004, JPK Instruments AG.

[58] Hutter, J.L. and J. Bechhoefer, *Calibration of atomic-force microscope tips.* Review of Scientific Instruments, 1993. **64**: p. 1868-1873.

[59] Rong, M.Z., M.Q. Zhang, Y. Liu, G.C. Yang, and H.M. Zeng, *The effect of fiber treatment on the mechanical properties of unidirectional sisal-reinforced epoxy composites.* Composites Science and Technology, 2001. **61**(10): p. 1437-1447.

[60] Sreekala, M.S., M.G. Kumaran, and S. Thomas, *Oil palm fibers: Morphology, chemical composition, surface modification, and mechanical properties.* Journal of Applied Polymer Science, 1997. **66**(5): p. 821-835.

[61] Adebajo, M.O. and R.L. Frost, *Acetylation of raw cotton for oil spill cleanup application: an FTIR and 13C MAS NMR spectroscopic investigation.* Spectrochimica Acta Part A: Molecular and Biomolecular Spectroscopy, 2004. **60**(10): p. 2315-2321.

[62] Duarte, M.L., M.C. Ferreira, M.R. Marvao, and J. Rocha, *An optimised method to determine the degree of acetylation of chitin and chitosan by FTIR spectroscopy.* International Journal of Biological Macromolecules, 2002. **31**(1-3): p. 1-8.

[63] Rana, A.K., R.K. Basak, B.C. Mitra, M. Lawther, and A.N. Banerjee, *Studies of acetylation of jute using simplified procedure and its characterization.* Journal of Applied Polymer Science, 1997. **64**(8): p. 1517-1523.

[64] Eastman, T. and D.M. Zhu, *Adhesion forces between surface-modified AFM tips and a mica surface.* Langmuir, 1996. **12**: p. 2859-2862.

[65] Piner, R.D., J. Zhu, F. Xu, S. Hong, and C.A. Mirkin, *"Dip-Pen" Nanolithography.* Science, 1999. **283**: p. 661-662.

[66] Olsson, L., P. Tengvall, R. Wigren, and R. Erlandsson, *Interaction forces between a tungsten tip and methylated SiO_2 surfaces studied with scanning force microscopy.* Ultramicroscopy, 1992. **42-44**: p. 73-79.

[67] Binggeli, M. and C.M. Mate, *Influence of capillary condensation of water on nanotribology studied by force microscopy.* Appl Phys Let, 1994. **65**: p. 415-417.

[68] Cappella, B. and G. Dietler, *Force-distance curves by atomic force microscopy.* Surface Science Reports, 1999. **34**: p. 1-104.

[69] Jang, J., G.C. Schatz, and M.A. Ratner, *How Narrow Can a Meniscus Be?* Phys. Rev. Let., 2004. **92**: p. 55041-55044.

[70] Burnham, A.N., D.D. Dominguez, R.L. Mowery, and R.J. Colton, *Probing the Surface Forces of Monolayer Films with an atomic-force microscope.* Phys. Rev. Let., 1990. **64**: p. 1931.

[71] French, R.H., *Origins and applications of London dispersion forces and Hamaker constants in ceramics.* J Am Ceram Soc, 2000. **83**: p. 2117-2146.

[72] Xu, L., A. Lio, J. Hu, D.F. Ogletree, and S. Miquel, *Wetting and capillary phenomena on mica.* J. Phys. Chem. B., 1998. **102**: p. 540-548.

[73] Pietak, A., S. Korte, E. Tan, A. Downard, and M.P. Staiger, *Atomic Force Microscopy Characterization of the Surface Wettability of Natural Fibres.* To be published, 2006.

[74] AB enzymes GmbH, *QS-Arbeitsanweisung - Bestimmung der Pektinesterase (PE) - Aktivität, Revision 3.* 1998.

[75] AB enzymes GmbH, *QS-Arbeitsanweisung - Photometrische Bestimmung der Polygalacturonase (PGP-Handmethode).* 2005.

[76] Novozymes Switzerland AG, Application Sheet Bioprep® 3000L, corporate homepage accessed on 19.07.2005

[77] Novozymes Switzerland AG, Product Sheet Scourzyme® L, corporate homepage accessed on 19.07.2005

[78] Novozymes Switzerland AG, Product Sheet Pectinex® Ultra SP-L, 2005

[79] Novozymes Switzerland AG, Corporate Homepage, accessed on 08.08.2005

[80] AB enzymes GmbH, *Rohament(R) PL - Description and Specification*. 2005.

[81] AB enzymes GmbH, *Rohapect(R) PTE - Description and Specification*. 2005.

[82] AB enzymes GmbH, *Rohapect(R) MPE - Description and Specification*. 2005.

[83] Winter, B., *EL 2005023 - Personal Communication*. 2005, AB Enzymes GmbH.

[84] Faix, O. and J.H. Böttcher, *The influence of particle size and concentration in transmission and diffuse refectance spectroscopy of wood.* Holz als Roh- und Werkstoff, 1992. **50**: p. 221-226.

[85] ASTM International, *D 3822 - 01 Standard Test Method for Tensile Properties of Single Textile Fibers*. 2001.

[86] PerkinElmer Life and Analytical Sciences, Mechanical Analysis - Diamond Thermomechanical Analyzer / Diamond Dynamic Mechanical Analyzer, 2003

[87] Mieck, K.-P., T. Reussmann, and A. Nechwatal, *About the characterization of the mechanical properties of natural fibres.* Materialwissenschaften und Werkstofftechnik, 2003(34): p. 285-289.

[88] Struers A/S, Material Safety Data Sheet - Epofix Hardener, 2005

[89] Struers A/S, Material Safety Data Sheet - Epofix Resin, 2005

[90] ASTM International, *D 790 - 00 Standard Test Methods for Flexural Properties of Unreinforced and Reinforced Plastics and electrical Insulating Materials*. 2000.

[91] Korte, S., *Processing and Characterisation of Hemp Fibre for Composite Reinforcement*, Diplomarbeit, Institut für Textiltechnik, RWTH Aachen, 106 p., 2005

[92] Synytsya, A., J. Copikova, P. Matejka, and V. Machovic, *Fourier transform Raman and infrared spectroscopy of pectins.* Carbohydrate Polymers, 2003. **54**(1): p. 97-106.

[93] Sene, C., M.C. McCann, R.H. Wilson, and R. Grinter, *Fourier-Transform Raman and Fourier-Transform Infrared Spectroscopy (An Investigation of Five Higher Plant Cell Walls and Their Components).* Plant Physiology, 1994. **106**: p. 1623-1631.

[94] Chatjigakis, A.K., C. Pappas, N.Proxenia, O.Kalantzi, P.Rodis, and M. Polissiou, *FT-IR spectroscopic determination of the degree of esterification of cell wall pectins from stored peaches and correlation to textural changes.* Carbohydrate Polymers, 1998. **37**(4): p. 395-408.

[95] Manrique, G.D. and F.M. Lajolo, *FT-IR spectroscopy as a tool for measuring degree of methyl esterification in pectins isolated from ripening papaya fruit.* Postharvest Biology and Technology, 2002. **25**(1): p. 99-107.

[96] Kacurakova, M. and R.H. Wilson, *Developments in mid-infrared FT-IR spectroscopy of selected carbohydrates.* Carbohydrate Polymers, 2001. **44**(4): p. 291-303.

[97] Kamnev, A.A., M. Colina, J. Rodriguez, N.M. Ptitchkina, and V.V. Ignatov, *Comparative spectroscopic characterization of different pectins and their sources.* Food Hydrocolloids, 1998. **12**(3): p. 263-271.

[98] Filippov, M.P., *Practical infrared spectroscopy of pectic substances.* Food Hydrocolloids, 1992. **6**(1): p. 115-142.

[99] Barros, A.S., I. Mafra, D. Ferreira, S. Cardoso, A. Reis, J.A. Lopes da Silva, I. Delgadillo, D.N. Rutledge, and M.A. Coimbra, *Determination of the degree of methylesterification of pectic polysaccharides by FT-IR using an outer product PLS1 regression.* Carbohydrate Polymers, 2002. **50**(1): p. 85-94.

[100] Schwanninger, M., J.C. Rodrigues, H. Pereira, and B. Hinterstoisser, *Effects of short-time vibratory ball milling on the shape of FT-IR spectra of wood and cellulose.* Vibrational Spectroscopy, 2004. **36**(1): p. 23-40.

[101] Ishikawa, M., H. Kuroyama, Y. Takeuchi, and Y. Tsumuraya, *Characterization of pectin methyltransferase from soybean hypocotyls.* Planta, 2000. **210**(5): p. 782-791.

[102] Losonczi, A., E. Csiszár, G. Szakács, and L. Bezúr, *Role of the EDTA Chelating Agent in Bioscouring of Cotton.* Textile Research Journal, 2005. **75**(5): p. 411-418.

[103] Demarty, M., C. Morvan, and M. Thellier, *Calcium and the cell wall.* Plant, Cell and Environment, 1984. **7**(6): p. 441-448.

[104] Taragano, V., V.E. Sanchez, and A.M.R. Pilosof, *Combined effect of water activity depression and glucose addition on pectinases and protease production by Aspergillus niger.* Biotechnology Letters, 1997. **19**(3): p. 233-236.

[105] Ferreira, D., A. Barros, M.A. Coimbra, and I. Delgadillo, *Use of FT-IR spectroscopy to follow the effect of processing in cell wall polysaccharide extracts of a sun-dried pear.* Carbohydrate Polymers, 2001. **45**(2): p. 175-182.

[106] Nelson, M.L. and R.T. O'Connor, *Relation of Certain Infrared Bands to Cellulose Crystallinity and Crystal Lattice Type. Part II. A New Infrared Ratio for Estimation of Crystallinity in Celluloses I and II.* Journal of Applied Polymer Science, 1964. **8**: p. 1325-1341.

[107] Nelson, M.L. and R.T. O'Connor, *Relation of Certain Infrared Bands to Cellulose Crystallinity and Crystal Lattice Type. Part I. Spectra of Lattice Types I, II, III and of Amorphous Cellulose.* Journal of Applied Polymer Science, 1964. **8**: p. 1311-1324.

[108] Stuart, T., Q. Liu, M. Hughes, R.D. McCall, H.S.S. Sharma, and A. Norton, *Structural biocomposites from flax—Part I: Effect of bio-technical fibre modification on composite properties.* Composites Part A: Applied Science and Manufacturing, 2005.

[109] Dreyer, J., J. Müssig, N. Koschke, W.-D. Ibenthal, and H. Harig, *Comparison of Enzymatically Separated Hemp and Nettle Fibre to Chemically Separated and Steam Exploded Hemp Fibre.* Journal of industrial hemp, 2002. **7**(1): p. 43-59.

[110] Grant, G.T., E.R. Morris, D.A. Rees, P.J.C. Smith, and D. Thom, *Biological interactions between polysaccharides and divalent cations: The egg-box model.* FEBS Letters, 1973. **32**(1): p. 195-198.

[111] Windeisen, E., C. Strobel, and G. Wegener, *Chemische Charakterisierung von thermisch belastetem Holz: Bestimmung des Acetylgruppengehalts und FTIR-Spektroskopie.* Holz als Roh- und Werkstoff, 2003. **61**: p. 471-472.

[112] Cao, Y. and H. Tan, *Structural characterization of cellulose with enzymatic treatment.* Journal of Molecular Structure, 2004. **705**(1-3): p. 189-193.

[113] Cao, Y. and H. Tan, *Effects of cellulase on the modification of cellulose.* Carbohydrate Research, 2002. **337**(14): p. 1291-1296.

[114] Liang, C.Y. and R.H. Marchessault, *Infrared spectra of crystalline polysaccharides. II. Native celluloses in the region from 640 to 1700 cm^{-1}.* Journal of Polymer Science, 1959. **39**(135): p. 269-278.

[115] Colom, X., F. Carrillo, F. Nogues, and P. Garriga, *Structural analysis of photodegraded wood by means of FTIR spectroscopy.* Polymer Degradation and Stability, 2003. **80**(3): p. 543-549.

[116] Li, Y., Y.-W. Mai, and L. Ye, *Sisal fibre and its composites: a review on recent developments.* Composites Science and Technology, 2000. **60**: p. 2037-2055.

[117] Cox, H.L., *The Elasticity and Strength of Paper and Other Fibreous Materials.* British Journal of Applied Physics, 1952. **3**: p. 72-79.

[118] Krenchel, H., *Fibre Reinforcement - Theoretical and Practical Investigations of the Elasticity and Strength of Fibre-Reinforced Materials*. Thesis. 1964, Copenhagen, Akademisk Forlag.

[119] Thomason, J.L. and M.A. Vlug, *Influence of fibre length and concentration on the properties of glass fibre-reinforced polypropylene: 1. Tensile and flexural modulus.* Composites Part A: Applied Science and Manufacturing, 1996. **27**(6): p. 477-484.

[120] van den Oever, M.J.A., H.L. Bos, and M.J.J.M. van Kemenade, *Influence of the Physical Structure of Flax Fibres on the Mechanical Properties of Flax Fibre Reinforced Polypropylene Composites.* Applied Composite Materials, 2000. **7**: p. 387–402.

[121] Thomason, J.L., M.A. Vlug, G. Schipper, and H.G.L.T. Krikor, *Influence of fibre length and concentration on the properties of glass fibre-reinforced polypropylene: Part 3. Strength and strain at failure.* Composites Part A: Applied Science and Manufacturing, 1996. **27**(11): p. 1075-1084.

[122] De Neef America Inc., REMR Material Safety Data Sheet CM-CR-1.4 - Denepox 40, accessed on 11.08.2006

[123] Rana, A.K., A. Mandal, B.C. Mitra, R. Jacobson, R. Rowell, and A.N. Banerjee, *Short Jute Fiber-Reinforced Polypropylene Composites: Effect of Compatibilizer.* Journal of Applied Polymer Science, 1998. **69**: p. 329-338.

[124] http://www.matweb.com/reference/flexuralstrength.asp, accessed on 11.08.2006

[125] http://www.matweb.com/reference/tensilestrength.asp, accessed on 11.08.2006

[126] Zhandarov, S. and E. Mäder, *Characterization of fiber/matrix interface strength: applicability of different tests, approaches and parameters.* Composites Science and Technology, 2005. **65**: p. 149-160.

[127] Curtis, P.T., M.G. Bader, and J.E. Bailey, *The stiffness and strength of a polyamide thermoplastic reinforced with glass and carbon fibres.* Journal of Materials Science, 1978. **13**(2): p. 377-390.

[128] Datta, C., D. Basu, and A. Banerjee, *Mechanical and Dynamic Mechanical Properties of Jute Fibers–Novolac–Epoxy Composite Laminates.* Journal of Applied Polymer Science, 2002. **85**: p. 2800-2807.

[129] Wielage, B., T. Lampke, H. Utschick, and F. Soergel, *Processing of natural-fibre reinforced polymers and the resulting dynamic–mechanical properties.* Journal of Materials Processing Technology, 2003. **139**: p. 140-146.

[130] Koimtzoglou, C., V. Kostopoulos, N.E. Melanitis, and S.A. Paipetis, *The effect of cyclic loading on the micromechanics of the interface.* Advanced Composites Letters, 1995. **4**: p. 151-155.

[131] Pietak, A., Personal communication, 2005

7 Appendix

Table A 1 . Data sheets for the applied enzyme solutions

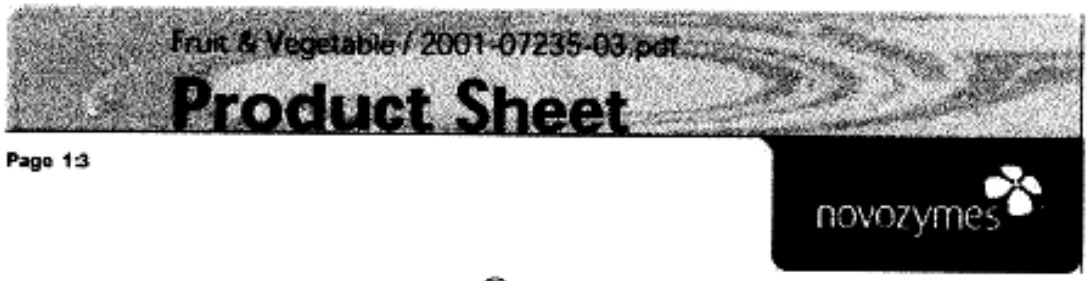

Pectinex ® Ultra SP-L

Description

Pectinex Ultra SP-L is a highly active pectolytic enzyme preparation produced by a selected strain of *Aspergillus aculeatus*. This enzyme preparation contains pectolytic and a range of hemicellulolytic activities. It has the ability to disintegrate plant cell walls.

Product Properties

Product Type

Pectinex Ultra SP-L is a brownish liquid with a slight smell typical of fermented products and a pH of approx. 4.5.

Activity

Pectinex Ultra SP-L has a standard activity of 26,000 PG/ml (pH 3.5). The standard activity is determined by the measurement of the viscosity reduction of a solution of pectic acid at pH 3.5 and 20°C (68°F). See the Analytical Method for further information.

Solubility

The active components of Pectinex Ultra SP-L are readily soluble in water at all concentrations that occur in normal usage. Turbidity which may occur in the enzyme preparation has no influence on the volumetric activity or handling characteristics of the product.

Food-grade status

The product complies with FAO/WHO, JECFA and FCC specifications for food-grade enzymes, supplemented by maximum limits of 10^7 moulds/g. The product is bott[redacted]tically after sterile filtration and therefore practically germ-free.

Packaging

See the standard Packaging List for more packaging information.

Application

The preparation is especially designed for the treatment of fruit and vegetable mashes and the maceration of plant tissues. Soluble and insoluble pectins as well as haze-provoking polysaccharides are also efficiently degraded. Pectinex Ultra SP-L applied on fruit and vegetable mashes and/or pomaces leads to drastically increased capacities in solid/liquid separation (e.g. press, decanter) and higher juice yields.

Table A 1 . Data sheets for the applied enzyme solutions

Reaction Parameters

Pectinex Ultra SP-L Activity

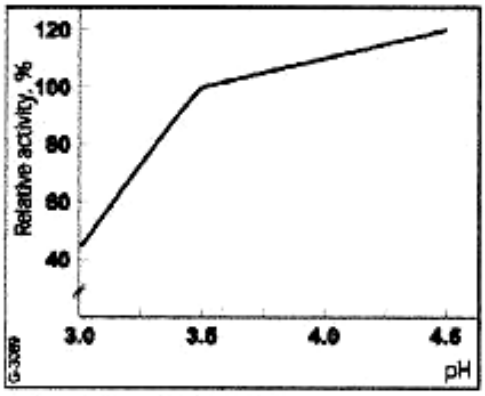

Fig. 1. Pectinase activity versus pH.
Polygalacturonase activity at 20°C (68°F)

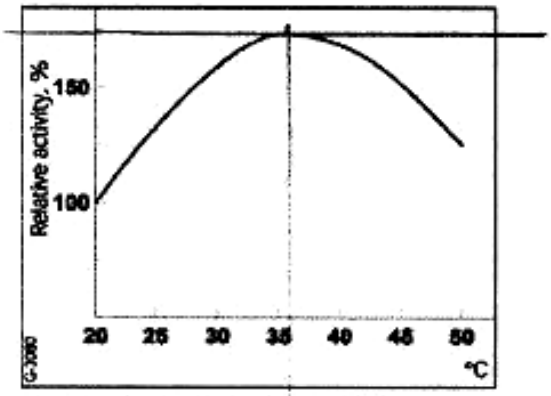

Fig. 2. Pectinase activity versus temperature.
Polygalacturonase activity at pH 3.5

Safety

Enzymes are proteins and inhalation of dust or aerosols may induce sensitization and may cause allergic reactions in sensitized individuals. Some enzymes may irritate the skin, eyes and mucous membranes upon prolonged contact.

The product may create easily inhaled aerosols if splashed or vigorously stirred. Spilled product may dry out and create dust.

Spilled material should be flushed away with water (avoid splashing). Left-over material may dry out and create dust.

A Material Safety Data Sheet is supplied with all products. See the Safety Manual for further information regarding how to handle the product safely.

novozymes

Table A 1 . Data sheets for the applied enzyme solutions

Storage

When the product is stored at a temperature of 20°C (68°F), the declared activity is maintained for three months. For longer storage periods, a loss in activity of 1-2% per month may occur. When stored at 0-10°C (32-50°F), this product will maintain the declared activity for at least one year.

novozymes

Novozymes Switzerland AG
Neumatt
4243 Dittingen
Switzerland

Tel. +41 61 7656111
Fax +41 61 7656333

Novozymes A/S
Krogshoejvej 36
2880 Bagsvaerd
Denmark

Tel. +45 8824 9999
Fax +45 8824 9998
info@novozymes.com
www.novozymes.com

Table A 1 . Data sheets for the applied enzyme solutions

Textile Distribution

Application Sheet

novozymes®

Content:
- Benefits
- Products
- Usage

The biological way to scour (ready-to-use products)

Traditional scouring involves the use of chemicals such as caustic soda, which is not only harsh on the fabric but also on the environment. Disadvantages of traditional scouring include chemical handling, excessive rinsing, effluent concerns, and possible fibre damage.
To counter this, Novozymes introduced a scouring process called Bio-Scouring. Bio-Scouring is an enzymatic process offering a milder and gentler alternative to traditional scouring.
Scourzyme® L is a specially developed alkaline pectate lyase for end-users. Pectate lyase degrades the pectin from the primary cell wall of cotton without degrading the cotton itself. Research has shown that pectin acts like glue between the fibre core and the waxes, but that it can be removed by an alkaline pectate lyase, making the residual waxes easy to eradicate in the subsequent hot rinse.

Benefits

Bio-Scouring has a number of potential benefits over traditional scouring, including:

- Gentler on fabrics
- Improved dyeing
- Lower yarn coefficient of friction
- Increased yarn elongation for improved weaving efficiencies
- Improved emerising and brushing properties
- No degradation of cellulose
- Lower weight loss
- Environment-friendly
- Safe and easy to use

Table A 1 . Data sheets for the applied enzyme solutions

novozymes

Products

Scourzyme L is a liquid product and is available as:

Scourzyme L ..... 375 APSU/g
APSU = Alkaline Pectinase Standard Units

There is more information about the above-mentioned products available at the Customer Centre.

Usage

Product	Temp. (°C)	pH	Application		
			Continuous	CPB	Jet, jig, winch
Scourzyme L	50-65	7.5-9.0	+/-	++	++
	25-65	7.5-9.0	NR	++	NR

NR – Not Recommended
++ – very good
+/- – suitable in certain circumstances

Application/process type
Scourzyme L can be used with in any equipment normally used for wet textile processing.

Bio-Scouring on cotton includes the following basic steps: treatment with Scourzyme L; emulsification; hot rinsing followed by cold rinsing (optional). To obtain all of the benefits of the Bio-Scouring concept on yarn or jet dyeing equipment, Scourzyme L should be run at its optimum parameters as stated below:

- Dosage 0.4-0.6%
- Application pH range 8-9
- Process temperature 45-60°C
- Process time 10-30 minutes
- Wetting agent 0.25-1.0 g/l (anionic not recommended)
- Emulsifier 0.5-1.0 g/l
- Chelating agent 0.25-1.0 g/l

Table A 1 . Data sheets for the applied enzyme solutions

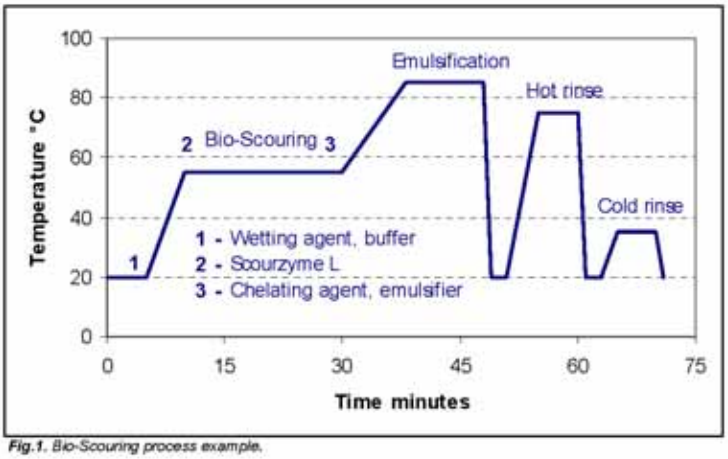

Fig.1. Bio-Scouring process example.

Storage in application

Enzymes are proteins and inhalation of dust or aerosols may induce sensitisation and may cause allergic reactions in sensitised individuals. Some enzymes may irritate the skin, eyes and mucous membranes upon prolonged contact.

The product may create easily inhaled aerosols if splashed or vigorously stirred. Spilled product may dry out and create dust. Spilled material should be flushed away with water. Avoid splashing. Left-over material may dry out and create dust.

A Material Safety Data Sheet is supplied with all products. Please refer to the Safety Manual for further information on the safe handling of the product.

Safety, handling and storage

Safety, handling and storage guidelines are provided with all products.

Novozymes A/S
Krogshoejvej 36
2880 Bagsvaerd
Denmark

Tel. +45 8824 9999
Fax +45 8824 9998

For more information
and addresses of
international offices,
please see
www.novozymes.com
info@novozymes.com

Table A 1 . Data sheets for the applied enzyme solutions

ROHAPECT® PTE

Description and Specification

2005-03-01
Rev. Nr. 07

Description

ROHAPECT® PTE is a special pectolytic enzyme preparation for the processing of fruits and vegetables. The pectinase is derived from Aspergillus.

- IUB-No.: 4.2.2.10
- CAS-No.: 9033-35-6

Properties

The product has the following characteristics:

a) liquid product
b) brown coloured with aromatic smell
c) specific weight: ~ 1.15 g/ml

Activity

ROHAPECT® PTE contains a declared minimum activity of 75 PTF/mg.
1 PTF/mg corresponds an enzyme activity, which leads to an increase of the extinction of 0,01 after 1 min., at pH 5,8 and 30 °C at 235 nm in a 0,5 % pectin solution.

Application

ROHAPECT® PTE is a special enzyme preparation which contains mainly the specific pectintranseliminase or endo pectin lyase activity.
The pectin degradation occurs by transelimative pattern without previous deesterification.
ROHAPECT® PTE suits perfectly for a fast viscosity reduction in the processing of fruit and vegetables. In fruit brandy production the enzyme treatment supplies a better fermentation, without additional formation of methanol. For the processing of carrot juice, the treatment increases the yield on juice and colouring matter.

Table A 1 . Data sheets for the applied enzyme solutions

AB Enzymes GmbH
Postfach 101239
64212 Darmstadt
Germany
Tel: +49 (0) 6151 3680 100
Fax: +49 (0) 6151 3680 120

ROHAPECT® PTE

Dosage

Application	Reaction conditions	Dosage
Citrus juice (orange, grape fruit)	10 - 25 ° C, 10-20 min	5 - 10 ppm
Citrus pulp wash	30 - 45° C, 10 - 30 min	20 - 40 ppm
Fruit brandies: Pears, Cherries, Plums, ect.	mash: ambient temperature, during fermentation Combination with ROHAMENT® PL	30 - 60 ppm
Carrot juice	mash: 45 - 50 °C, 1 - 2 hrs Combination with ROHAMENT® CL	100 ppm
Puree concentrates, i.e. mango, banana, maracuja, apricot, peaches etc.	35 - 55° C, 10 - 20 min	20 - 40 ppm

Specification

The product fulfils the requirements of the FAO/WHO's Joint Expert Committee for Food Additives (JECFA) and Food Chemicals Codex (FCC).
The total viable counts are within the upper limit of 5×10^4 g^{-1}

Storage

Stored in a cool place (4 °C) the activity loss will be less than 10 % within one year.

Table A 1 . Data sheets for the applied enzyme solutions

ROHAMENT® PL

Description and Specification

2005-03-01
Rev. Nr. 05

Description

ROHAMENT® PL is a special pectolytic enzyme preparation for the maceration of fruit and vegetable tissue. It contains almost exclusive polygalacturonase activity. The pectinase is derived from Aspergillus.

- IUB-No.: 3.2.1.15
- CAS-No.: 9032-75-1

Properties

The product has the following characteristics:

a) liquid product
b) brown coloured with aromatic smell
c) specific weight: 1.1 - 1.2

Activity

ROHAMENT® PL contains a declared minimum activity of 28.000 PGU/mg.
The PGU activity is determined by the measurement of the viscosity reduction of a standard pectin solution at pH 3.9 and 30 °C.

Application

ROHAMENT® PL is particularly suitable for the production of fruit and vegetable purees.
During the breakdown of protopectin in fruit or vegetable mash the fruit tissue disintegrates and a soluble but still high molecular-weight pectin is produced. Cloud-stable juices or purees can be obtained from a mash treated in this manner.
ROHAMENT® PL is also suitable for mash treatment in the production of fruit brandies, particularly in combination with **ROHAPECT® PTE**.

Table A 1 . Data sheets for the applied enzyme solutions

AB Enzymes GmbH
Postfach 101239
64212 Darmstadt
Germany
Tel: +49 (0) 6151 3680 100
Fax: +49 (0) 6151 3680 120

ROHAMENT® PL

Dosage

Application	Reaction conditions	Dosage
Fruit and Vegetable Purees	pH 4.5 - 5.0, 40 - 45° C, 1 - 2 Std.	300 - 500 ppm
Fruit Brandy Production: Cherries, Plums, Greengages, Apricots	approx .20° C during fermentation	50 - 100 ppm
Apples, Pears	approx. 20° C during fermentation	100 - 150 ppm

Specification

The product fulfils the requirements of the FAO/WHO's Joint Expert Committee for Food Additives (JECFA) and Food Chemicals Codex (FCC).
The total viable counts are within the upper limit of 5×10^4 g^{-1}

Storage

Stored in a cool place (4 °C) the activity loss will be less than 10 % within one year.

Table A 1 . Data sheets for the applied enzyme solutions

ROHAPECT® MPE

Description and Specification

2005-04-08
Rev. No. 04

Description

ROHAPECT® MPE is a special pectolytic enzyme preparation with mainly pectin esterase activitiy, used for the de-esterification of pectin. The enzyme is derived from Aspergillus.

- IUB-No.: 3.1.1.11
- CAS-No.: 9025-98-3

Properties

The product has the following characteristics:

a) liquid product
b) brown coloured with aromatic smell
c) specific weight: 1.1 - 1.2 g/ml

Activity

Rohapect® MPE contains a declared minimum activity of 1000 PE/g.
1 PE/g is defined as that enzyme quantity which releases 1 µval acid per minute under the given conditions (30 °C, 0.55 % substrate solution, pH 4.5).

Application

ROHAPECT® MPE is particularly suitable for the modification of pectin and in the process of "Défécation" for the production of apple cider.

Table A 1 . Data sheets for the applied enzyme solutions

AB Enzymes GmbH
Postfach 101239
64212 Darmstadt
Germany
Tel: +49 (0) 6151 3680 100
Fax: +49 (0) 6151 3680 120

ROHAPECT® MPE

Dosing

Application	Reaction conditions	Dosage
Pectin De-Esterification	pH 4.5 - 5.0, 20 - 30° C, 1 - 2 hrs	5.000 - 10.000 ppm
Cider "Défécation"	approx . 10 - 20° C addition of Calcium Chloride	10 - 20 ppm

Specification

Requirements correspond to the recommendations given by the FAO/WHO's Joint Expert Committee for Food Additives (JECFA) and Food Chemicals Codex (FCC).
The total viable counts are within the upper limit of 5×10^4 g^{-1}.

Storage

Stored in a cool place (4 °C) the activity loss will be less than 10 % within one year.

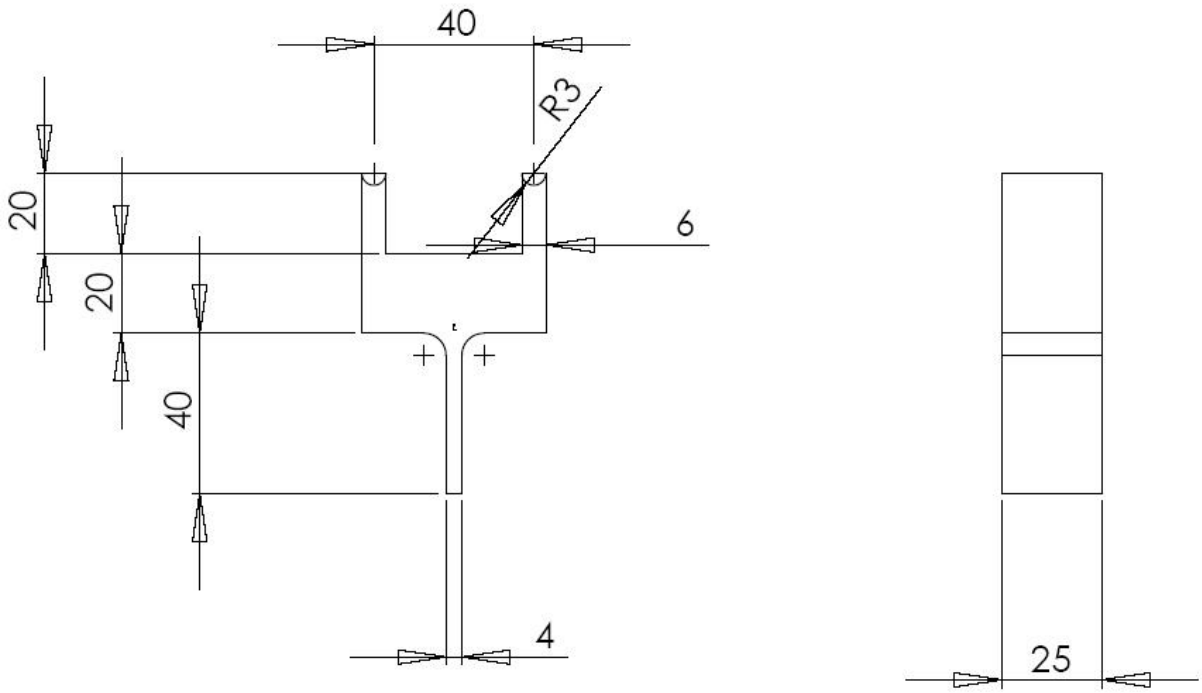

(a) Specimen support

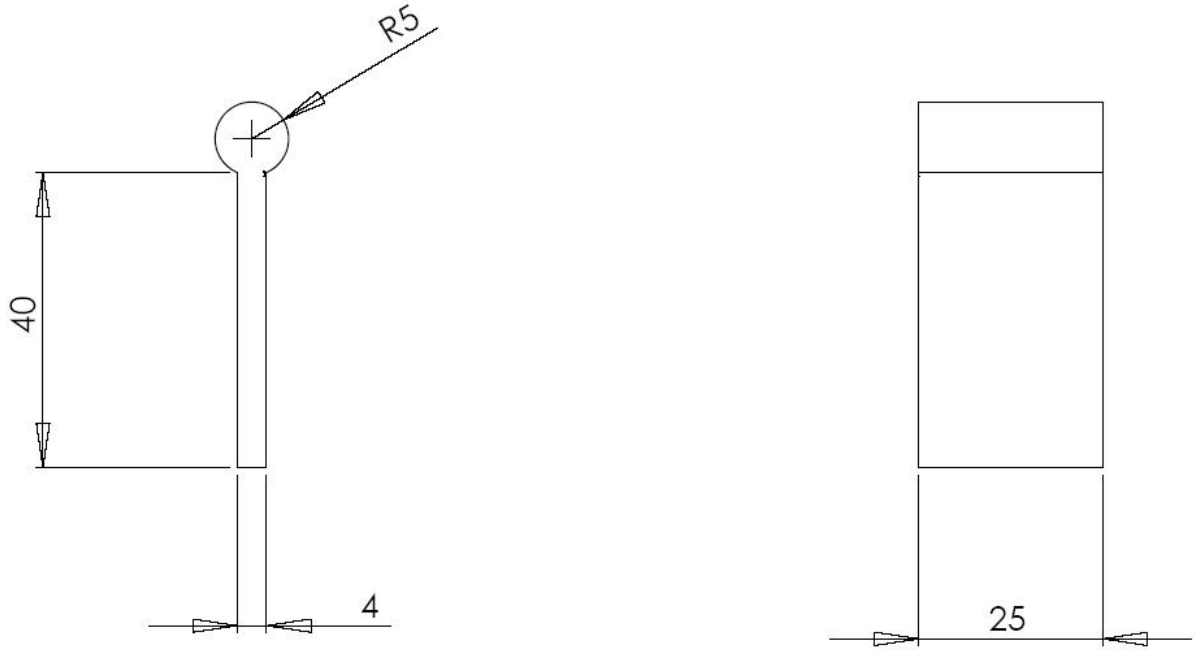

(b) “Loading nose“

Figure A 1: Three-point-bending assembly designed for the conducted composite tests

Table A 2: Visual Basic macro for automated analysis of data files from DMA tensile tests and creation of a data summary in Excel

```
Option Explicit
Dim strFilePath, strFileSaveNew, strNameFile, strFileName, strFileSearcher, dummy, stCurrentFile As String
Dim i, intGetData, intAktuellesWorkbook, intFolder, intAnzahl, intEnde, intCounter, b As Integer
Public intLineinMerge, intFoundFiles As Integer
Public arrFolder(1 To 5) As String
Dim boolConvert, boolFehler As Boolean
Dim stOutputFileName As String
Dim stSampleName As String
Dim sYoungsModulus As Single
Dim sElongation As Single
Dim sStrength As Single
Dim sRadius1 As Variant
Dim sRadius2 As Single
Dim sRadius3 As Single
Dim sRadius4 As Single
Dim sRadius5 As Single
Dim sRadius6 As Single
Dim sRadius7 As Single
Dim sRadius8 As Single
Dim sArea As Single
Public iOutputColumn As Integer
```

```
Sub Main()

Call StartUP
Call MakeSummaryFile
Call ImportLoop

'Workbooks("MainImportWorkbook.xls").Sheets("Merge").Select
MsgBox (intGetData - 1 & " data file(s) out of " & intFoundFiles & " processed!")


End Sub
```

```
Sub StartUP()

   ThisWorkbook.SaveAs ("MainImportWorkbook_incl_Summary.xls")
   Application.ScreenUpdating = False
   arrFolder(1) = "\Import Files"

   Sheets("Merge").Activate
   Sheets("Merge").Range("A5:D2000").Select
   Selection.ClearContents
   Sheets("Merge").Cells(5, 3).Select

      With Application

         .FileSearch.LookIn = ThisWorkbook.Path & arrFolder(1)
         .FileSearch.SearchSubFolders = False
         .FileSearch.Filename = "*.xls"
         intFoundFiles = .FileSearch.FoundFiles.Count
         If .FileSearch.Execute() > 0 Then

            For intGetData = 1 To .FileSearch.FoundFiles.Count
               dummy = Split(.FileSearch.FoundFiles(intGetData), "\")
               intAnzahl = UBound(dummy)
               strFileName = dummy(intAnzahl)
               Sheets("Merge").Cells(intGetData + 4, 3) = strFileName
            Next intGetData

         Else

            If Not boolConvert Then
               boolFehler = True
            End If
         End If

      End With

   If boolFehler Then
      MsgBox "No files found.", vbCritical, "Error..."
      boolFehler = False
   End If
   Application.ScreenUpdating = True
End Sub
```

```
Sub ImportLoop()
intLineinMerge = 5
    While intLineinMerge < intGetData + 4

        Call ImportDMAdata

        intLineinMerge = intLineinMerge + 1
    Wend

End Sub
```

Table A 2: Visual Basic macro for automated analysis of data files from DMA tensile tests and creation of a data summary in Excel

```
Sub ImportDMAdata()
'
    Workbooks.Add Template:= _
        "C:\Dokumente und Einstellungen\sandra\Anwendungsdaten\Microsoft\Vorlagen\DMA analysis1 more auto.xlt"

    stCurrentFile = Workbooks("MainImportWorkbook_inclSummary.xls").Sheets("Merge").Cells(intLineinMerge, 3).Value
'SaveAs "ANALYZED_" & first filename
    ActiveWorkbook.SaveAs ("ANALYZED_" & stCurrentFile)
    ChDir ("Import Files")
    Workbooks.Open (stCurrentFile)
    ChDir (Workbooks("ANALYZED_" & stCurrentFile).Path)
    Range("A1:E200").Select
    Selection.Copy

Workbooks("ANALYZED_" & stCurrentFile).Activate

    Call GeometryForm

'Paste data from DMA file
    Sheets("Data").Select
    Range("J6").Select
    ActiveSheet.Paste
    Application.CutCopyMode = False
    Workbooks(stCurrentFile).Close
    Application.CutCopyMode = True

 'Filter sigma, elongation, true elongation columns
    Columns("D:F").Select
    Range("D1:F200").AdvancedFilter Action:=xlFilterCopy, CriteriaRange:=Range( _
        "D1:F3"), CopyToRange:=Columns("O:Q"), Unique:=False

 'If original data is corrupt (DIV/0! warnings in filtered file shown on screen)
 'abort macro here and go to next file
    If MsgBox("Any good?", vbYesNo, "Starten...") = vbNo Then
         GoTo AbortLine

    End If

 Call SetOffset

 '***SUMMARY***
 Sheets("Radius etc").Select
 'Read all necessary values from Active Radius Sheet
    stSampleName = ActiveSheet.Range("B2").Value                'Reads the sample name
    'MsgBox (stSampleName)  'to check pointing to right kind of cell
    sYoungsModulus = ActiveSheet.Range("C7").Value              'Reads the Young's Modulus
    'MsgBox (sYoungsModulus)  'to check pointing to right kind of cell
    sElongation = ActiveSheet.Range("D7").Value                 'Reads the Elongation at break
    'MsgBox (sElongation)  'to check pointing to right kind of cell
    sStrength = ActiveSheet.Range("E7").Value                   'Reads the Tensile Strength
    'MsgBox (sStrength)  'to check pointing to right kind of cell
        sRadius1 = ActiveSheet.Range("A6").Value
    sRadius2 = ActiveSheet.Range("A8").Value
    sRadius3 = ActiveSheet.Range("A10").Value
    sRadius4 = ActiveSheet.Range("A12").Value
    sRadius5 = ActiveSheet.Range("A14").Value
    sRadius6 = ActiveSheet.Range("A16").Value
    sRadius7 = ActiveSheet.Range("A18").Value
    sRadius8 = ActiveSheet.Range("A20").Value
    sArea = ActiveSheet.Range("A22").Value

'Write values into outputfile
    With Workbooks(stOutputFileName).Worksheets("Tabelle1").Range("B2")  'Go to outputfile's upper left data cell
        .Cells(1, iOutputColumn).Value = stSampleName
        .Cells(2, iOutputColumn).Value = sYoungsModulus
        .Cells(3, iOutputColumn).Value = sElongation
        .Cells(4, iOutputColumn).Value = sStrength
        .Cells(5, iOutputColumn).Value = sRadius1
        .Cells(6, iOutputColumn).Value = sRadius2
        .Cells(7, iOutputColumn).Value = sRadius3
        .Cells(8, iOutputColumn).Value = sRadius4
        .Cells(9, iOutputColumn).Value = sRadius5
        .Cells(10, iOutputColumn).Value = sRadius6
        .Cells(11, iOutputColumn).Value = sRadius7
        .Cells(12, iOutputColumn).Value = sRadius8
        .Cells(13, iOutputColumn).Value = sArea
    End With

    iOutputColumn = iOutputColumn + 1


 '*** END SUMMARY
AbortLine:  'Macro jumps to this line if analysis is aborted for one file

 ActiveWorkbook.Save
 ActiveWorkbook.Close

End Sub
```

Table A 2: Visual Basic macro for automated analysis of data files from DMA tensile tests and creation of a data summary in Excel

```
Sub SetOffset()
'user looks at diagram and approximates trend-offset
    Sheets("Radius etc").Select
    Range("B32").Select
    ActiveCell.Value = InputBox("Approximate Offset")        ⇨ screenshot 1
 'Filter data again to get new true elongation
    Sheets("Data").Select
    Columns("D:F").Select
    Range("D1:F200").AdvancedFilter Action:=xlFilterCopy, CriteriaRange:=Range( _
        "D1:F3"), CopyToRange:=Columns("O:Q"), Unique:=False


    Sheets("Sigma-Epsilon").Select

'Visual check by user if stress-strain-curve is set to start in origin of diagram
'If not offset can be adjusted
    If MsgBox("Does the curve approach zero?", vbYesNo, "Check offset...") = vbNo Then
       Call SetOffset
    End If                                                   ⇨ screenshot 2
End Sub
```

Screenshot 1

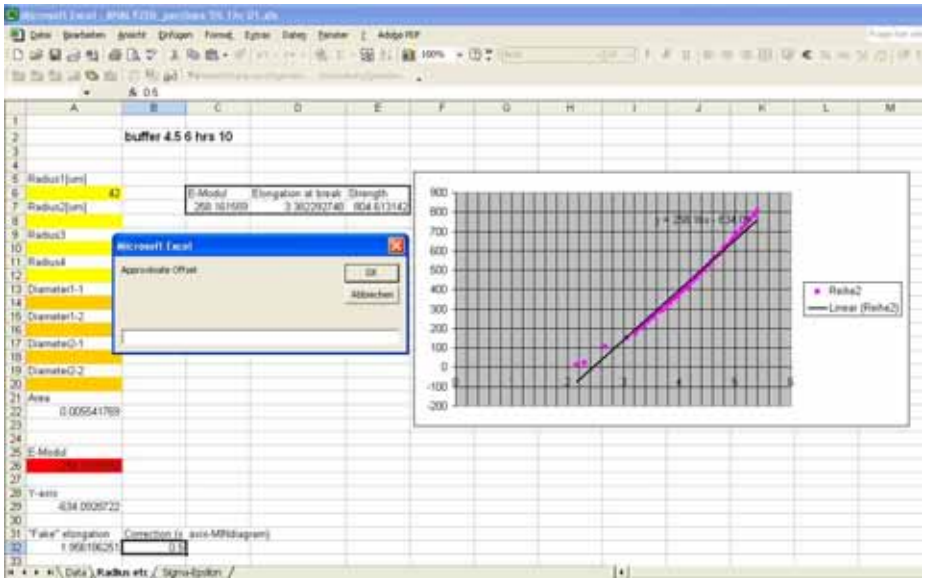

Screenshot 2

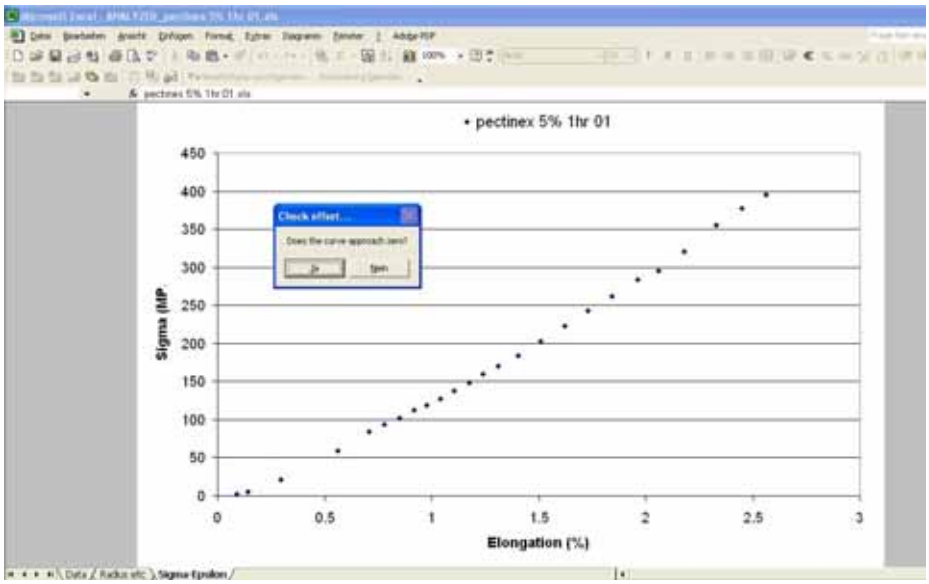

Table A 2: Visual Basic macro for automated analysis of data files from DMA tensile tests and creation of a data summary in Excel

```
Sub MakeSummaryFile()

'Create new output file
Workbooks.Add
stOutputFileName = InputBox("Please enter name of output file including '.xls'")
ActiveWorkbook.SaveAs (stOutputFileName)
'Defines structure and layout of summary
ActiveWorkbook.Sheets("Tabelle1").Range("A1").Value = "Summary of all tested samples"
With ActiveWorkbook.Sheets("Tabelle1").Range("A1").Font
    .Bold = True
    .Size = 12
End With
ActiveWorkbook.Sheets("Tabelle1").Range("A2").Value = "Sample Name"
ActiveWorkbook.Sheets("Tabelle1").Range("A3").Value = "Young's Modulus"
ActiveWorkbook.Sheets("Tabelle1").Range("A4").Value = "Elongation at failure"
ActiveWorkbook.Sheets("Tabelle1").Range("A5").Value = "Tensile Strength"
ActiveWorkbook.Sheets("Tabelle1").Range("A6").Value = "Radius1"
ActiveWorkbook.Sheets("Tabelle1").Range("A7").Value = "Radius2"
ActiveWorkbook.Sheets("Tabelle1").Range("A8").Value = "Radius3"
ActiveWorkbook.Sheets("Tabelle1").Range("A9").Value = "Radius4"
ActiveWorkbook.Sheets("Tabelle1").Range("A10").Value = "Sidelength1"
ActiveWorkbook.Sheets("Tabelle1").Range("A11").Value = "Sidelength2"
ActiveWorkbook.Sheets("Tabelle1").Range("A12").Value = "Sidelength3"
ActiveWorkbook.Sheets("Tabelle1").Range("A13").Value = "Sidelength4"
ActiveWorkbook.Sheets("Tabelle1").Range("A14").Value = "Area"


With ActiveWorkbook.Sheets("Tabelle1").Range("A2:A14")
    .Font.Bold = True
    .ColumnWidth = 20
End With

ActiveWorkbook.Save
iOutputColumn = 1

End Sub
```

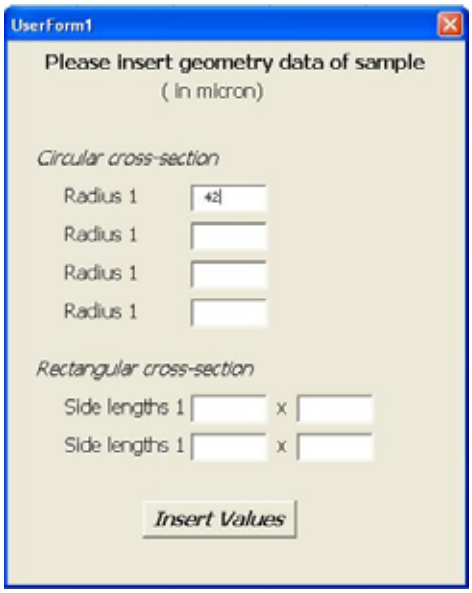


```
Sub GeometryForm()

    Load GeometryInput
    GeometryInput.Show

End Sub
```

```
Private Sub CommandButton1_Click()
With ActiveWorkbook.Sheets("Radius etc")
    .Range("A6") = TextBox1.Value
    .Range("A8") = TextBox2.Value
    .Range("A10") = TextBox3.Value
    .Range("A12") = TextBox4.Value
    .Range("A14") = TextBox5.Value
    .Range("A16") = TextBox6.Value
    .Range("A18") = TextBox7.Value
    .Range("A20") = TextBox8.Value
    Unload GeometryInput
End With


End Sub
```